UNIVERSIDAD NACIONAL AUTÓNOMA DE MEXICO
POSGRADO EN CIENCIAS FÍSICAS

NEUTRINO MASS GENERATION AND DARK MATTER MODELS

TESIS
QUE PARA OPTAR POR EL GRADO DE:
DOCTOR EN CIENCIAS (FÍSICAS)

PRESENTA:
JORGE MARIO LAMPREA GARZON

ASESOR:
DR. EDUARDO PEINADO RODRÍGUEZ
INSTITUTO DE FÍSICA – UNAM

MIEMBROS DEL COMITÉ TUTOR:
DR. GENARO TOLEDO SÁNCHEZ
INSTITUTO DE FÍSICA – UNAM

DR. MARIANO CHERNICOFF MINSBERG
FACULTAD DE CIENCIAS – UNAM

CUIDAD DE MÉXICO, SEPTIEMBRE 2018

Resumen de la tesis

Las masas de los neutrinos y la existencia de materia oscura son las pruebas más directas sobre la necesidad de nueva física más allá del Modelo Estándar de partículas elementales. Sin embargo, la naturaleza de esta nueva física sigue siendo al día de hoy desconocida. Esto ha imposibilitado determinar cuál es la extensión del Modelo Estándar que de cuenta de todos o la mayoría de los fenómenos que el Modelo Estándar no puede explicar. Por el lado de los neutrinos, se desconoce su naturaleza, es decir, si son fermiones de Dirac o Majorana, su escala de masas, el mecanismo detrás de la generación de sus masas tan pequeñas o si existe una razón detrás del patrón de masa y mezcla.
Adicionalmente, es interesante considerar que las masas y mezclas de los neutrinos pueden ser explicados por una teoría que de cuenta de los patrones de masa y mezcla de los todos los fermiones en el Modelo Estándar. Esto es posible ya que los acoplamientos de Yukawa, de los cuales dependen las masas y mezclas de los quarks y leptones, son parámetros complejos totalmente libres en el Modelo Estándar. A dicha arbitrariedad de los acoplamientos de Yukawa y, por tanto, falta de explicación para las masas y mezclas de los fermiones, es referido usualmente como el *problema del sabor* del Modelo Estándar.

Por otro lado, la existencia de materia oscura, inferida a través de sus efectos gravitacionales sobre la materia visible, urge por una explicación dentro del escenario de la física de partículas. Esto debido a que el Modelo Estándar falla en proporcionar un candidato viable a materia oscura. Además, tales candidatos a materia oscura deben satisfacer constricciones de experimentos de busqueda directa e indirecta cada vez más fuertes.

La idea de relacionar el mecanismo detrás del origen de las masas de los neutrinos y la materia oscura es, desde el punto de vista teórico, muy atractivo y puede generar interesantes desarrollos en ambos sectores. Basados en dicha premisa, la presente tesis está dedicada al estudio de tres realizaciones teóricas de la conexión entre los neutrinos y la materia oscura, teniendo en común la *mínima extensión del Modelo Estándar a través de la adición de simetrías discretas.*

Esta tesis está ordenada como se describe a continuación. Primero en el capítulo 1, desarrollamos una breve introdución al Modelo Estándar, la física de neutrinos y la materia oscura. Esto con el fin de establecer la notación y convenciones usadas a lo largo del documento. A continuación en el capítulo 2, se presentan dos extensiones al Modelo Estándar donde la materia oscura y la masa de los neutrinos están relacionadas por medio de una simetría de sabor no Abeliana. Dicha simetría de sabor es responsable por la fenomenología de los neutrinos. Además, su rompimiento en una simetría residual, genera un mecanismo para la estabilizacíon de la materia oscura. Las masas de los neutrinos son generadas a través del mecanismo de seesaw tipo I. Las predicciones de sabor se deben a que la matriz de masas de los neutrinos izquierdos posee una textura con dos ceros. A partir de dicha textura, es posible obtener correlaciones entre los parámetros de oscilación y, por lo tanto, los observables de los neutrinos. Una de estas correlaciones lleva a una cota inferior a la masa de Majorana efectiva del neutrino del electrón, la cual es proporcional a la amplitud del decaimiento beta doble sin neutrinos ($0\nu\beta\beta$). Dicha cota está en la región de sensitividad de futuros experimentos.

En el capítulo 3, se estudia una extensión del modelo Escotogénico de Ma, donde las masas de los neutrinos son generadas a través de correcciones radiativas a un lazo. En dichas correcciones radiativas la materia oscura participa en el lazo. El modelo de Ma añade tres neutrinos derechos y un doblete de Higgs inerte al Modelo Estándar, todos ellos cargados ante una simetría discreta exacta. De tal modo, los neutrinos izquierdos adquieren sus masas mediante una corrección radiativa a un lazo. Sin embargo, existe una tensión en el modelo Escotogénico. Cuando el candidato a materia oscura es el neutrino derecho más ligero y solo su aniquilación es responsable por la densidad reliquia, el espacio de parámetros que satisface las cotas experimentales de los procesos con violación de sabor es severamente restringido. De este modo, se muestra que al añadir un campo escalar complejo singlete bajo el grupo de norma del Modelo Estándar se reduce significativamente dicha tensión. Esto debido a que el campo escalar puede generar dinámicamente la masa de los neutrinos derechos, introduciendo un nuevo canal de aniquilación para la materia oscura.

Posteriormente en el capítulo 4, se explora un modelo de simetría de sabor donde los neutrinos adquieren masas por medio de un mecanismo de seesaw para neutrinos de Dirac. El modelo resuelve parcialmente el problema de sabor en el Modelo Estándar. Por un lado, el patrón de masa de los fermiones es explicado por medio de una relación de masas derivada de la simetría de sabor, entre los leptones cargados y los quarks tipo down. Dicha relación ha sido propuesta anteriormente en otros trabajos. Por otro lado, el patrón de

mezcla de los fermiones está relacionado por la estructura de la simetría de sabor, la cual puede reproducir los elementos de la matriz CKM, y de este modo, fijar la contribución de los leptones cargados a la matriz de mezcla leptónica. El modelo tiene predicciones respecto a la fenomenología de los neutrinos, siendo solo consistente con un ordenamiento invertido de las masas de los neutrinos y un ángulo de mezcla atmosférico no maximal. Además, se tiene que la fase de violación de CP es no nula cuando la masa más ligera de neutrinos menor a 2 meV, mientras que para masas mayores es compatible con un escenario con conservación de la simetría de CP.

Por último damos nuestras conclusiones y comentarios finales en el capítulo 5.

Abstract

Neutrino masses and dark matter existence are the most direct proves for the need of new physics beyond the Standard Model (SM). On the neutrino side, we do not know their nature, that is, whether they are Dirac or Majorana fermions, their mass scale and which is the mechanism behind their small masses. Furthermore, it is interesting to consider that neutrino mass and mixing patterns could be explained within a theoretical framework relating mass and mixing patterns for quarks and leptons in the SM. On the dark matter side, its existence, inferred through gravitational effects on visible matter, needs to be explained within particle physics theoretical framework, as the SM fails on providing a viable dark matter candidate. Additionally, these dark matter candidates have to satisfy current experimental constraints.

The idea of relating the mechanism behind the neutrino mass generation and the dark matter is, form the theoretical point of view, quite appealing and could lead to interesting developments in both sectors. Based on such idea, this thesis is intended to investigate three possible theoretical realisations of this connection based on minimal SM extensions using discrete symmetries. Thus, this thesis is organised as follows.

In chapter 1, we develop a brief introduction to the Standard Model, neutrino physics and dark matter, setting notation and convention used throughout the document. Following, the chapter 2 is devoted to the study of an A_4 symmetric SM extension, where neutrino mass generation and dark matter are related by the breaking of such non-Abelian discrete flavour symmetry into a residual symmetry, which stabilises the dark matter. Neutrino phenomenology follows from the flavour symmetry assignments and its specific breaking. Correlations between neutrino oscillation parameters and, then observables, are found. One of such correlations leads to a lower bound on the neutrinoless double beta decay ($0\nu\beta\beta$) amplitude, lying within the sensitivity range of near-future experiments.

In chapter 3, we study an extension of Ma's Scotogenic model, where neutrino mass generation is due to one-loop radiative correction involving dark matter particles in the loop. Previous works have shown that when the lightest right-handed (RH) neutrino is the dark matter and the right relic abundance is coming only from its annihilation, lepton flavour violating processes (LFV) severely constrain the parameter region for the model. We have shown that by adding a complex scalar singlet of the SM gauge, which generates dynamically RH neutrinos masses, an additional dark matter annihilation channel opens up relaxing the aforementioned tension.

In chapter 4, we study an A_4 flavour symmetric realisation of a type-II Dirac seesaw. This model partially addresses the flavour problem in the SM. First, the fermion mass patterns are explained by a flavour dependent mass relation between down-type quarks and charged leptons, proposed in previous works. Secondly, the model can fit the CKM matrix elements, then fixing the charged lepton contribution to lepton mixing matrix. Regarding neutrino phenomenology, this model is only consistent with an inverted ordering of neutrino masses and non-maximal atmospheric mixing angle. The model also predicts a non-zero CP violating phase when the lightest neutrino mass is less than 2 meV, while for bigger masses it is consistent with a vanishing value of the CP violating phase.
Finally, we draw our summary and final remarks in chapter 5.

This work is based on the following publications:

- *Seesaw scale discrete dark matter and two-zero texture Majorana neutrino mass matrices.* J. M. Lamprea, E. Peinado. Phys. Rev. D 94 (2016).
- *Flavour-symmetric type-II Dirac neutrino seesaw.* C. Bonilla, J.M. Lamprea, E. Peinado, J. W. F. Valle. Phys. Lett. B 779 (2018).
- *Fermionic dark matter from radiative neutrino mass.* C. Bonilla, L. M. Garcia de la Vega, J. M. Lamprea, R. Lineros, E. Peinado, *in prep.*

Table of contents

List of figures xi

List of tables xv

1 Introduction 1

2 A_4 flavour symmetric models for Majorana neutrinos and dark matter 31
- 2.1 Preliminaries . . . 31
- 2.2 The models . . . 33
- 2.3 Neutrino phenomenology . . . 36
- 2.4 Results and discussion . . . 40
- 2.5 Dark matter phenomenology . . . 44
- 2.6 Conclusions . . . 44

3 Radiative Majorana neutrino mass generation and fermionic dark matter 53
- 3.1 Preliminaries . . . 53
- 3.2 The model . . . 56
- 3.3 Constraints . . . 61
- 3.4 Results and discussion . . . 64
- 3.5 Conclusion . . . 66

4 A_4 flavour symmetric model for a type-II Dirac neutrino seesaw 73
- 4.1 Preliminaries . . . 73
- 4.2 The model . . . 75
  - 4.2.1 Lepton sector . . . 76
- 4.3 Results and discussion . . . 78
  - 4.3.1 The generalised bottom-tau mass relation . . . 78

4.3.2 CKM fitting 81
4.3.3 Lepton masses and mixing 83
4.4 Conclusions 86

5 Summary and final remarks **89**

Appendix A The A_4 group **93**
A.1 A_4 irreducible representations product 94

Appendix B Radiative one-loop mass calculation for Scotogenic model **97**

Appendix C Oblique parameters for a radiative Majorana neutrino mass generation **101**

References **103**

List of figures

1.1 *Feynman diagram of the type-I seesaw. The tree level completion of the dimension-5 Weinberg operator is done by the exchange of RH neutrinos* $N = \nu_R$. 14

1.2 *Feynman diagram for the type-II seesaw mechanism. The tree level completion of the dimension-5 Weinberg operator is done by the exchange of a* $SU(2)_L$ *triplet complex scalar* Δ. 15

1.3 *Feynman diagram for the type-III seesaw mechanism. The tree level completion of the dimension-5 Weinberg operator is done by the exchange of* $SU(2)_L$ *triplet RH fermions* Σ. 17

1.4 *One-loop radiative mass generation for LH Majorana neutrinos in the Zee model [61, 62].* 18

1.5 *Two-loops radiative mass generation for LH Majorana neutrinos in the Zee–Babu model [65, 64].* 19

1.6 *Feynman diagram for a type-I Dirac neutrino seesaw. The tree level completion of the generalised dimension-5 operator in Eq. (1.52), is done by the exchange of Dirac fermions* $N = N_L + N_R$. 21

1.7 *Feynman diagram for a type-II Dirac neutrino seesaw. The tree level completion of the generalised dimension-5 operator in Eq. (1.52) is done by the exchange of* ϕ *a complex scalar doublet of* $SU(2)_L$. 22

1.8 *Feynman diagram for a type-III Dirac neutrino seesaw. The tree level completion of the generalised dimension-5 operator in Eq. (1.52) is done by the exchange of vector-like fermions* E^0. 23

2.1 *Correlation between* $\sin^2\theta_{23}$ *and the sum of the light neutrino masses,* $\sum m_\nu$, *in model A (with the* B_3 *texture) at the top and model B (with the* B_4 *texture) at the bottom, where NO (IO) allowed region is in magenta (cyan). The horizontal red (blue) shaded region corresponds to the* 1σ *value in* $\sin^2\theta_{23}$ *for NO (IO) from [121]. The red (blue) horizontal dashed line represent the* θ_{23} *best fit value in NO (IO), while the doted horizontal red line represents the value of local minimum in NO from from [121]. The vertical grey shaded region is disfavoured by Planck data [124].* 46

2.2 *Correlation between* $\sin^2\theta_{23}$ *and the sum of the light neutrino masses,* $\sum m_\nu$, *in model A (with the* B_3 *texture) at the top and model B (with the* B_4 *texture) at the bottom, where NO (IO) allowed region is in magenta (cyan). The horizontal red (blue) shaded region corresponds to the* 1σ *value in* $\sin^2\theta_{23}$ *for NO (IO) from [122]. The red (blue) horizontal dashed line represents the best fit value in NO (IO) from [122]. The vertical grey shaded region is disfavoured by the Planck data [124].* 47

2.3 *Correlation between* $\sin^2\theta_{23}$ *and the sum of the light neutrino masses,* $\sum m_\nu$, *in model A (with the* B_3 *texture) at the top and model B (with the* B_4 *texture) at the bottom, where NO (IO) allowed region is in magenta (cyan). The horizontal red (blue) shaded region correspond to the* 1σ *in* $\sin^2\theta_{23}$ *for NO (IO) from [123]. The case for IO has two* 1σ *regions in the data used. The red (blue) horizontal dashed line represents the best fit value in NO (IO) from [123]. The vertical grey shaded region is disfavoured by Planck data [124].* 48

2.4 *Effective* $0\nu\beta\beta$ *parameter* $|m_{ee}|$ *versus the lightest neutrino mass* $m_{\nu_{light}}$ *in model A (B) at the top (bottom). The* $m_{\nu_{light}}$ *is* $m_1(m_3)$ *for NO (IO). The model allowed region for NO is in magenta (dark magenta) for the* 1σ *(*3σ*) atmospheric mixing angle and for IO in cyan (dark cyan) for the* 1σ *(*3σ*) atmospheric mixing angle region from [121]. The yellow (green) band correspond to the "flavour–generic" IO (NO) neutrino spectra at* 3σ*. The horizontal red shaded region is the experimental limit on* $0\nu\beta\beta$*, while the red (blue) horizontal (vertical) lines are the forthcoming experimental sensitivities on* $|m_{ee}|$ *(*$m_{\nu_{light}}$*) from [125–130]. The vertical blue shaded region is disfavoured by Planck data [124].* 49

2.5 *Effective $0\nu\beta\beta$ parameter $|m_{ee}|$ versus the lightest neutrino mass $m_{\nu_{light}}$ in model A (B) at the top (bottom). The $m_{\nu_{light}}$ is $m_1 (m_3)$ for NO (IO). The $m_{\nu_{light}}$ is $m_1 (m_3)$ for NO (IO). The model allowed region for NO is in magenta (dark magenta) for the 1σ (3σ) atmospheric mixing angle and for IO in cyan (dark cyan) for the 1σ (3σ) atmospheric mixing angle region from [122]. The yellow (green) band correspond to the "flavour–generic" IO (NO) neutrino spectra at 3σ. The horizontal red shaded region is the experimental limit on $0\nu\beta\beta$, while the red (blue) horizontal (vertical) lines are the forthcoming experimental sensitivities on $|m_{ee}|$ ($m_{\nu_{light}}$) from [125–130]. The vertical blue shaded region is disfavoured by Planck data [124].* 50

2.6 *Effective $0\nu\beta\beta$ parameter $|m_{ee}|$ versus the lightest neutrino mass $m_{\nu_{light}}$ in model A (B) at the top (bottom). The $m_{\nu_{light}}$ is $m_1 (m_3)$ for NO (IO). The model allowed region for NO is in magenta (dark magenta) for the 1σ (3σ) atmospheric mixing angle and for IO in cyan (dark cyan) for the 1σ (3σ) atmospheric mixing angle region from [123]. The yellow (green) band correspond to the "flavour–generic" IO (NO) neutrino spectra at 3σ. The horizontal red shaded region is the experimental limit on $0\nu\beta\beta$, while the red (blue) horizontal (vertical) lines are the forthcoming experimental sensitivities on $|m_{ee}|$ ($m_{\nu_{light}}$) from [125–130]. The vertical blue shaded region is disfavoured by Planck data [124].* 51

3.1 *One-loop neutrino mass generation in Ma's Scotogenic model [133].* 54

3.2 *Relevant annihilation channels for scalar DM η_0 in Ma's Scotogenic model.* 56

3.3 *Relevant annihilation channel for fermionic DM N_1 in Ma's Scotogenic model.* 57

3.4 *One-loop neutrino mass generation in the model.* 59

3.5 *New annihilation channels for fermionic DM, N_1, in the model. Up: t-channel. Down: s-channel resonance.* 61

3.6 *Up: Dark matter velocity averaged annihilation cross section to gammas $\langle\sigma v\rangle_\gamma$ as a function of the dark matter mass m_{N_1}. The Fermi-LAT [146] indirect detection exclusion curve is shown in blue. Bottom: Dark matter–nucleon spin independent scattering cross section σ_{SI} as a function of dark matter mass m_{N_1}. The PandaX–II [145] 54 ton-day exclusion curve is shown in blue.* 67

3.7 *Up: SM Higgs total width Γ_{h_1} as a function of dark matter mass m_{N_1}. Bottom: SM Higgs total width Γ_{h_1} as a function of the mixing parameter $\sin\theta$.* 68

3.8 *Correlation between the of SM Higgs branching ratio to invisible* $Br(h_1 \to inv)$ *and the effective coupling* $\sin\theta/v_\phi$. 69
3.9 *Up: lightest LH neutrino mass* m_{ν_1} *as a function of dark matter mass* m_{N_1}. *Bottom: gauge singlet scalar–dark matter Yukawa coupling* h_{N_1} *as a function of inert Higgs–neutrinos Yukawa couplings* Y_i^ν. 70
3.10 *Correlation between the dark matter spin-independent scattering cross section* σ_{SI} *as a function of the Higgs portal effective coupling* h_{N_1}. 71

4.1 *Neutrino mass generation in the type-II seesaw for Dirac neutrinos, as in [69, 153, 154].* 75
4.2 *The regions in the atmospheric mixing angle* θ_{23} *and the lightest neutrino mass* m_3 *allowed by oscillation data in shaded (green) areas. The horizontal dashed line represents the best-fit value for* $\sin^2\theta_{23}$, *whereas the horizontal shaded region corresponds to the* 1σ *allowed region from Ref. [33].* 86
4.3 *Correlation between the CP violation and the lightest neutrino mass. Up: correlation between the Jarlskog invariant* J *and the lightest neutrino mass* m_3 *allowed by the current oscillation data [33]. Bottom: Allowed regions for the correlation between the Dirac CP phase* δ_{CP} *and the lightest neutrino mass* m_3. 87
4.4 *The allowed regions of the atmospheric mixing angle and* δ_{CP} *are indicated in green shaded. The unshaded contour regions represent the 90 and 99%CL regions obtained directly in the unconstrained three neutrino oscillation global fit [33].* 88

B.1 *Feynman diagram for the Scotogenic neutrino mass generation in mass eigenstates.* 97

List of tables

1.1 *Fundamental fermions in the Standard Model arranged by generations.* . . . 2
1.2 *Fundamental fermions in the Standard Model, where* $a = 1, 2, 3$ *is the generation index. Particle electric charges are given by the Gell-Mann – Nishijima formula* $Q = I_3 + Y$ *[15–17], where the third component of weak* $SU(2)_L$ *is* $I_3 = \pm 1/2$ *for doublets and* $I_3 = 0$ *in the case of singlets.* 3
1.3 *Fundamental scalars in the Standard Model. Particle electric charges are given by the Gell-Mann–Nishijima formula* $Q = I_3 + Y$ *[15–17], where the third component of weak* $SU(2)_L$ *is* $I_3 = \pm 1/2$ *for the doublet.* 3
1.4 *Summary of relevant particle content and quantum numbers in the Zee model [61, 62].* 18

2.1 *Summary of the relevant particle content and quantum numbers for model A.* 36
2.2 *Summary of the relevant particle content and quantum numbers for model B.* 38

3.1 *Relevant particle content and quantum numbers in Scotogenic model* 53
3.2 *Summary of the relevant particle content and quantum numbers in the model.* 57

4.1 *Charge assignments for the particles involved in the type-II Dirac neutrino seesaw realisation, as in [69].* 76
4.2 *Charge assignments for the particles involved in the neutrino mass generation mechanism, where* $\omega^3 = 1$ 76
4.3 *Particle content and quantum numbers for the complete model.* 79
4.4 *Experimental and predicted quark masses and mixing parameters from the CKM fit.* 83

Chapter 1

Introduction

This chapter is intended as an introduction to the thesis and to survey the notation and convention we will use throughout the document. Here we will briefly review the Standard Model of Particle Physics, neutrino physics and dark matter as the necessary background to our work.

The Standard Model in a nutshell

In this section, we will give a short review of the Standard Model properties. A more detailed discussion can be found in several textbooks, for instance in [1, 2]. The description of the fundamental interactions, excluding gravitation, is given quite accurately by the SM. This is a renormalisable gauge theory [3] based upon the symmetry group

$$G_{\rm SM} = SU(3)_C \otimes SU(2)_L \otimes U(1)_Y,$$

where C, L and Y stands for colour, left-handed (LH) chirality and hypercharge, and the corresponding coupling constants are g_s, g and g' respectively. Each part in this direct product of symmetry groups is responsible for an interaction. The $SU(3)_C$ group describes the strong interaction in what is known as Quantum Chromodynamics (QCD) [4–8], while the product $SU(2)_L \otimes U(1)_Y$ is responsible for an unified description of the Electroweak interaction [9–11].

The gauge symmetry group choice in the SM fixes the gauge bosons content as well as their irreducible representations (*irreps.*) to be the adjoint *irreps.*, although it does not fix the content of fermion and scalar fields. There are four Electroweak gauge bosons: three

weak gauge boson $W^{1,2,3\ \mu}$ in a $SU(2)_L$ triplet and a B^μ associated with $U(1)_Y$. There are also eight QCD gauge bosons (or gluons) labelled as $G^{1,\cdots,8\ \mu}$ forming up a $SU(3)_C$ octet. These gauge bosons account for the 12 generators of G_{SM}.

Additionally, as the bare mass terms for gauge bosons and chiral fermions are forbidden by the gauge invariance, the SM incorporates the Electroweak spontaneous symmetry breaking mechanism (EWSB) [12–14], or Brout–Englert–Higgs (BEH) mechanism, responsible for giving mass to the Electroweak gauge bosons W and Z and the whole fermions. This mechanism leads to the breaking of $SU(2)_L \otimes U(1)_Y \to U(1)_Q$, with Q the electric charge. Such spontaneous symmetry breaking is triggered by the field H, a complex scalar doublet of $SU(2)_L$ with hypercharge $Y = 1/2$, which is referred as the Higgs doublet.

The SM includes three generations of quarks and leptons. These are shown in Tab. 1.1. Each fermion generation contains 15 two-component spinors[1]: two charged leptons and 12 quarks, all of them in both chiral components left- (LH) and right-handed (RH) forming up seven Dirac fermions[2], plus one left-handed neutrino. Particle content and gauge symmetry

Family	1st	2nd	3rd
Quarks	u	c	t
	d	s	b
Leptons	ν_e	ν_μ	ν_τ
	e	μ	τ

Table 1.1 *Fundamental fermions in the Standard Model arranged by generations.*

assignments of the fermions and scalar in the SM are displayed in Tabs. 1.2 and 1.3 respectively. The LH fermions transform as $SU(2)_L$ doublets, while RH fermions are $SU(2)_L$ singlets, as a consequence that weak interactions violate parity maximally.

The Standard Model Lagrangian can be written as:

$$\mathcal{L} = \mathcal{L}_{\text{Gauge}} + \mathcal{L}_{\text{Dirac}} + \mathcal{L}_{\text{Yuk}} + \mathcal{L}_{\text{Higgs}}, \tag{1.1}$$

[1]The homogeneous Lorentz group *irreps.* for spin 1/2 particles are labelled as $(1/2, 0)$ and $(0, 1/2)$, which are known as left-handed (LH) χ_L and right-handed (RH) χ_R Weyl or Majorana fields or two-component spinors.

[2]Dirac fermions or four-component spinors are made of both homogeneous Lorentz group *irreps.* $\psi = (\chi_L\ \chi_R)^T$. Left and right projectors $P_L = \frac{1-\gamma_5}{2}$ and $P_R = \frac{1+\gamma_5}{2}$ are defined through the relations $P_L\psi := (\chi_L\ 0)^T$ and $P_R\psi := (0\ \chi_R)^T$.

Fields	$SU(3)_C$	$SU(2)_L$	$U(1)_Y$
$L_a = \begin{pmatrix} \nu_{aL} & \ell_{aL} \end{pmatrix}^T$	**1**	**2**	$-1/2$
ℓ_{aR}	**1**	**1**	-1
$Q_a = \begin{pmatrix} u_{aL} & d_{aL} \end{pmatrix}^T$	**3**	**2**	$1/6$
u_{aR}	**3**	**1**	$2/3$
d_{aR}	**3**	**1**	$-1/3$

Table 1.2 *Fundamental fermions in the Standard Model, where $a = 1, 2, 3$ is the generation index. Particle electric charges are given by the Gell-Mann – Nishijima formula $Q = I_3 + Y$ [15–17], where the third component of weak $SU(2)_L$ is $I_3 = \pm 1/2$ for doublets and $I_3 = 0$ in the case of singlets.*

Fields	$SU(3)_C$	$SU(2)_L$	$U(1)_Y$
$H = \begin{pmatrix} H^+ & H^0 \end{pmatrix}^T$	**1**	**2**	$1/2$

Table 1.3 *Fundamental scalars in the Standard Model. Particle electric charges are given by the Gell-Mann–Nishijima formula $Q = I_3 + Y$ [15–17], where the third component of weak $SU(2)_L$ is $I_3 = \pm 1/2$ for the doublet.*

where each term represents a contribution conceptually different. In order, these are the kinetic energy of the gauge bosons (Yang–Mills theory), kinetic energy of the fermion content, Yukawa interactions between fermions and scalars and finally Higgs interactions. Ghost and gauge fixing terms could be excluded working in the unitary gauge.

The gauge part in Eq. (1.1) describes the behaviour of the gauge bosons. This term is written as:

$$\mathcal{L}_{\text{Gauge}} = -\frac{1}{2}\text{Tr}(G^{\mu\nu}G_{\mu\nu}) - \frac{1}{2}\text{Tr}(W^{\mu\nu}W_{\mu\nu}) - \frac{1}{4}B^{\mu\nu}B_{\mu\nu}, \tag{1.2}$$

with $G^{\mu\nu}$, $W^{\mu\nu}$ and $B^{\mu\nu}$ the field strength tensors[3] of $SU(3)_C$, $SU(2)_L$ and $U(1)_Y$ respectively.

The Dirac Lagrangian in Eq. (1.1) contains the kinematic and gauge interactions of the whole fermions in the SM. Such Lagrangian is given by:

$$\mathcal{L}_{\text{Dirac}} = \bar{\psi}^a(i\gamma^\mu D_\mu)\psi_a, \tag{1.3}$$

[3]The field strength tensor for a non-Abelian gauge theory is defined as $F^i_{\mu\nu} := \partial_\mu A^i_\nu - \partial_\nu A^i_\mu - g\, c_{ijk}\, A^j_\mu A^k_\nu$, with A^i_μ the gauge boson fields, g the coupling constant and c_{ijk} the group structure constants.

where the index a refers to all the fermion fields and D_μ is the covariant derivative defined as:

$$D_\mu =: \partial_\mu - ig_s G^a_\mu \lambda_a - igW^a_\mu \tau_a - iY g' B_\mu, \tag{1.4}$$

with λ_a and τ_a the $SU(3)$ and $SU(2)$ generators in the same representation that ψ, and Y the hypercharge of ψ.

The Higgs interactions term in Eq. (1.1) is given by the Lagrangian

$$\mathcal{L}_{\text{Higgs}} = D_\mu H^\dagger D^\mu H - \mu^2 (H^\dagger H) - \lambda (H^\dagger H)^2, \tag{1.5}$$

where the Higgs doublet, H, can be written as[4]:

$$H = \begin{pmatrix} H^+ \\ \frac{1}{\sqrt{2}}(v + h + i\ A) \end{pmatrix}. \tag{1.6}$$

When $\mu^2 < 0$, the Higgs potential in Eq. (1.5) has a non-zero minimum value, then the Higgs vacuum expectation value (*vev.*) is non-zero. Thus, when H develops a *vev.*, denoted as $\langle H \rangle = v/\sqrt{2}$, it triggers the spontaneous EWSB.
The tree level Higgs boson h mass is given in terms of the parameters in Eq. (1.5) as

$$m_h^2 = -\mu^2 \lambda = 2\lambda v^2. \tag{1.7}$$

This mass has been experimentally determinated approximately as $m_h \approx 125$ GeV [18, 19].

After EWSB, the fields $H^\pm$ and A will be the pseudo Nambu-Goldstone bosons [20–22] corresponding to the broken generators of $SU(2)_L \otimes U(1)_Y$. Such fields will become the longitudinal degrees of freedom of the gauge fields $W^{i\ \mu}$ and B^μ (W and Z in mass basis), thus generating masses for them. At tree level, the W and Z gauge boson masses yield

$$m_W = \frac{g}{2} v \sim 78 \text{ GeV} \qquad \text{and} \qquad m_Z = \frac{\sqrt{g^2 + g'^2}}{2} v = \frac{m_W}{\cos\theta_W} \sim 89 \text{ GeV}, \tag{1.8}$$

with g and g' the coupling constants associated with $SU(2)_L$ and $U(1)_Y$, $v \simeq 246$ GeV, the weak scale, and $\sin^2\theta_W = \frac{g'^2}{g^2+g'^2} \simeq 0.23$ the sine of the weak mixing angle. This mixing angle parametrises the mixing between the neutral gauge bosons in the interaction basis

[4] The Higgs doublet in the unitary gauge is $H = \frac{1}{\sqrt{2}} (0\ v + h)^T$.

$W^{3\mu}$ and B^{μ} in terms of the physical eigenstates Z^{μ} and A^{μ}, the latter being the photon field which remains massless.

Finally, Yukawa Lagrangian in Eq. (1.1) is responsible for giving mass to the fermions through EWSB. This Lagrangian is given by:

$$\mathcal{L}_{\rm Yuk} = \Gamma^{e}_{ij}\,\bar{L}_i\,H\,\ell_{Rj} + \Gamma^{u}_{ij}\,\bar{Q}_i\,\tilde{H}\,u_{Rj} + \Gamma^{d}_{ij}\,\bar{Q}_i\,H\,d_{Rj} + h.c., \tag{1.9}$$

where i, j are generation indices, Γ^{a} are 3×3 general complex Yukawa coupling matrices and $\tilde{H} = i\sigma^2 H^*$, with σ^2 the Pauli matrix, is the Higgs doublet charge conjugate which has $Y = -1/2$. Notice that fields in Eq. (1.9) are written in the flavour (interaction) basis not as mass eigenstates.

After EWSB, from Eq. (1.9) fermion mass matrices are give by

$$M^{a}_{ij} = \Gamma^{a}_{ij}\,\frac{v}{\sqrt{2}},$$

where $a = \{e, u, d\}$. As Γ^{a} are general complex matrices, they can be diagonalised by two unitary matrices U and V as:

$$V^{a\,\dagger}\;M^{a}\;U^{a} = M^{a}_{D} := \mathrm{diag}\,(m_1, m_2, m_3)\,, \tag{1.10}$$

with m_i the running masses.

Since neutrinos in the Standard Model are massless, one has the freedom to redefine charged lepton fields making them diagonal. However, such field redefinitions cannot be done for quarks as u- and d-type quarks couple both to the Higgs, then quark mass matrix will be non-diagonal in flavour space. Thus, we can redefine quarks in flavour space in term of the unitary matrices that diagonalise the quark mass matrix, Eq. (1.10), as $u_L = V^{u} u'_L$, $d_L = V^{d} d'_L$ and $u_R = U^{u} u'_R$, $d_R = U^{d} U'_L$, where the prime refers to mass eigenstates. Therefore, the quark weak charged current:

$$\mathcal{L}_{\rm CC} = -\frac{g}{2\sqrt{2}}\sum_{i=1}^{3}\left(\bar{u}_{iL}\gamma_{\alpha}d_{iL}\right)W^{+\alpha} + \;\; h.c., \tag{1.11}$$

will be diagonal in flavour space. We can define the quark mixing matrix or the Cabibbo–Kobayashi–Maskawa (CKM) matrix [23] from the mismatch between flavour and mass eigenstates as:

$$V_{CKM} = V^{u\,\dagger}V^{d}. \tag{1.12}$$

The CKM matrix is parametrised (PDG parametrisation [24]) by three mixing angles θ_{12}, θ_{23} and θ_{13} and one complex phase δ which allows charge-parity (CP) violation in quark sector. Thus,

$$V_{CKM} = \begin{pmatrix} 1 & 0 & 0 \\ 0 & c_{23} & -s_{23} \\ 0 & s_{23} & c_{23} \end{pmatrix} \begin{pmatrix} c_{13} & 0 & -e^{-i\delta}s_{13} \\ 0 & 1 & 0 \\ e^{i\delta}s_{13} & 0 & c_{13} \end{pmatrix} \begin{pmatrix} c_{12} & -s_{12} & 0 \\ s_{12} & c_{12} & 0 \\ 0 & 0 & 1 \end{pmatrix}, \tag{1.13}$$

where $s_{ij} = \sin\theta_{ij}$ and $c_{ij} = \cos\theta_{ij}$.

The CP violating δ phase in V_{CKM}, Eq. (1.13), depends on the chosen parametrisation. An independent way to have a CP violation quantification is through the Jarlskog invariant $J_{\rm CP}$ [25]:

$$J_{\rm CP} = -{\rm Im}[V_{us}V_{cd}V_{cs}^{*}V_{ud}^{*}] = \cos\theta_{12}\,\cos\theta_{23}\,\cos^{2}\theta_{13}\,\sin\theta_{12}\,\sin\theta_{23}\,\sin\theta_{13}\,\sin\delta. \tag{1.14}$$

Finally, it is worth to notice that in its minimal extension the Standard Model has 19 free parameters: nine fermions (quark and charged lepton) masses, four parameters in CKM matrix, three gauge couplings, the Higgs mass, the weak scale and $\theta_{\rm QCD}$ (related with the strong CP problem).

Open questions in the Standard Model

The SM has shown to be a successful theory in the last decades, even the latest LHC results have confirmed its astounding accuracy describing fundamental interactions. However, we know this is not a complete theory. There are some open theoretical issues and phenomena that the SM cannot account for, as the existence of dark matter and neutrino masses.

First, the SM gives no prediction or explanation on the number of generations of fermions, the mass hierarchy between generations and the mixing patterns of quarks and leptons. In addition, it does not explain either electric charge quantisation or CP conservation in the strong interaction (strong CP problem). Moreover, it is necessary a fine-tuning in the radiative corrections to the Higgs mass to account for the observed one.

There are in addition some phenomena that the SM fails explaining. The most relevant include the smallness of the neutrino masses, the existence of dark matter (DM), the origin of the asymmetry between matter and antimatter in the Universe, also called Baryonic

Asymmetry of the Universe (BAU), and finally the accelerated expansion of the Universe or Dark Energy.

The quest for an unified description of the forces in Nature leads to consider the Standard Model as an effective theory valid at most to the Planck scale $M_{\text{Planck}} = G_N^{-1/2} \sim 10^{19}$ GeV, when the quantum theory of gravity has to be taken into account. One hopes that such new physics beyond Standard Model (BSM) be at a sufficiently low scale, near to energy scale achievable by next-generation experiments, as the latest LHC runs have not spotted any new physics.

Neutrino Physics

Nowadays it is known that neutrinos have masses, as it has been inferred from neutrino oscillation experiments. Solar, atmospheric, reactor and accelerator neutrino experiments [26–30] have provided convincing evidence for the oscillation of three flavours of active (LH) neutrinos: ν_{eL}, $\nu_{\mu L}$ and $\nu_{\tau L}$.

Experimental data analysis has shown that such flavour neutrino oscillations are consistent with the mixing of three mass eigenstates ν_i with masses m_i, $i = \{1, 2, 3\}$. Such mixing is given by

$$\nu_{aL} = \sum_{i=1}^{3} V_{ai}^{\dagger}\, \nu_i, \tag{1.15}$$

with $a = \{e, \mu, \tau\}$ the flavour index and V_{ai} a 3×3 unitary mixing matrix. This mixing matrix, as for quarks, comes from the left-diagonalising matrices for the charged leptons V^{ℓ} and neutrinos V^{ν} making the weak neutral current flavour diagonal.

We can redefine the LH flavour fields as $\nu_L = V^{\nu}\nu'_L$ and $\ell_L = V^{\ell}\ell'_L$, where prime refers to mass eigenstates. Thus, from the weak charged current

$$\mathcal{L}_{\text{CC}} = -\frac{g}{2\sqrt{2}} \sum_{a=1}^{3} (\bar{\nu}_{aL}\gamma_{\alpha}\ell_{aL})W^{+\alpha} + h.c., \tag{1.16}$$

we define the lepton mixing matrix [31] as

$$V = V^{\nu\dagger}V^{\ell}. \tag{1.17}$$

In the canonical case, three flavours and three mass eigenstates, the lepton mixing matrix for Dirac neutrinos can be parametrised by three mixing angles θ_{12}, θ_{23} and θ_{13}, and

one CP violating phase δ as

$$V = \begin{pmatrix} c_{12}c_{13} & s_{12}c_{13} & s_{13}e^{-i\delta} \\ -s_{12}c_{23} - c_{12}s_{23}s_{13}e^{i\delta} & c_{12}c_{23} - s_{12}s_{23}s_{13}e^{i\delta} & s_{23}c_{13} \\ s_{12}s_{23} - c_{12}c_{23}s_{13}e^{i\delta} & -c_{12}s_{23} - s_{12}c_{23}s_{13}e^{i\delta} & c_{23}c_{13} \end{pmatrix}, \tag{1.18}$$

with $c_{ij} = \cos\theta_{ij}$, $s_{ij} = \sin\theta_{ij}$ and $0 \leq \theta_{ij} \leq \pi/2$. As for quarks, the magnitude of CP violation is determined by the rephasing Jarlskog $J_{\rm CP}$ invariant [25]:

$$J_{\rm CP} = -{\rm Im}[V_{\mu 3}V_{e3}^{*}V_{e2}V_{\mu 2}^{*}] = \frac{1}{8}\cos\theta_{13}\,\sin 2\theta_{12}\,\sin 2\theta_{23}\,\sin 2\theta_{13}\,\sin\delta. \tag{1.19}$$

Neutrino oscillation experiments are only sensitive to mass square differences $\Delta m_{ij}^2 = m_i^2 - m_j^2$. From three mass eigenstates, only two independent mass squared differences could be defined. By convention these are: Δm_{21}^2 and Δm_{3i}^2, with $i = 1, 2$ depending on the mass ordering. In summary, neutrino oscillation experiments are sensitive to six parameters. These are, three mixing angles: solar $\theta_{12}(\sim 34.5^{\circ})$, atmospheric $\theta_{23}(\sim 48^{\circ})$ and reactor $\theta_{13}(\sim 8.49)$, the CP phase $\delta(\sim 3\pi/2)$ and two mass squared differences $\Delta m_{21}^2(\sim 7.5 \times 10^{-5}$ eV$^2)$ and $|\Delta m_{3i}^2| \sim (2.5 \times 10^{-3}$ eV$^2)$. However, we do not know what is the sign for the latter mass squared difference. This enables two possible arrangements for the neutrino masses:

$$\begin{aligned} &\text{Normal ordering (NO):} && m_1 < m_2 < m_3, \\ &\text{Inverted ordering (IO):} && m_3 < m_1 < m_2, \end{aligned}$$

for which $\Delta m_{31}^2 > 0$ in NO and $\Delta m_{32}^2 < 0$ for IO.

It is worth to mention that values for δ are not directly measured but inferred from neutrino oscillation experiment global fits. In addition, as θ_{23} is quite close to the maximal mixing value $\sin^2\theta_{23} \sim 1/2$, precise determination of such mixing angle and the sign of the corresponding mass squared difference, Δm_{3i}^2 is challenging. Currently, both θ_{23} and δ are the less precise measured neutrino oscillation parameters. This situation is expected to improve in forthcoming years when new experiments, as NOvA or Hyper-Kamiokande, start reporting results. Finally, it is worth to stress that latest global fits on neutrino oscillation parameters [32, 33] have a preference for a normal ordering of the neutrino masses at $3\,\sigma$ confidence level.

The neutrino mass scale can be determined from another type of experiments rather than oscillation experiments. Currently, the strongest limit is obtained from the measurement of the energy spectrum of electrons near to the end point in ^{3}H β-decay experiments. Such limit sets [34, 35]

$$m_{\nu_e} < 2.05 \text{ eV}, \qquad \text{at } 95\% \text{ CL}. \tag{1.20}$$

However, it is expected that near future experiments improve this bound. The KATRIN experiment plans to achieve a sensitivity of $m_{\nu_e} \sim 0.20$ eV [36]. Also from Cosmology, Planck collaboration has reported an upper bound on the sum of masses of active neutrinos. This limit comes from the global fit that combines data from the cosmic microwave background (CMB) temperature power spectrum anisotropies, polarisation, gravitational lensing effects, low ℓ CMB polarisation spectrum, supernovae and Baryonic Acoustic Oscillations (BAO) and assuming three actives neutrinos and ΛCDM as fiducial model. This bound relies highly on the assumptions made, but gives important information on neutrinos masses [37]:

$$\sum_j m_j < 0.23 \text{ eV}, \qquad \text{at } 95\% \text{ CL}. \tag{1.21}$$

Given the neutrality properties of neutrinos, these could be Majorana fermions. Determining their nature, whether they are Majorana or Dirac fermions, remains as an open question in neutrino physics. If LH neutrinos are Majorana fermions $\nu_R = \nu_L^c$, then two phases of the lepton mixing matrix, Eq. (1.17), cannot be re-absorbed by the LH fields. Thus, lepton mixing matrix for Majorana neutrinos has the form [38]

$$V = V^D D, \tag{1.22}$$

where V^D is the lepton mixing matrix for Dirac neutrinos, Eq. (1.18), and

$$D = \text{diag}(1, e^{i\alpha_{21}/2}, e^{i\alpha_{31}/2}), \tag{1.23}$$

is a matrix of Majorana phases α_{ij}.

Regarding nature of neutrinos, there are some processes which can happen only for Majorana neutrinos, as lepton number L is violated by two units for Majorana neutrinos while for Dirac neutrinos it is conserved. The neutrinoless double beta decay ($0\nu\beta\beta$), where a nucleus undergoes: $(A, Z) \to (A, Z+2) + 2e^-$, is one of such processes where $\Delta L = 2$ [39]. The amplitude for $0\nu\beta\beta$ in the case of the exchange of three active neutrinos, generated only

through a (V–A) charged current, long-range contribution, is proportional to the effective Majorana mass (see e.g. Refs. [40–42]):

$$\begin{aligned} |m_{ee}| &= |m_1 V_{e1}^2 + m_2 V_{e2}^2 + m_3 V_{e3}^2| \\ &= |(m_1 c_{12}^2 + m_2 s_{12}^2 e^{i\alpha_{21}}) c_{13}^2 + m_3 s_{13}^2 e^{i(\alpha_{31}-\delta)}|. \end{aligned} \tag{1.24}$$

Finally, the black box theorem [43, 44] states that observation of such process would suffice to prove the Majorana nature of neutrinos.

Neutrino masses

As mentioned before, neutrinos can be either Majorana or Dirac fermions due to their neutrality properties. Each case leads to different mass terms for them. In the case of Dirac neutrino lepton number, $L = L_e + L_\mu + L_\tau$, is an accidental global symmetry, as their mass term does not break L, while Majorana neutrino mass term breaks L by two units. With this on mind, we will examine the mass terms for Dirac and Majorana neutrinos and the ways to generate such masses.

Dirac neutrino masses

Even though neutrinos are massless in the SM, there is nothing forbidding them of having Dirac masses. A Dirac mass term can be incorporated to the SM in the same way as for quarks and charged leptons. For this, it suffices to add three RH neutrino chiral components ν_R^i, $i = 1, 2, 3$, which are $\mathrm{SU(3)_C} \otimes \mathrm{SU(2)_L} \otimes \mathrm{U(1)_Y}$ singlet, and use the BEH mechanism. Thereby, Dirac neutrino fields will be $\nu_D^i = \nu_L^i + N^i$, having four independent degrees of freedom: ν_L, ν_R, ν_L^c and ν_R^c. Thus, a Dirac mass term is given by:

$$-\mathcal{L}_D = m_D(\bar{\nu}_L \nu_R + \bar{\nu}_R \nu_L), \tag{1.25}$$

where the index i has been omitted. Note that if we assign $L = 1$ to $\nu_{L,R}$, thus $L = -1$ to $\bar{\nu}_{L,R}$, the mass term in Eq. (1.25) does not violate global lepton number symmetry.

The Dirac mass term, Eq. (1.25), could be generated through the BEH mechanism by the Yukawa interaction Lagrangian

$$\mathcal{L}_Y = \Gamma^\nu \, \bar{L} \, \tilde{H} \, \nu_R + h.c., \tag{1.26}$$

where Γ^ν is a general 3×3 complex matrix and y_ν^i its eigenvalues. Then, Dirac neutrino masses will be $M_D^i = v\, y_\nu^i$.

Finally, we notice that rather small neutrino masses require quite small Yukawa couplings compared with Yukawa couplings for the remaining same generation fermions (charged lepton and quarks), whose Yukawa couplings are approximately of the same order. For instance, electron neutrino Yukawa coupling is at most of the order $\mathcal{O}(y_{\nu_e}) \lesssim 10^{-11}$, for $m_{\nu_e} < 1$ eV. Such Yukawa coupling is at its greater value five orders of magnitude smaller than the electron Yukawa coupling $\mathcal{O}(y_e) \sim 10^{-6}$; up and down quark Yukawa couplings are of the order $\mathcal{O}(y_{u,d}) \sim 10^{-5}$, just an order of magnitude larger than the electron Yukawa, but at least seven orders of magnitude larger than the neutrino Yukawa. Such disparity between Yukawa couplings in the same generation is referred to *the unnatural value of the neutrino masses*.

Majorana neutrino masses

In the case of Majorana neutrinos, RH components are not independent form the LH ones. The Majorana condition relates them as: $\nu^i = \nu^{c\,i}$, where the c stands for the charge conjugation operator[5]. The LH Majorana fields ν_M^i have only two independent degrees of freedom ν_L^i and $\nu_R^{c\,i}$, and therefore $\nu_M^i = \nu_L^i + \nu_R^{c\,i}$. Then, Majorana mass term for LH Majorana neutrinos is given by

$$-\mathcal{L}_M = M_M(\bar{\nu}_L \nu_R^c + \bar{\nu}_R^c \nu_L), \tag{1.27}$$

where we have omitted the index i.

The bilinear term $\bar{\nu}_L \nu_R^c$ in the mass Lagrangian, Eq. (1.27), has weak isospin third component $I_3 = 1$. Therefore, it cannot be coupled to a $SU(2)_L$ doublet as the Higgs doublet, H, and cannot be generated by EWSB as the Dirac neutrino mass term. However, this mass term could be generated within the SM via non-renormalisable operators violating L by two units and whose high energy completion need additional heavy fields to the SM ones, which we will discuss in more detail later.

[5]The charge conjugation is defined as:

$$\mathcal{C} : \psi^c := C(\bar{\psi}\gamma_0)^T = C\bar{\psi}^T.$$

Analogously, the Majorana mass term for RH (or sterile) neutrinos $\nu_s = \nu_R + \nu_L^c$ is

$$-\mathcal{L}_S = \frac{M_s}{2}(\bar{\nu}_L^c \nu_R + \bar{\nu}_R \nu_L^c). \tag{1.28}$$

This mass term, Eq. (1.28), is a $\mathrm{SU(3)_C} \otimes \mathrm{SU(2)_L} \otimes \mathrm{U(1)_Y}$ singlet and therefore it should be added to the SM when RH neutrinos are incorporated unless there is some new symmetry forbidding it. The mass term for sterile neutrinos can be generated by the *vev.* of a scalar field singlet under $\mathrm{SU(3)_C} \otimes \mathrm{SU(2)_L} \otimes \mathrm{U(1)_Y}$.

Finally, LH as well as RH Majorana mass terms, Eqs. (1.27) and (1.28), violate L by two units. As in the SM L is an accidental symmetry, processes with lepton number violation by two units can occur for Majorana neutrinos. The discovery of one of these processes, the neutrinoless double beta decay, will imply the Majorana nature of neutrinos as has been stated by in the black-box theorem [43].

General neutrino mass term

In the case where LH and RH neutrinos are present, neutrinos can have Majorana as well as Dirac mass terms at the same time. Then, the general mass term takes the form:

$$-\mathcal{L} = \frac{1}{2}\begin{pmatrix}\bar{\nu}_L & \bar{\nu}_L^c\end{pmatrix}\begin{pmatrix}M_M & M_D \\ M_D^T & M_s\end{pmatrix}\begin{pmatrix}\nu_R^c \\ \nu_R\end{pmatrix} + \ h.c., \tag{1.29}$$

where the mass matrix defined in this Lagrangian is a complex symmetric matrix.

Neutrino mass models

Now, we will review the ways to naturally generate small masses for Dirac and LH Majorana neutrinos. In general, one has the freedom to add extra fermions and scalars to the SM, as the particle content is not fixed by the gauge symmetry. We will focus on generating light neutrino masses through (non-renormalisable) high dimension effective operators. This can be done writing down the lowest dimension effective operator generating neutrino masses using only SM fields and then looking for its possible high energy realisations.

Majorana mass models

Using only SM fields, the lowest dimensional operator with lepton number violation is the dimension-5 Weinberg operator [45]. Such effective operator can be written as

$$\mathcal{O}^{(5)} = \frac{g}{\Lambda}(\bar{L}^c \otimes H \otimes H \otimes L). \tag{1.30}$$

The fact that dimension-5 Weinberg operator violates lepton number by two units has been exploited in the generation of mass for Majorana neutrinos. The suppression for LH Majorana neutrino masses can be explained by the combination of a large lepton number breaking scale Λ and a small coupling g. Higher order operators would lead to further neutrino mass suppression. For instance, taking a coupling $g \simeq \mathcal{O}(1)$ and a scale $\Lambda \simeq 10^{13-15}$ GeV one can generate LH neutrino masses in the range of 1 eV with the dimension-5 Weinberg operator.

Canonical seesaw mechanisms

The canonical or high energy seesaw mechanisms are specific high energy realisations at tree level of the dimension-5 Weinberg operator, Eq. (1.30). The idea is that lightness of LH neutrinos is due to new physics effects at low energy (as the EW scale) of the exchange of heavy mediators associated with breaking of lepton number. Depending on whether the mediator is scalar or fermionic and its $SU(2)_L \otimes U(1)_Y$ *irreps.*, there are three canonical ways to complete at three level the dimension-5 Weinberg operator. These are called type-I [46–52], -II [53, 50, 54, 52, 55] and -III [56–58] seesaw mechanisms. Finally, there also exists the possibility of tree level completion of the dimension-5 Weinberg operator with a lower scale than the canonical seesaw mechanisms. This can be done by a further suppression to the neutrino masses trough additional small couplings in violating lepton number terms. The inverse and linear seesaw are some examples [59, 60].

Type-I seesaw

The type-I seesaw is the high energy completion of the dimension-5 Weinberg operator realised by the addition of n_s RH neutrinos $\nu_{Ri} = N_i$, $i = \{1, \ldots, n_s\}$. The Feynman diagram for the type-I seesaw is shown in Fig. 1.1. The relevant terms in the Lagrangian are:

$$\mathcal{L} = Y_N^{ij}\ \bar{L}_i \tilde{H} N_j + M_R\, \bar{N}^c N + h.c., \tag{1.31}$$

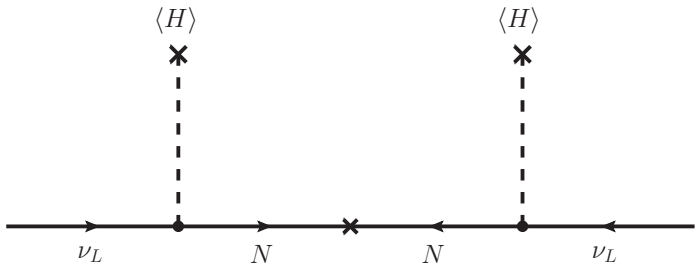

Fig. 1.1 *Feynman diagram of the type-I seesaw. The tree level completion of the dimension-5 Weinberg operator is done by the exchange of RH neutrinos* $N = \nu_R$.

where Y_N is a $3 \times n_s$ general complex Yukawa coupling matrix and M_R is the RH neutrino Majorana mass matrix, which is a $n_s \times n_s$ complex and symmetric matrix. The addition of the n_s RH neutrinos induce a Dirac mass matrix $M_D = v\, Y_N$. The M_D is a $3 \times n_s$ complex matrix. Therefore, in this scenario general neutrino mass matrix M_{D+M} will be similar to the general case, Eq. (1.29), with a vanishing LH Majorana mass matrix $M_M = 0$. Then,

$$M_{D+M} = \begin{pmatrix} 0 & M_D \\ M_D^T & M_R \end{pmatrix}. \tag{1.32}$$

The mass matrix in Eq. (1.32) can be diagonalised by an unitary matrix, as it is a complex symmetric $(3 + N_s)$ square matrix. Let W be a unitary matrix, then

$$M = W^\dagger M_{D+M} W, \tag{1.33}$$

where M is a block diagonal matrix.

One expects that the mass scale $\Lambda \sim M_R$ to be much greater than M_D. Therefore, the mass matrix in Eq. (1.32) can be approximately block diagonalised as

$$W^\dagger M_{D+M} W \approx \begin{pmatrix} M_{\text{light}} & 0 \\ 0 & M_{\text{heavy}} \end{pmatrix}, \tag{1.34}$$

with

$$W = \begin{pmatrix} 1 - \frac{1}{2} M_D^\dagger (M_R M_R^\dagger)^{-1} M_D & [(M_R)^{-1} M_D]^\dagger \\ -(M_R)^{-1} M_D & 1 - \frac{1}{2} (M_R)^{-1} M_D M_D^\dagger (M_R^\dagger)^{-1} \end{pmatrix}, \tag{1.35}$$

and the mass sub-matrices M_{light} and M_{heavy} are given by

$$M_\nu^{\text{T-I}} = M_{\text{light}} \approx -M_D^T (M_R)^{-1} M_D \quad \text{and} \quad M_{\text{heavy}} \approx M_R, \tag{1.36}$$

where only terms up to first order in $M^D(M^R)^{-1}$ are kept in the expansion.

Finally, it is worth to notice that in order to generate at least two non-zero LH neutrino masses, as indicated by neutrino oscillation experiments, M_{light} has to be a matrix of rank at least two. Then, the number of RH neutrinos participating in the type-I seesaw has to be $n_s \geq 2$.

Type-II seesaw

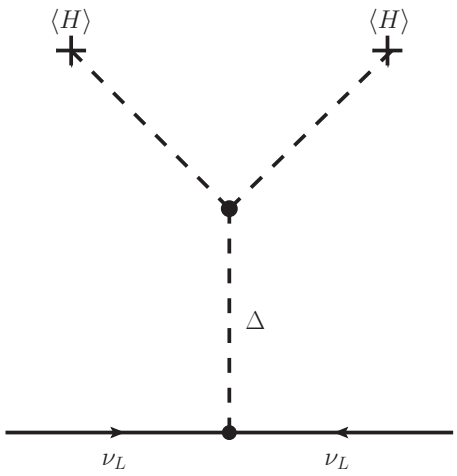

Fig. 1.2 *Feynman diagram for the type-II seesaw mechanism. The tree level completion of the dimension-5 Weinberg operator is done by the exchange of a $SU(2)_L$ triplet complex scalar Δ.*

The type-I seesaw is the only tree level canonical realisation of the dimension-5 Weinberg operator using $SU(2)_L$ singlets as heavy mediators. However, there also exists the possibility of using $SU(2)_L$ triplets as the heavy mediators. In the case in which this iso-triplet is a scalar Δ carrying hypercharge $Y = +1$, one has the type-II seesaw mechanism. The Feynman diagram showing the type-II seesaw mechanism is displayed in Fig. 1.2.

This scalar triplet, Δ, can be represented in the $SU(2)_L$ space as the 2×2 matrix:

$$\Delta = \begin{pmatrix} \Delta^+/\sqrt{2} & \Delta^{++} \\ \Delta^0 & -\Delta^+/\sqrt{2} \end{pmatrix}. \tag{1.37}$$

Accordingly, the relevant Lagrangian terms are

$$\mathcal{L} = Y_\Delta^{ij}\, \bar{L}_i^c\, \sigma_2 \Delta\, L_j + h.c., \tag{1.38}$$

with Y_Δ a 3×3 complex and symmetric Yukawa coupling matrix. This Lagrangian leads to the LH Majorana neutrino mass matrix

$$M_\nu^{\text{T-II}} = Y_\Delta \left\langle \Delta^0 \right\rangle . \tag{1.39}$$

The scalar potential involving the Higgs doublet, H, and the scalar iso-triplet, Δ, is thus,

$$\begin{aligned} V = -m_h^2 H^\dagger H + \frac{\lambda}{4}(H^\dagger H)^2 + M_\Delta^2 \,\text{Tr}(\Delta^\dagger \Delta) + \lambda_1 \text{Tr}[\Delta^\dagger \Delta]^2 + \lambda_2 \text{Tr}[(\Delta^\dagger \Delta)^2] \\ + \lambda_3 H^\dagger H \,\text{Tr}[\Delta^\dagger \Delta] + \lambda_4 H^\dagger \Delta \Delta^\dagger H + (\mu H^T i\sigma^2 \Delta^\dagger H + h.c.). \end{aligned} \tag{1.40}$$

The minimisation of such scalar potential leads to

$$\left\langle \Delta^0 \right\rangle = \frac{\mu v^2}{M_\Delta^2}, \tag{1.41}$$

where the iso-triplet *vev.* has to be $\langle \Delta^0 \rangle < v$, and could be at most of the order of a few GeV to evade ρ parameter constraints.

Assuming Y_Δ of the order one, the smallness of the LH neutrino masses, and $\langle \Delta^0 \rangle$, could come from either choosing the scale M_Δ large or the coupling μ small. In the first case, if the seesaw scale is large enough effects of new physics will appear at very high energies (not in forthcoming experiments). While in the latter, making μ small will reduce the scale of the seesaw, bringing phenomena associated with the triplet Δ at sight in forthcoming experiments, e.g. collider signatures associated with the decay of the doubly charged scalar $\Delta^{\pm\pm}$.

Type-III seesaw

Finally, the canonical type-III seesaw mechanism is realised from the three level exchange of n_T $SU(2)_L$ triplet RH fermions Σ^i, with $i = \{1, \cdots, n_T\}$ a mass eigenstate index. Fig. 1.3 shows the Feynman diagram for the type-III seesaw. The RH Majorana fermions can be represented in the same way as the scalar triplet in Eq. (1.37) as:

$$\Sigma = \begin{pmatrix} \Sigma^0/\sqrt{2} & \Sigma^+ \\ \Sigma^- & -\Sigma^0/\sqrt{2} \end{pmatrix}. \tag{1.42}$$

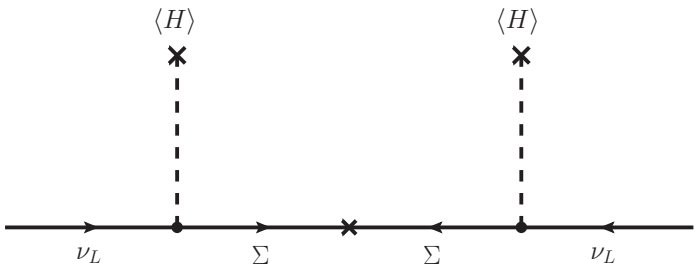

Fig. 1.3 *Feynman diagram for the type-III seesaw mechanism. The tree level completion of the dimension-5 Weinberg operator is done by the exchange of $SU(2)_L$ triplet RH fermions Σ.*

The relevant terms in the Lagrangian are analogous to the type-I seesaw, though field contractions change accordingly,

$$\mathcal{L} = Y_\Sigma \; \bar{L}^c \tilde{H} \Sigma + M_\Sigma \mathrm{Tr}(\bar{\Sigma}^c \Sigma) + h.c., \tag{1.43}$$

where Y_Σ is a $3 \times n_T$ general complex Yukawa coupling matrix and M_Σ is $n_T \times n_T$ Majorana mass matrix. The LH Majorana neutrino mass matrix is obtained in a similar fashion as type-I seesaw. Then, assuming $M_\Sigma \gg v$, LH Majorana mass matrix will be

$$M_\nu^{\text{T-III}} = -v^2 \; Y_\Sigma^T \, (M_\Sigma)^{-1} \, Y_\Sigma. \tag{1.44}$$

As in type-I seesaw mechanism, at least two RH fermions Σ_R are needed to generate two non-zero masses for LH Majorana neutrinos.

Radiative mass generation

Now we turn our attention to a different class of mass generation mechanisms, where LH neutrino mass suppression is generated by the combination of loop factors and Yukawa couplings. This radiative mass generation could be realised at one, two or more loops. In the following we will review two models: the Zee model [61, 62] and the Cheng–Li–Babu–Zee [63–65] model. These models were the first works where the dimension-5 Weinberg operator is completed at one and two loops respectively.

	L_i	ℓ_{Ri}	ϕ_1	ϕ_2	η^+
$SU(2)_L$	**2**	**1**	**2**	**2**	**1**
L	1	1	0	0	-2

Table 1.4 *Summary of relevant particle content and quantum numbers in the Zee model [61, 62].*

The Zee model

The Zee model is one of the simplest setups for radiative neutrino mass generation at one loop. The particle content in the model enhances the SM adding two scalars: a singly charged $\mathrm{SU(3)_C} \otimes \mathrm{SU(2)_L} \otimes \mathrm{U(1)_Y}$ singlet η^+ and an additional $SU(2)_L$ iso-doublet $\phi_2 = \left(\phi_2^+ \;\; \phi_2^0\right)^T$. For sake of simplicity in the notation, the SM Higgs will be denoted as ϕ_1. The two Higgses $\phi_{1,2}$ can develop *vevs*.

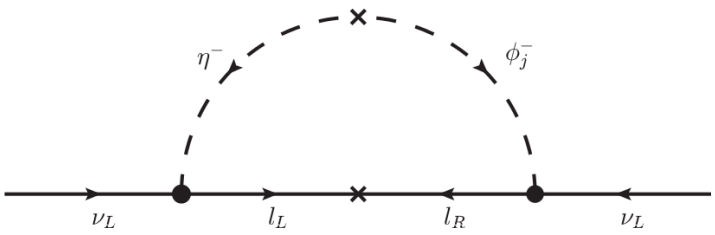

Fig. 1.4 *One-loop radiative mass generation for LH Majorana neutrinos in the Zee model [61, 62].*

The LH Majorana neutrinos acquire their masses through the Feynman diagram in Fig. 1.4. One vertex comes from the Yukawa interaction of the LH leptons and the singly charged scalar, while the other vertex comes from the Yukawa interaction between leptons and Higgses.

From the particle assignments in Tab. 1.4, the relevant part of the Lagrangian is given by:

$$-\mathcal{L} = Y^{\phi_{1,2}}\; \bar{L}\, \phi_{1,2}\, \ell_R + f_{\alpha\beta}\; \bar{L}^c_\alpha\, i\sigma_2 L_\beta \eta^+ - \mu\; \phi_1^\dagger\, i\sigma_2\, \phi_2^* \eta^+ + h.c., \tag{1.45}$$

where $f_{\alpha\beta}$ is an antisymmetric Yukawa coupling matrix between η^+ and LH neutrinos. In the base where charged leptons are diagonal α, β are flavour indices. The violation in lepton number, needed to generate Majorana neutrino masses, comes from the last term in Eq. (1.45).

There exists a restricted version of the Zee model, called Zee–Wolfenstein [66], where only the ϕ_1 scalar iso-doublet couples to leptons. In this model, LH Majorana mass matrix has zeros in the diagonal, as consequence of the Yukawa matrix $f_{\alpha\beta}$ anti-symmetry. After removing all the unphysical phases, LH neutrino mass matrix is parametrised by three real parameters as

$$M_\nu = \begin{pmatrix} 0 & f_{\mu e}(m_\mu^2 - m_e^2) & f_{\tau e}(m_\tau^2 - m_e^2) \\ f_{\mu e}(m_\mu^2 - m_e^2) & 0 & f_{\tau\mu}(m_\tau^2 - m_\mu^2) \\ f_{\tau e}(m_\tau^2 - m_\mu^2) & f_{\tau\mu}(m_\tau^2 - m_\mu^2) & 0 \end{pmatrix}. \tag{1.46}$$

From Eq. (1.46), the model predicts a pattern for neutrino masses and mixing which are ruled out by nowadays oscillation parameters.

Even though the Zee–Wolfenstein model is ruled out, there are no conflicts with experimental oscillation parameter values for the original Zee model. As both Higgses $\phi_{1,2}$ couple to leptons, there are two different Yukawa coupling matrices entering in the right vertex of Fig. 1.4, then M_ν has non-zero diagonal components.

The Zee–Babu model

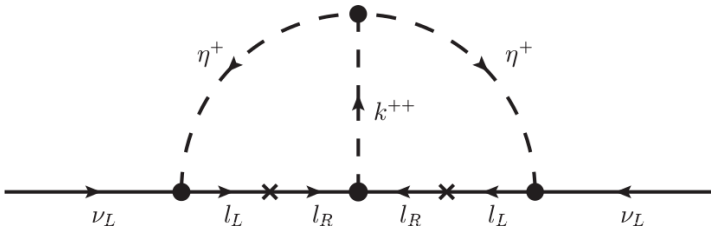

Fig. 1.5 *Two-loops radiative mass generation for LH Majorana neutrinos in the Zee–Babu model [65, 64].*

The Zee–Babu model [65, 64] adds to the SM particle content two $\mathrm{SU(3)_C} \otimes \mathrm{SU(2)_L} \otimes \mathrm{U(1)_Y}$ singlets: a singly charged η^+ and a doubly charged k^{++}. The LH Majorana masses are generated by the two-loop diagram in Fig. 1.5. The relevant part of the Lagrangian is given by

$$-\mathcal{L} = f_{\alpha\beta}\ \bar{L}^c_\alpha\, i\sigma_2\, L_\beta\, \eta^+ + h_{\alpha\beta}\ \bar{\ell}^c_{\alpha R}\, \ell_{\beta R}\, k^{++} - \tilde{\mu}\, \eta^- \eta^- k^{++} + h.c., \tag{1.47}$$

where $f_{\alpha\beta}$ and $h_{\alpha\beta}$ are antisymmetric Yukawa coupling matrices. The lepton number assignment is similar to the Zee model, $L(k^{++}) = -2$ and $L(\eta^+) = -2$. The breaking of lepton number is given explicitly by the $\tilde{\mu}$ term in Eq. (1.47).

The LH neutrino mass is calculated from the diagram, Fig. 1.5, giving:

$$M_\nu = \tilde{f}\, m_{\ell_i}\, \tilde{h}^*\, m_{\ell_j}\, \tilde{f} I_{\ell_i \ell_j}, \tag{1.48}$$

where $\tilde{f} = f_{\alpha\beta}$, $\tilde{h} = h_{\alpha\beta}$, $m_\ell = \mathrm{diag}\,(m_e, m_\mu, m_\tau)$ and $I_{\ell_i \ell_j}$ is a loop function defined by:

$$I_{\ell_i \ell_j} = \int \frac{d^4p}{(2\pi)^4} \int \frac{d^4q}{(2\pi)^4} \frac{1}{p^2 - m_{\ell_1}^2} \frac{1}{q^2 - m_{\ell_2}^2} \frac{1}{p^2 - m_\eta^2} \frac{1}{q^2 - m_\eta^2} \frac{1}{(p-q)^2 - m_k^2}. \tag{1.49}$$

One interesting feature of this model is that, as $\tilde{f}$ is antisymmetric, the determinant of M_ν is zero for three generations. Thus the lightest neutrino mass is zero. This only implies that at two loops, the lightest neutrino mass is zero, however at higher loop corrections this mass will be different from zero, but much smaller than the other two.

Dirac neutrino mass models

Turning back to Dirac neutrinos, there are alternative models to generate naturally small Dirac neutrino masses to the BEH mechanism in the SM extension discussed previously, Eq. (1.26). The classification of such models is analogous to the Majorana mass cases: through (non-renormalisable) higher dimensional operators and their corresponding high energy completions at tree level or involving loops. However, in order to achieve Dirac neutrino masses, a new conserved symmetry in the model has to be imposed forbidding the Majorana mass terms for the RH neutrinos, Eq. (1.28). Such symmetry has been realised as an extra $U(1)$ lepton number symmetry [67, 68] or as the discrete parity Z_n (n>2) [69, 70].

In addition, one also has to forbid the usual SM Yukawa coupling, Eq. (1.26), which has been done by means of a Z_2 parity [71], flavour symmetries [72, 73] or even trough an unconventional $U(1)_{B-L}$ symmetry [74, 68].

In the context of the SM, an effective operator leading to Dirac neutrino masses has the form:

$$\frac{1}{\Lambda^{2n}}\, \bar{L}\, \tilde{H}\, \nu_R (H^\dagger H)^n, \qquad \mathrm{n} \in \{0,\, 1,\, 2,\, ...\}, \tag{1.50}$$

as H and L are $SU(2)_L$ doublets, the operator only involves odd number of Higgses. The lowest order operator is the dimension-4 or tree level Dirac mass, Eq. (1.26), while the first non-renormalisable one is a dimension-6 operator. However, as models for natural Dirac

neutrino masses forbid such tree level mass term, then any higher order operator is also forbidden.

One simple way to generate higher order operators leading to small Dirac neutrino masses is through non-renormalisable operators involving additional scalar fields. Thus, a generalised dimension-5 Weinberg operator for Dirac neutrinos could be written as

$$\mathcal{O}^{(5)} = \frac{g}{\Lambda} \bar{L} \otimes H \otimes X \otimes \nu_R, \tag{1.51}$$

where X is a scalar field transforming under $SU(2)_L$ either as a singlet or a doublet and zero hypercharge.

We will focus on the high energy completions for the simplest generalised dimension-5 operator, that is, when $X = \sigma$ is $\mathrm{SU(3)_C} \otimes \mathrm{SU(2)_L} \otimes \mathrm{U(1)_Y}$ singlet. Thus, Eq. (1.51) yields

$$\mathcal{O}^{(5)} = \frac{g}{\Lambda} (\bar{L}\tilde{H})\, \sigma \nu_R, \tag{1.52}$$

whose tree level completions by heavy mediators can be considered as the Dirac counterpart of the canonical Majorana seesaws.

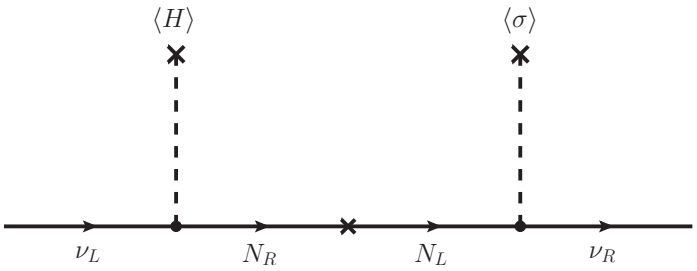

Fig. 1.6 *Feynman diagram for a type-I Dirac neutrino seesaw. The tree level completion of the generalised dimension-5 operator in Eq. (1.52), is done by the exchange of Dirac fermions* $N = N_L + N_R$.

In this context, a *type-I Dirac seesaw* is the high energy completion of the generalised dimension-5 operator in Eq. (1.52). This is realised by the tree level exchange of n heavy fermions, with chiral components N_L^i, N_R^i, $i = \{1, \cdots, n\}$, transforming as singlets under $SU(2)_L \otimes U(1)_Y$. The Feynman diagram for this type-I Dirac seesaw is shown in Fig. 1.6. The relevant terms in the Lagrangian are

$$\mathcal{L} = Y^H\, \bar{L}\, \tilde{H}\, N_R + Y^\sigma \bar{N}_L \nu_R \sigma + M_N\ \bar{N}_R N_L + h.c., \tag{1.53}$$

where $Y^{H(\sigma)}$ are $3 \times n$ $(n \times 3)$ general complex Yukawa matrices and M_N is a $n \times n$ Dirac mass matrix for the heavy fermions $N^i_{L,R}$. It is worth to stress that there must be a symmetry forbidding the Majorana mass terms for N_L as well as N_R in addition to a symmetry forbidding the tree level Dirac mass term.

The $(3+n)$ square mass matrix for the neutrinos and heavy fermions, N_L, N_R, in the basis (ν_L, N_L) and $(\nu_R, N_R)^T$ is given by:

$$M_{\nu,\,N} = \begin{pmatrix} 0 & vY^H \\ uY^\sigma & M_N \end{pmatrix}, \tag{1.54}$$

with $\langle H \rangle = v$ and $\langle \sigma \rangle = u$.

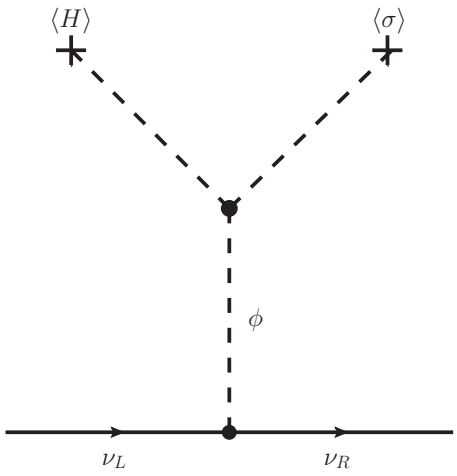

Fig. 1.7 *Feynman diagram for a type-II Dirac neutrino seesaw. The tree level completion of the generalised dimension-5 operator in Eq. (1.52) is done by the exchange of ϕ a complex scalar doublet of $SU(2)_L$.*

Finally, the Dirac neutrino mass matrix is found in the limit where $M_N \gg v, u$ in a similar fashion as the expansion in the type-I Majorana seesaw mechanism. This leads to,

$$M_\nu^{\text{T-I}} = u\, v\, Y^\sigma\, M_N^{-1}\, Y^H, \tag{1.55}$$

and the smallness of neutrino masses in due to a large scale M_N and small $\langle \sigma \rangle$.

The *type-II Dirac seesaw* realisation is shown in Fig. 1.7. In this case, the high energy completion of the generalised dimension-5 operator, Eq. (1.52), is through the tree level exchange of ϕ a heavy scalar doublet of $SU(2)_L$ with $Y = -1/2$. Thus, the relevant part of

the Lagrangian is

$$-\mathcal{L} = Y^{\nu}\,\bar{L}\,\phi\nu_R + h.c., \tag{1.56}$$

and the relevant part of the scalar potential include

$$V(H,\phi,\sigma) \supset \kappa\,\tilde{H}\,\phi\,\sigma, \tag{1.57}$$

where $\langle\phi\rangle = v_\phi$, M_ϕ is the scalar field ϕ mass and κ the coupling in the scalar potential term involving the fields H, σ and χ.

From Eqs. (1.56) and (1.57), the Dirac neutrino mass matrix is given by:

$$M_\nu^{\text{T-II}} = \kappa\frac{v v_\phi}{M_\phi^2}Y^{\nu}, \tag{1.58}$$

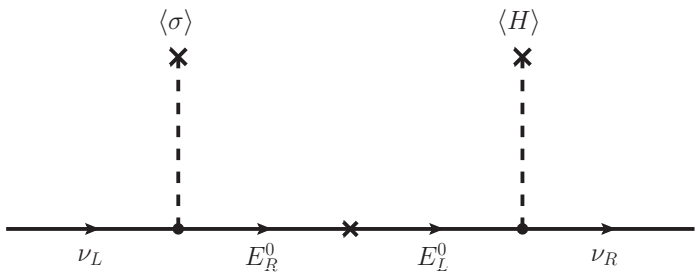

Fig. 1.8 *Feynman diagram for a type-III Dirac neutrino seesaw. The tree level completion of the generalised dimension-5 operator in Eq. (1.52) is done by the exchange of vector-like fermions* E^0.

Finally, the *type-III Dirac seesaw* realisation is shown in Fig. 1.8. In this case, the high energy completion of the generalised dimension-5 operator, Eq. (1.52), is through the tree level exchange of heavy vector-like fermions, with chiral components E_L and E_R, transforming as $SU(2)_L$ doublets. In contrast with type-I and type-II Dirac seesaws, mentioned before, a complete high energy theory using type-III seesaw has not been explicitly developed. Finally, it is worth to mention that radiative mass generation for Dirac neutrinos has been shown to exist in several realisations, as for example in [70, 75].

Dark Matter

In the following section, we will review the main aspects of the dark matter (DM), which together with neutrino masses are one of the compelling evidence for BSM physics.

Evidence of dark matter

The first indication of DM presence comes from the dynamical study in our galaxy. In 1922, the astronomer James Jeans [76], re-analysed the vertical motion of stars near the galactic plane [77]. He showed that spatial density of visible stars cannot explain their vertical motion, it was needed to have two non-visible (dark) stars to each visible star.

The second indication of DM was made by Fritz Zwicky. In 1933, he measured the galaxy radial velocities of the Coma galaxy cluster. Zwicky [78] found that the galaxy orbital velocities were larger by a factor of ten than what was expected from the total mass sum of galaxies in the Cluster. Then, he concluded that the galaxy cluster should contain larger amounts of non-visible (dark) matter. Later in the 70's, Vera Rubin and others [79, 80] analysed the rotation curves of several galaxies, showing that the virial mass and the observed mass, inferred from spectroscopical observations, did not match in every single observation suggesting the evidence of dark matter at galactic scales.

Another cosmological evidence of DM is related with the spatial distribution of galaxies in the Universe. It was shown in the 70's, that the galaxy spatial distribution is not uniform, as was assumed earlier. Posterior observation of the redshifts of visible galaxies [81] showed that such galaxies are clustered in a filamentary cosmic web and the space between filaments is practically devoid of galaxies. These voids have diameters of the order of ten Megaparsecs [82]. Nowadays, it is known that structure formation in the Universe is due to gravitational clustering [83], originated by small initial fluctuations in matter density. This process is very slow, so in order to achieve the observed large scale structure, initial matter density amplitude has to be at least 1/1000th of the matter density at the recombination epoch, when the CMB was originated. Finally, when these matter fluctuations were inferred from CMB measurements, they showed to be two orders of magnitude smaller than expected from only baryonic matter density evolution. Therefore, a dark matter component is needed to explain the structure formation.

The next evidence of DM came from Cosmology in the 80's. From the expansion rate of the Universe, it is possible to calculate the critical energy density of the Universe. The mean energy density has to be close to the critical one, as it is known that the Universe is flat [37]. This means that the energy density can be estimated from the masses of the galaxies and the gas between them. Such estimate shows that the baryonic matter (mostly from stars in galaxies and the interstellar and intergalactic gas) only accounts for a small percentage of the critical density, which however is consistent with the bounds from Big Bang Nucleosynthesis of light elements: ^1H, D, ^{3}He, ^{4}He, and ^{7}Li [84]. Finally, in the

middle 80's the DM existence was confirmed by other independent sources: the weak lensing mass estimates [85, 86] and the X-ray studies of galaxy clusters [87].

Currently, the most precise estimation for the dark matter energy density as well as baryonic energy density, is obtained combining the CMB temperature anisotropies and the spatial distribution of galaxies [37], which has found that the DM abundance[6] is

$$\Omega_{\rm c}h^2 = 0.11933 \pm 0.00091 \quad \text{at } 68\% \text{ CL.},$$

and

$$\Omega_{\rm b}h^2 = 0.02242 \pm 0.00014 \quad \text{at } 68\% \text{ CL.},$$

where h is the Hubble constant in units of 100 Km (s Mpc)$^{-1}$.

Production mechanisms of dark matter

The first and more studied dark matter production mechanism is the thermal production. In this setup, the DM particles are in chemical and thermal equilibrium with ordinary matter in the early Universe, until the DM annihilation rate falls below the expansion rate of the Universe [88, 89] and the DM particles "freeze-out". Among the physical processes that could modify this simple thermal production mechanism, one can mention the co-annihilation of DM with degenerate particles. There are some alternatives to the thermal production mechanism as gravitational production, through the decaying of heavy particles, and scenarios with a non-standard expansion rate of the Universe.

Now, we will explain the thermal freeze-out in detail. Let be X a DM stable particle interacting with the SM particles Y through some process $X\bar{X} \leftrightarrow Y\bar{Y}$ or alternatively $XX \leftrightarrow Y\bar{Y}$ if X is its own antiparticle. In the early Universe, when the temperature was much larger than the X mass $m_{\rm X}$, the annihilation and creation processes were equally efficient, leading to the DM partiwcles X to be in the same amount than the SM particles. However, when the temperature drops below $m_{\rm X}$, the $X\bar{X}$ creation process is exponentially suppressed, while the $X\bar{X}(XX)$ (co-)annihilation process remains unaffected.

In thermal equilibrium at temperature T, the number density of the non-relativistic species X (and $\bar{X}$) is given by

$$n_{\rm X,\,eq} = g_{\rm X}\left(\frac{m_{\rm X}T}{2\pi}\right)e^{-m_X/T}, \tag{1.59}$$

[6] Where $\Omega_X = \rho_x/\rho_{\rm crit}$, being $\rho_{\rm crit}$ the critical density, i.e. $\Omega_{\rm tot} = 1$, which correspond to a flat Universe.

with $g_{\rm X}$ the number of internal degrees of freedom of X. If the DM particle X remains indefinitely in thermal equilibrium, its number density would further suppress as the Universe cools due to the expansion, diluting them quickly. The annihilation of DM particles can be countered by the Hubble expansion rate H.
As the expansion and corresponding dilution of the X dominates over the annihilation rate, the particle number density becomes small enough, then the X interactions cease, surviving until the present epoch.

The expansion and (co-)annihilation effects are described by the Boltzmann equation:

$$\frac{dn_{\rm X}}{dt} + 3Hn_{\rm X} = -\langle\sigma_{X\bar{X}}v\rangle\left(n_{\rm X}^2 - n_{\rm X,\,eq}^2\right), \tag{1.60}$$

where $n_{\rm X}$ is the number density of X, $H := \dot{a}/a = (8\pi^3\rho/3M_{\rm Pl})^{1/2}$ is the expansion rate of the Universe, and $\langle\sigma_{X\bar{X}}v\rangle$ is the thermally average annihilation cross section times its relative velocity.

One can identify two limits in the Boltzmann equation. At high temperatures ($T \gg m_{\rm X}$), the X density is given by its equilibrium value $n_{\rm X,\,eq}$. At low temperatures ($T \ll m_{\rm X}$), the equilibrium density is very small, allowing to the terms $3Hn_{\rm X}$ and $\langle\sigma_{X\bar{X}}v\rangle n_{\rm X}^2$ further reduce the number density of X. For small enough $n_{\rm X}$ values, the annihilation term becomes negligible with respect to the Hubble expansion dilution. When this happens, the comoving number density of X does not change, i.e. it freezes–out.

The freeze out temperature is found numerically solving the Boltzmann equation. Let $x := m_{\rm x}/T$ and $T_{\rm FO}$ be the freeze out temperature, this is approximately given by

$$x_{\rm FO} \approx \log\left[c(c+2)\sqrt{\frac{45}{8}}\frac{g_{\rm X}}{2\pi^3}\frac{m_{\rm X}M_{\rm Pl}(a+6b/x_{\rm FO})}{g_*^{1/2}x_{\rm FO}^{1/2}}\right], \tag{1.61}$$

where $c \sim 0.5$ is a quantity determined numerically, g_* is the number of degrees of freedom (in the SM $g_* \sim 120$ at $T \sim 1$ TeV and $g_* \sim 65$ at $T \sim 1$ GeV), and a and b are non-relativistic expansion terms of the annihilation cross section, $\langle\sigma_{X\bar{X}}v\rangle \simeq a + b\langle v^2\rangle + \mathcal{O}(v^4)$. The DM relic density in the Universe today is approximately

$$\Omega_{\rm X}h^2 \approx \frac{1.04\times10^9\,GeV^{-1}}{M_{\rm Pl}}\frac{x_{\rm FO}}{g_*(a+3b/x_{\rm FO})}. \tag{1.62}$$

Finally, if the DM particle X has a mass scale between GeV and TeV and annihilation cross section at the scale of the generic weak interaction, the freeze out occurs at $x_{\rm FO} \approx$

$20 - 30$, leading to a relic density of

$$\Omega_{\rm X} h^2 \approx 0.1 \left(\frac{x_{\rm FO}}{20}\right) \left(\frac{g_*}{80}\right) \left(\frac{a + 3b/x_{\rm FO}}{3 \times 10^{-26} cm^3/s}\right)^{-1}. \tag{1.63}$$

In other words, if the mass scale of a thermally produced particle with a relic density similar to the relic density of DM is in the GeV–TeV range, this has to have a thermally average cross section of the order of $3 \times 10^{-26}\, cm^3/s$. This is value is similar to the value of the cross section for a generic weak interaction, which has been referred as the "WIMP miracle".

Dark matter candidate profile

The dark matter cannot be made of SM particles, therefore it is necessary to postulate new particles coming from beyond Standard Model theories (BSM) as dark matter candidates. In fact, a possible connection between DM and BSM physics has proliferated the creation of DM candidates, which currently are under search in accelerators and direct and indirect detection experiments.

A particle can be considered as a good DM candidate if it fulfils the following conditions [90]:

- It has the right relic density,
- It is cold,
- It is neutral under colour and electric charges[7],
- It is consistent with the BBN limits,
- It is consistent with the stellar evolution,
- It is compatible with the direct and indirect detection searches limits.

Dark matter candidates

The first obvious DM candidate were the SM neutrinos. However, this scenario leads to troubles with the large scale structure of the universe, as active neutrinos were ultra-relativistic particles (because of their small masses) at the time of formation of galaxies,

[7] Rigorously, there exist some electric charge and colour bounds for the DM, though they are model dependent.

which leads to few amounts of small scale structure formation, i.e. galaxies. This sets an upper bound to the free-streaming contribution of neutrinos [91] in structure formation, which is transformed to a bound on neutrino energy density

$$\Omega_\nu h^2 \leq 0.0062, \qquad \text{at } 95\ \%\ \text{C.L.} \tag{1.64}$$

In the case of non–relativistic DM particles at the beginning of structure formation, or cold dark matter (CDM), unlike ultra-relativistic particles, or hot dark matter (HDM), are consistent with structure formation. N-body numerical simulations of the structure evolution in the Universe show that the filamentary superclusters formation and voids are consistent with a CDM dominated Universe [92].

The most popular candidates to DM include axions (and axion–like particles), sterile neutrinos and WIMPS (motivated in BSM physics). Axions were postulated to solve the strong CP problem in the SM [93, 94]. These are the pseudo Nambu–Goldstone bosons associated with the spontaneous symmetry breaking of a new global $U(1)$ symmetry, the Peccei–Quinn symmetry, at the f_a scale, where the θ_{QCD} is replaced by a dynamic field that goes to zero at the potential minimum. Axions are CDM candidates, as they can be produced non–thermally at temperatures larger than the QCD phase. There are two invisible axion models, the Kim–Shifman–Vainshtein–Zakharov (KSVZ) model [95, 96] and the Dine–Fischler–Sredniki–Zhitnitky (DFSZ) model [97, 98]. The best Peccei–Quinn (PQ) scale and axion masses bounds for these models come from astrophysical reasoning. For instance, bounds in the axion flux in stars which leaves the stellar evolution unaffected. The strongest bound comes from the (SN) 1987A supernova observations, which sets a bound to PQ scale $f_a \lesssim 4 \times 10^8$ GeV.

Sterile neutrinos with masses above the keV could solve the cusp core problem present in CDM models. This problem comes from structure formation simulations, where in places with large DM density such value tends to quickly increase, which seems to be in contradiction with the observation of DM density in galaxy cores. If sterile neutrinos are non-thermally produced by the mixing with SM neutrinos, this could eventually decay into an active neutrino and a photon. Though this leads to sterile neutrinos to be not stable.

The WIMPs are particles with masses between 10 GeV and few TeV and annihilation cross section approximately equal to the weak interactions scale. Its relic density can be calculated by the standard thermal freeze-out. One WIMP candidate could be a heavy Dirac neutrino, though a $SU(2)_L$ doublet would have too few relic density if its masses

exceed the LEP bound $m_\nu > M_Z/2$. The annihilation cross section can be suppressed and then increase the relic density by, for instance, mixing this heavy $SU(2)_L$ doublet with sterile Majorana neutrinos. However, it has to be required some mechanism that forbids the decaying of such heavy neutrino.

Another WIMP DM candidate is the lightest super-symmetrical particle (LSP) [99]. This could be either the sneutrino or the neutralino. The negative result in WIMPs searches, ruled out the sneutrinos as primary components in our galaxy DM halo, leading to the neutralino as a much more viable candidate. The neutralino relic density can be produced thermally in right amounts. The neutralino is a mixing of a bino a photino and a Higgsino, it could be mainly one of them if its mass m_χ is below 150 GeV or m_χ is close to the mass of some other sfermion (and the relic density is reduced by the co-annihilations with the sfermion) or if $2m_\chi$ is close to the CP-odd Higgs boson mass present in supersymmetric models.

There are several non-SUSY SM extensions which provide viable WIMP candidates, as the lightest T-odd particle (LTP) in little Higgs models [100], where T is a conserved parity, or techni-baryons in a scenario with additional strongly interacting gauge group (technicolour or similar). There are also models where the DM particles interact weakly with ordinary matter but have strong interactions with a dark sector. This kind of models was motivated by the excess in positrons and electron fluxes from cosmic rays measured by satellites as PAMELA, ATIC and Fermi. However, such excesses could be due to oversimplification of the estimates, though if they are real, are too large to be accounted by WIMPs, they can be explained by astrophysical sources [101].

Axions (and axion-like particles), sterile neutrinos and WIMPS are detectable in principle with the current and near future technology. However, there are some other DM candidates whose detection is impossible unless they decay. There exists a lower bound on the mean time of 10^{25} to 10^{26} seconds to a 100 GeV decaying DM particle, which includes the gravitino and axino [100].

Chapter 2

A_4 flavour symmetric models for Majorana neutrinos and dark matter

In this chapter, we present a scenario where the stability of the DM arises from the family symmetry explaining neutrino masses and oscillation pattern. A non-Abelian discrete group is chosen as the family symmetry group, as its breaking could yield to a remanent parity symmetry Z_2. Such parity has been assumed in the literature as the simplest mechanism behind the stability of the DM. This is the main idea behind the *discrete dark matter model* (DDM) [102], a minimal extension of the SM and the basis for the work presented in this chapter. In particular, we will discuss two realisations of such a scenario.

2.1 Preliminaries

The model studied in [102] assumes A_4 as flavour group, being A_4 the group of the even permutations of four elements. The A_4 group has order 12 and four *irrreps.*, which are three one-dimensional $\mathbf{1}$, $\mathbf{1}'$ and $\mathbf{1}''$ and one three-dimensional $\mathbf{3}$. A review on the A_4 group properties is given in the Appendix A. The breaking of this flavour symmetry is induced by means of the EWSB.

The three LH Majorana neutrinos ν_{iL}, $i = \{1, 2, 3\}$, get their masses through the type-I seesaw mechanism, for which four RH Majorana neutrinos N_j, $j = \{1, \ldots, 4\}$, are introduced in this model. Three of these RH neutrinos transform as a triplet $N_T \sim \mathbf{3}$ of A_4 and the remaining neutrino N_4 is assigned as the (trivial) singlet $\mathbf{1}$. The scalar sector also has to be extended because the flavour symmetry requires a way to break it spontaneously without

spoiling the EWSB. The scalar H doublet of $SU(2)_L$ is assigned to the trivial singlet, **1**, of A_4, and is responsible for giving masses to quarks and charged leptons. Three additional scalar $SU(2)_L$ iso-doublets labelled as η_i, $i = \{1, 2, 3\}$, are also added forming up a triplet of A_4, $\eta \sim \mathbf{3}$. The SM Higgs is a combination mostly of H and the CP-even component of η_1.

The breaking of the flavour symmetry is driven by the triplet η. The A_4 is spontaneously broken into the sub-group Z_2 when this triplet acquires a *vev.* with alignment $\langle\eta\rangle \sim (1, 0, 0)$. Such alignment is consistent with the minimum conditions of the scalar potential and leads to the breaking of A_4 into Z_2, the latter will be explained in more detail later. After EWSB, the residual Z_2 charges two components of the A_4 triplets. Two scalar iso-doublets $\eta_{2,3}$ in the triplet η as well as two RH Majorana neutrinos $N_{2,3}$ in the triplet N_T will be Z_2-odd.

Regarding DM phenomenology, residual Z_2 provides the mechanism of stability for the DM. Then, the DM candidate will be lightest neutral Z_2-odd particle. The only neutral Z_2-odd particles are the two CP-even and CP-odd neutral components of the two inert Higgses and two RH Majorana neutrinos. The inert Higgses masses are around the EW scale and the RH neutrino masses are expected to be at a larger scale (the seesaw scale). Then, $M_{N_i} > M_{\eta_i}$ and therefore the DM candidate are the lightest neutral scalar combination arising from the neutral components of the inert Higgses, $\eta_{2,3}$.

This first realisation of the DDM with A_4 has viable and interesting DM phenomenology, which was studied in [103]. Unfortunately, it also has strong neutrino phenomenological predictions as a vanishing reactor mixing angle $\theta_{13} = 0$, an inverted mass ordering (IO) with a massless lightest LH neutrino $m_3 = 0$[1] and no CP violation for the lepton sector. The vanishing reactor mixing angle and the CP conservation for leptons are in contradiction with measurements of the reactor mixing angle [104–106] and current hints on the CP violating phase, δ [33].

In a follow-up work [107], a fifth RH Majorana neutrino N_5 is added to the first A_4 DDM setup. The fourth RH neutrino changes its flavour assignment from **1** to **1′** while the fifth RH neutrino is assigned as the singlet **1″**. This new model gives a non-vanishing reactor mixing angle, besides it predicts a normal ordering (NO) with a non-zero lightest LH neutrino mass[2] and a lower bound for the neutrinoless double beta decay ($0\nu\beta\beta$) effective mass, Eq. (1.24), large enough to be in the range of sensitivity of near-future experiments.

[1] This is a consequence of only two RH neutrinos participate in the seesaw. The LH neutrino mass matrix, Eq. (1.36), has rank two and therefore only two non-zero neutrino masses can be generated.

[2] In this model, the addition of the fifth neutrino and the flavour assignments cause that three RH neutrinos to participate in the seesaw and therefore the LH neutrino mass matrix has rank three.

Nevertheless, even at its maximum predicted value for the reactor mixing angle, θ_{13}, this is still too small and ruled out by nowadays more precise measurements [104–106].

Other realisations of the DDM with non-Abelian discrete groups as family symmetries rather than A_4 have been also implemented. For instance, in [108] the family group used is the dihedral group of order four D_4 and in [109] the group $\Delta(54)$ is chosen. In the former model, the vanishing reactor mixing angle issue is not solved, while in the latter besides of addressing this problem the model has further interesting phenomenological features.

2.2 The models

The models studied in [110], hereafter referred to A and B, are extensions of the A_4 realisation of the DDM made in [102]. The relevant particle content and quantum numbers of the models are shown in Tab. 2.1 for model A and in Tab. 2.2 for model B. The particle content is similar to the one presented in [107], with some changes in assignments of the flavour symmetry for the RH neutrinos and the addition of complex scalar $\mathrm{SU(3)_C} \otimes \mathrm{SU(2)_L} \otimes \mathrm{U(1)_Y}$ singlets, also known as flavon fields.

In total there are five RH Majorana neutrinos N_i, $i = \{1, \ldots, 5\}$, three of them arranged in a triplet of the family symmetry $\mathbf{3} \sim N_T = (N_1, N_2, N_3)^T$, the fourth N_4 is assigned as the singlet **1** and the remaining RH neutrino is assigned as the singlet **1'** or **1"** on the model A or B respectively. The scalar sector contains in addition to SM Higgs doublet, H, which is flavour blind (**1**), three extra scalar $SU(2)_L$ iso-doublets as a triplet $\eta = (\eta_1, \eta_2, \eta_3)^T$ and three flavons also as a triplet $\phi = (\phi_1, \phi_2, \phi_3)^T$ of A_4. The iso-doublet LH leptons, $L_i = (\nu_{iL}, \ell_{iL})^T$, $i = \{e, \mu, \tau\}$, transform under the family symmetry as the *irreps.* **1**, **1'** and **1"** and the corresponding RH iso-singlets charged leptons, ℓ_i^c, as the *irreps.* **1**, **1"** and **1'** respectively. Under these assignments of the flavour symmetry, the charged leptons only couple to the SM-like Higgs doublet, H, and are automatically diagonal by A_4. Then, charged leptons do not contribute to the lepton mixing matrix. Regarding quark sector, these are assumed to be flavour blind (**1**) and their masses and mixing could possible arise from an extra family symmetry, which is not considered in the models. Finally, the LH neutrino masses arise via type-I seesaw mechanism by the contributions of H and η in the Dirac mass terms and ϕ on the RH Majorana masses.

When the ϕ fields acquire *vev.* at some scale, for instance around the seesaw scale, they trigger the spontaneous breaking of the family symmetry into a residual Z_2. Unlike the previous realisations of A_4 DDM models, where the flavour symmetry breaking were at EW

scale, in the present models the scale changes at the scale set by the flavons, which is larger than the EW scale. In order to drive the breaking of A_4 into the residual Z_2, the flavon triplet ϕ have to pick up a *vev.* alignment $\langle\phi\rangle$ which has to be invariant under Z_2 and also be consistent with the global minimum conditions of the scalar potential. This A_4 invariant scalar potential is the same in both models and is given by

$$V_{A_4} = V_H + V_\eta + V_\phi + V_{\phi H} + V_{\phi\eta} + V_{\phi H\eta}, \tag{2.1}$$

with

$$\begin{aligned}
V_{A_4} = {} & \mu_1^2\left(\eta_1^\dagger\eta_1\right) + \mu_2^2\left(h^\dagger h\right) + \mu_3^2\left(h^\dagger\eta_1 + \eta_1^\dagger h\right) + \mu_4^2\left(\eta_2^\dagger\eta_2 + \eta_3^\dagger\eta_3\right) + \mu_5^2\left(\eta_2^\dagger\eta_3 + \eta_3^\dagger\eta_2\right) \\
& + \lambda_1\left((\eta_1^\dagger\eta_1)^2 + (\eta_2^\dagger\eta_2)^2 + (\eta_3^\dagger\eta_3)^2\right) + \lambda_2\left(h^\dagger h\right)^2 + \lambda_3\left(\eta_1^\dagger\eta_1\,\eta_2^\dagger\eta_2 + \eta_1^\dagger\eta_1\,\eta_3^\dagger\eta_3 + \eta_2^\dagger\eta_2\,\eta_3^\dagger\eta_3\right) \\
& + \lambda_4\left(h^\dagger h\right)\left(\eta_1^\dagger\eta_1 + \eta_2^\dagger\eta_2 + \eta_3^\dagger\eta_3\right) + \lambda_5\left(\eta_2^\dagger\eta_1\,\eta_1^\dagger\eta_2 + \eta_3^\dagger\eta_1\,\eta_1^\dagger\eta_3 + \eta_3^\dagger\eta_2\,\eta_2^\dagger\eta_3\right) \\
& + \lambda_6\left(\eta_1^\dagger h\,h^\dagger\eta_1 + \eta_2^\dagger h\,h^\dagger\eta_2 + \eta_3^\dagger h\,h^\dagger\eta_3\right) + \Big[\lambda_7\left((\eta_3^\dagger\eta_1)^2 + (\eta_1^\dagger\eta_2)^2 + (\eta_2^\dagger\eta_3)^2\right) \\
& + \lambda_8\left((\eta_1^\dagger h)^2 + (\eta_2^\dagger h)^2 + (\eta_3^\dagger h)^2\right) + \lambda_9\left(\eta_1^\dagger h\,\eta_2^\dagger\eta_3 + \eta_2^\dagger h\,\eta_3^\dagger\eta_1 + \eta_3^\dagger h\,\eta_1^\dagger\eta_2\right) \\
& + \lambda_{10}\left(\eta_3^\dagger\eta_2\,\eta_1^\dagger h + \eta_1^\dagger\eta_3\,\eta_2^\dagger h + \eta_2^\dagger\eta_1\,\eta_3^\dagger h\right) + h.c.\Big],
\end{aligned}$$

and the couplings $\lambda_{1,\ldots,6}$ are real and the remaining couplings $\lambda_{7,\ldots,10}$ could be complex. For simplicity, we assume the case of a CP conserving potential, i.e. all the couplings λ are real. The minimum conditions of the potential, Eq. (2.1), are

$$\frac{\partial V_{A_4}}{\partial v_i} = 0,$$

where v_i stands for the *vevs.* of H, η_i and ϕ_i, which lead to the *vevs.* alignment conditions

$$\left\langle H^0\right\rangle = v_h \neq 0, \quad \left\langle\eta_1^0\right\rangle = v_\eta \neq 0, \quad \left\langle\eta_{2,3}^0\right\rangle = 0, \quad \langle\phi_1\rangle = v_\phi \neq 0, \qquad \langle\phi_{2,3}\rangle = 0, \tag{2.2}$$

where all the v_i are real.

The *vev.* for the A_4 triplet $\langle\eta\rangle$ has the alignment $v_{Z_2} = (1,\,0,\,0)^T$ which is Z_2 invariant, and therefore spontaneously breaks A_4 into a remanent Z_2. In the three dimensional basis

where the Z_2 generator S is real and diagonal,

$$S = \begin{pmatrix} 1 & 0 & 0 \\ 0 & -1 & 0 \\ 0 & 0 & -1 \end{pmatrix}. \tag{2.3}$$

Then one can see that v_{Z_2} is manifestly invariant under the Z_2 generator S:

$$S\, v_{Z_2} = v_{Z_2}. \tag{2.4}$$

Let $a = (a_1, a_2, a_3)^T$ be a generic A_4 triplet, then the S generator (a Z_2 transformation) acts over a as:

$$S\, a = \begin{pmatrix} 1 & 0 & 0 \\ 0 & -1 & 0 \\ 0 & 0 & -1 \end{pmatrix} \begin{pmatrix} a_1 \\ a_2 \\ a_3 \end{pmatrix} = \begin{pmatrix} a_1 \\ -a_2 \\ -a_3 \end{pmatrix}. \tag{2.5}$$

This defines the remanent Z_2 symmetry over the triplets N_T, η and ϕ as:

$$\begin{aligned} &N_1 \to N_1, && \eta_1 \to \eta_1, && \phi_1 \to \phi_1, \\ &N_2 \to -N_2, && \eta_2 \to -\eta_2, && \phi_2 \to -\phi_2, \\ &N_3 \to -N_3, && \eta_3 \to -\eta_3, && \phi_3 \to -\phi_3. \end{aligned} \tag{2.6}$$

Therefore, two RH neutrinos, two Higgs doublets and two flavons will be Z_2-odd after the flavour symmetry breaking. As the remaining Z_2 parity is chosen to be conserved, after EWSB only the Z_2-even component of the triplet η could acquire a *vev.*, and the remaining components will be inert Higgses.

After EWSB and minimisation of the potential, Eq. (2.1), the scalar fields can be written as:

$$\begin{aligned} H &= \begin{pmatrix} H^+ \\ \frac{1}{\sqrt{2}}(v_h + h_0 + i\, A_0) \end{pmatrix}, & \eta_1 &= \begin{pmatrix} H_1^+ \\ \frac{1}{\sqrt{2}}(v_\eta + h_1 + i\, A_1) \end{pmatrix}, \\ \eta_2 &= \begin{pmatrix} H_2^+ \\ \frac{1}{\sqrt{2}}(h_2 + i\, A_2) \end{pmatrix}, & \eta_3 &= \begin{pmatrix} H_3^+ \\ \frac{1}{\sqrt{2}}(h_3 + i\, A_3) \end{pmatrix}, \\ \phi_1 &= \frac{1}{\sqrt{2}}(v_\phi + \phi_{R_1} + i\, \phi_{I_1}), & \phi_{2,3} &= \frac{1}{\sqrt{2}}(\phi_{R_{2,3}} + i\, \phi_{I_{2,3}}). \end{aligned} \tag{2.7}$$

The physical spectrum of the scalars is: three charged scalars ($H_{1,2,3}$), seven CP-even scalars ($h_{0,1,2,3},\ \phi_{1,2,3}$) and seven CP-odd scalars ($A_{1,2,3},\ \phi_{1,2,3}$). Integrating out the heavy scalars ϕ_i, whose masses are assumed to be of the order of the seesaw scale, at energies below the seesaw scale the number of CP-even and CP-odd scalars reduces to four, and the potential will be Z_2-symmetric rather than A_4-symmetric.

2.3 Neutrino phenomenology

In this section, the neutrino phenomenology from the models is presented. The models have similar features, as they arise from similar flavour symmetry assignments, though predicting different LH neutrino mass matrices textures.

Model A

	L_e	L_μ	L_τ	ℓ_e	ℓ_μ	ℓ_τ	N_T	N_4	N_5	H	η	ϕ
$SU(2)_L$	**2**	**2**	**2**	**1**	**1**	**1**	**1**	**1**	**1**	**2**	**2**	**1**
A_4	1	$1''$	$1'$	1	$1''$	$1'$	**3**	1	$1'$	1	**3**	**3**

Table 2.1 *Summary of the relevant particle content and quantum numbers for model A.*

From the particle content and assignments under the flavour group for model A, Table 2.1, the lepton part of the Yukawa Lagrangian is given by

$$\begin{aligned}\mathcal{L}_{\rm Y}^{(\rm A)} &= y_e \bar{L}_e \ell_e H + y_\mu \bar{L}_\mu \ell_\mu H + y_\tau \bar{L}_\tau \ell_\tau H \\ &+ y_1^\nu \bar{L}_e [N_T\,\tilde{\eta}]_1 + y_2^\nu \bar{L}_\mu [N_T\,\tilde{\eta}]_{1''} + y_3^\nu \bar{L}_\tau [N_T\,\tilde{\eta}]_{1'} + y_4^\nu \bar{L}_e\, N_4\, \tilde{H} + y_5^\nu \bar{L}_\tau\, N_5\, \tilde{H} \\ &+ M_1\, \bar{N}_T^c N_T + M_2\, \bar{N}_4^c N_4 + y_1^N [\bar{N}_T^c\,\phi]_3 N_T + y_2^N [\bar{N}_T^c\,\phi]_1 N_4 + y_3^N [\bar{N}_T^c\,\phi]_{1''} N_5 + h.c.,\end{aligned} \tag{2.8}$$

where $[a\,b]_j$, stands for the product of the two triplet *irreps.* a and b contracted into the j *irrep.* of A_4, and the contributions of the form $[a\,b]_3$ account for the symmetric part of the two ways two triplets can be contracted, namely $[a\,b]_{3_1}$ and $[a\,b]_{3_2}$.

As mentioned previously, the iso-doublet H is flavour blind and responsible for giving mass to the charged leptons (as well as quarks), which can be calculated straightforward from Eq. (2.8) giving

$$M_l = \frac{v_h}{\sqrt{2}}\,\mathrm{diag}\,(\,y_e,\,y_\mu,\,y_\tau\,)\,, \tag{2.9}$$

where $\langle H \rangle = v_h/\sqrt{2}$. Then, the lepton mixing matrix $V = V^{\nu\dagger}V^{\ell}$, Eq. (1.17), comes from the neutrino part as $V^{\ell} = \mathbb{1}$.

The three LH neutrinos obtain their masses through the type I-seesaw. The Dirac neutrino mass matrix $M_D^{(A)}$ arises from the contribution of H and η, while the flavon fields ϕ contribute to the RH neutrino Majorana mass matrix M_R. From Eqs. (2.8), the Dirac neutrino mass matrix in the basis $(\bar{\nu}_e, \bar{\nu}_\mu, \bar{\nu}_\tau)^T$, $(N_1, N_2, N_3, N_4, N_5)$ is given by

$$M_{\rm D}^{\rm (A)} = \begin{pmatrix} y_1^\nu \eta_1^0 & y_1^\nu \eta_2^0 & y_1^\nu \eta_3^0 & y_4^\nu H^0 & 0 \\ y_2^\nu \eta_1^0 & \omega^* y_2^\nu \eta_2^0 & \omega y_2^\nu \eta_3^0 & 0 & 0 \\ y_3^\nu \eta_1^0 & \omega y_3^\nu \eta_2^0 & \omega^* y_3^\nu \eta_3^0 & 0 & y_5^\nu H^0 \end{pmatrix}, \tag{2.10}$$

where H^0 and η_i^0, $i = \{1, 2, 3\}$ the neutral component of the iso-doublets H and η_i. After EWSB, Eq. (2.2) leads to

$$M_{\rm D}^{\rm (A)} = \frac{1}{\sqrt{2}} \left(\begin{array}{c|cc|cc} y_1^\nu v_\eta & 0 & 0 & y_4^\nu v_h & 0 \\ y_2^\nu v_\eta & 0 & 0 & 0 & 0 \\ y_3^\nu v_\eta & 0 & 0 & 0 & y_5^\nu v_h \end{array} \right). \tag{2.11}$$

The RH Majorana neutrino mass matrix is calculated from Eq. (2.8) in the basis $(\bar{N}_1^c, \bar{N}_2^c, \bar{N}_3^c, \bar{N}_4^c, \bar{N}_5^c)^T$, $(N_1, N_2, N_3, N_4, N_5)$ as

$$M_{\rm R} = \begin{pmatrix} M_1 & y_1^N \phi_3 & y_1^N \phi_2 & y_2^N \phi_1 & y_3^N \phi_1 \\ y_1^N \phi_3 & M_1 & y_1^N \phi_1 & y_2^N \phi_2 & \omega^* y_3^N \phi_2 \\ y_1^N \phi_2 & y_1^N \phi_1 & M_1 & y_2^N \phi_3 & \omega y_3^N \phi_3 \\ y_2^N \phi_1 & y_2^N \phi_2 & y_2^N \phi_3 & M_2 & 0 \\ y_3^N \phi_1 & \omega^* y_3^N \phi_2 & \omega y_3^N \phi_3 & 0 & 0 \end{pmatrix}. \tag{2.12}$$

After EWSB, Eq. (2.2) leads to

$$M_{\rm R} = \frac{1}{\sqrt{2}} \left(\begin{array}{c|cc|cc} M_1 & 0 & 0 & y_2^N v_\phi & y_3^N v_\phi \\ \hline 0 & M_1 & y_1^N v_\phi & 0 & 0 \\ 0 & y_1^N v_\phi & M_1 & 0 & 0 \\ \hline y_2^N v_\phi & 0 & 0 & M_2 & 0 \\ y_3^N v_\phi & 0 & 0 & 0 & 0 \end{array} \right). \tag{2.13}$$

We can notice from mass matrix in Eq. (2.11) that the RH neutrinos N_2 and N_3 do not have any Dirac mass terms, because the breaking of A_4 charge them as Z_2-odd. Thus, N_2 and N_3 do not participate in the seesaw, i.e. from the five RH neutrinos only three, $N_{1,4,5}$, are active in the seesaw and the remaining two belong to the dark sector. This dark sector is shown within the lines in the mass matrices in Eqs. (2.11) and (2.13).

From the mass matrices Eqs. (2.11) and (2.13), the LH neutrinos get their Majorana masses through the type-I seesaw relation, Eq.(1.36), taking the form

$$M_\nu^{(\mathrm{A})} \simeq -\left(M_{\mathrm{D}_{3\times5}}^{(\mathrm{A})}\right)^{\mathrm{T}} \left(M_{\mathrm{R}_{5\times5}}\right)^{-1} M_{\mathrm{D}_{3\times5}}^{(\mathrm{A})} = \begin{pmatrix} a & 0 & b \\ 0 & 0 & c \\ b & c & d \end{pmatrix}, \tag{2.14}$$

where the parameters a, b, c and d are defined as

$$\begin{aligned} a &= \tfrac{(y_4^\nu v_h)^2}{M_2}, \quad b = \tfrac{y_1^\nu y_5^\nu v_\eta v_h}{y_3^N v_\phi} - \tfrac{y_2^N y_4^\nu y_5^\nu v_h^2}{y_3^N M_2}, \\ c &= \tfrac{y_2^\nu y_5^\nu v_\eta v_h}{y_3^N v_\phi}, \quad d = \tfrac{(y_2^N y_5^\nu v_h)^2}{(y_3^N)^2 M_2} - \tfrac{(y_5^\nu v_h)^2 M_1}{(y_3^N v_\phi)^2} + 2\,\tfrac{y_3^\nu y_5^\nu v_\eta v_h}{y_3^N v_\phi}. \end{aligned} \tag{2.15}$$

This LH Majorana neutrino mass matrix $M_\nu^{(\mathrm{A})}$, Eq. (2.14), has the two-zero B_3 texture, according to the nomenclature in [111]. This mass matrix texture is phenomenologically favourable, being consistent with both neutrino mass orderings (IO and NO), non-vanishing lightest neutrino mass and allows the current experimental value for the reactor mixing angle, as have been proved by several works [111–120].

Model B

In this model the particle content is shown in Tab. 2.2, where the difference with respect to the previous model is that the fifth RH neutrino, N_5, changes its assignment from $1' \to 1''$. The lepton sector of Yukawa Lagrangian is given by:

	L_e	L_μ	L_τ	ℓ_e	ℓ_μ	ℓ_τ	N_T	N_4	N_5	H	η	ϕ
$SU(2)_L$	**2**	**2**	**2**	**1**	**1**	**1**	**1**	**1**	**1**	**2**	**2**	**1**
A_4	1	$1''$	$1'$	1	$1''$	$1'$	**3**	1	$1''$	1	**3**	**3**

Table 2.2 *Summary of the relevant particle content and quantum numbers for model B.*

$$\begin{aligned}\mathcal{L}_{\rm Y}^{\rm (B)} &= y_e\,\bar{L}_e\ell_e H + y_\mu\,\bar{L}_\mu\ell_\mu H + y_\tau\,\bar{L}_\tau\ell_\tau H \\ &+ y_1^\nu \bar{L}_e[N_T\,\tilde{\eta}]_1 + y_2^\nu \bar{L}_\mu[N_T\,\tilde{\eta}]_{1''} + y_3^\nu \bar{L}_\tau[N_T\,\tilde{\eta}]_{1'} + y_4^\nu \bar{L}_e\,N_4\,\tilde{H} + y_5^\nu \bar{L}_\mu\,N_5\,\tilde{H} \\ &+ M_1\,\bar{N}_T^c N_T + M_2\,\bar{N}_4^c N_4 + y_1^N[\bar{N}_T^c\,\phi]_3 N_T + y_2^N[\bar{N}_T^c\,\phi]_1 N_4 + y_3^N[\bar{N}_T^c\,\phi]_{1'} N_5 + h.c.\ .\end{aligned} \tag{2.16}$$

The mass matrix for the charged leptons is also diagonal as their assignments have not changed from the model A. The Dirac neutrino mass matrix, from the Lagrangian Eq. (2.16), in the basis $(\bar{\nu}_e, \bar{\nu}_\mu, \bar{\nu}_\tau)^T$, $(N_1, N_2, N_3, N_4, N_5)$ is given by:

$$M_{\rm D}^{\rm (B)} = \begin{pmatrix} y_1^\nu\eta_1^0 & y_1^\nu\eta_2^0 & y_1^\nu\eta_3^0 & y_4^\nu H^0 & 0 \\ y_2^\nu\eta_1^0 & \omega^* y_2^\nu\eta_2^0 & \omega y_2^\nu\eta_3^0 & 0 & y_5^\nu H^0 \\ y_3^\nu\eta_1^0 & \omega y_3^\nu\eta_2^0 & \omega^* y_3^\nu\eta_3^0 & 0 & 0 \end{pmatrix}. \tag{2.17}$$

After EWSB, Eq. (2.2) leads to

$$M_{\rm D}^{\rm (B)} = \begin{pmatrix} y_1^\nu v_\eta & 0 & 0 & y_4^\nu v_h & 0 \\ y_2^\nu v_\eta & 0 & 0 & 0 & y_5^\nu v_h \\ y_3^\nu v_\eta & 0 & 0 & 0 & 0 \end{pmatrix}. \tag{2.18}$$

The Majorana neutrino mass matrix M_R is the same as in Eq. (2.13). Analogously, the LH neutrino Majorana mass matrix after the EWSB is given by the type-I seesaw relation:

$$M_\nu^{\rm (B)} \simeq -\left(M_{\rm D_{3\times5}}^{\rm (B)}\right)^{\rm T}\left(M_{\rm R_{5\times5}}\right)^{-1} M_{\rm D_{3\times5}}^{\rm (B)} = \begin{pmatrix} a & b & 0 \\ b & d & c \\ 0 & c & 0 \end{pmatrix}, \tag{2.19}$$

with the parameters a, b, c and d defined as:

$$\begin{aligned} a &= \tfrac{(y_4^\nu v_h)^2}{M_2}, \quad b = \tfrac{y_1^\nu y_5^\nu v_\eta v_h}{y_3^N v_\phi} - \tfrac{y_2^N y_4^\nu y_5^\nu v_h^2}{y_3^N M_2}, \\ c &= \tfrac{y_3^\nu y_5^\nu v_\eta v_h}{y_3^N v_\phi}, \quad d = \tfrac{(y_2^N y_5^\nu v_h)^2}{(y_3^N)^2 M_2} - \tfrac{(y_5^\nu v_h)^2 M_1}{(y_3^N v_\phi)^2} + 2\,\tfrac{y_2^\nu y_5^\nu v_\eta v_h}{y_3^N v_\phi}. \end{aligned} \tag{2.20}$$

Finally, the mass matrix $M_\nu^{\rm (B)}$ in Eq. (2.19) has another two-zero texture, B_4 according to the nomenclature in [111]. This B_4 texture is also consistent with both neutrino mass orderings (NO and IO), non-zero lightest neutrino mass and can accommodate the current reactor mixing angle as shown in several works [111–120].

2.4 Results and discussion

In the previous subsection, we show that both models display two different two-zero textures for the LH Majorana neutrino mass matrices, Eqs. (2.11) and (2.18). The properties of such two-zero mass matrices have been studied originally in [111] which coined the nomenclature used. There are seven two-zero textures for M_ν out of the fifteen logical possibilities that are compatible with the current neutrino oscillation data. These are labelled as:

$$\mathbf{A_1}: \begin{pmatrix} 0 & 0 & \times \\ 0 & \times & \times \\ \times & \times & \times \end{pmatrix}, \quad \mathbf{A_2}: \begin{pmatrix} 0 & \times & 0 \\ \times & \times & \times \\ 0 & \times & \times \end{pmatrix}, \tag{2.21}$$

$$\mathbf{B_1}: \begin{pmatrix} \times & \times & 0 \\ \times & 0 & \times \\ 0 & \times & \times \end{pmatrix}, \quad \mathbf{B_2}: \begin{pmatrix} \times & 0 & \times \\ 0 & \times & \times \\ \times & \times & 0 \end{pmatrix},$$
$$\mathbf{B_3}: \begin{pmatrix} \times & 0 & \times \\ 0 & 0 & \times \\ \times & \times & \times \end{pmatrix}, \quad \mathbf{B_4}: \begin{pmatrix} \times & \times & 0 \\ \times & \times & \times \\ 0 & \times & 0 \end{pmatrix} \tag{2.22}$$

and

$$\mathbf{C}: \begin{pmatrix} \times & \times & \times \\ \times & 0 & \times \\ \times & \times & 0 \end{pmatrix}, \tag{2.23}$$

with $\times$ any nonzero matrix element. Although, the C texture is currently only compatible with the inverted ordering of masses, see [118].

In order to spot the phenomenological consequences of the two-zero textures, one can see that in the standard case of three mass and three flavour neutrino oscillations, the Majorana neutrino mass matrix is given by:

$$M_\nu = M_\nu^T = V \,\mathrm{diag}\,(m_1, m_2, m_3)\, V^T, \tag{2.24}$$

with m_i the neutrino masses and $V = UD$, the lepton mixing matrix for Majorana neutrinos, Eq. (1.22). The Majorana phase matrix being $D = \mathrm{diag}\,(e^{i\alpha_1}, e^{i\alpha_2}, e^{i\alpha_3})$, where one of these

α phases can be dropped out. Then, Eq. (2.24) can be written as

$$(M_\nu)_{ij} = \sum_{k=1}^{3} m_k V_{ik} V_{jk} = \sum_{k=1}^{3} m_k e^{2i\alpha_k} U_{ik} U_{jk} = \sum_{k=1}^{3} \mu_k U_{ik} U_{jk}, \tag{2.25}$$

with $\mu_k = m_k e^{2i\alpha_k}$. The two independent zero conditions can be written as

$$(M_\nu)_{ij} = 0 \quad \left(\Leftrightarrow (M_\nu)^*_{ij} = 0\right), \tag{2.26}$$

for some different pair of indices (i, j). Replacing Eq. (2.25) in Eq. (2.26) gives

$$\sum_{k=1}^{3} \mu_k U_{ik} U_{jk} = 0. \tag{2.27}$$

This system of equations, Eq. (2.27), for the zeros $(i = a,\ j = b)$ and $(i = c,\ j = d)$ is equivalent system of equations

$$\begin{pmatrix} U_{a1}U_{b1} & U_{a2}U_{b2} \\ U_{c1}U_{d1} & U_{c2}U_{d2} \end{pmatrix} \begin{pmatrix} \mu_1 \\ \mu_2 \end{pmatrix} = -\mu_3 \begin{pmatrix} U_{a3}U_{b3} \\ U_{c3}U_{d3} \end{pmatrix}. \tag{2.28}$$

One can solve the system for μ_1 and μ_2 in terms of the lightest mass μ_3, leading to

$$\begin{pmatrix} \mu_1 \\ \mu_2 \end{pmatrix} = -\frac{\mu_3}{D} \begin{pmatrix} U_{c2}U_{d2} & -U_{a2}U_{b2} \\ -U_{c1}U_{d1} & U_{a1}U_{b1} \end{pmatrix} \begin{pmatrix} U_{a3}U_{b3} \\ U_{c3}U_{d3} \end{pmatrix}, \tag{2.29}$$

with

$$D = \det \begin{pmatrix} U_{a1}U_{b1} & U_{a2}U_{b2} \\ U_{c1}U_{d1} & U_{c2}U_{d2} \end{pmatrix}, \tag{2.30}$$

which is non-zero within the current 3σ values for the oscillation parameters. Therefore, finding non trivial solutions of Eq. (2.29) implies that μ_3 has to be different from zero, as $\mu_3 = 0$ in Eq. (2.29) implies $\mu_1 = \mu_2 = 0$.

Finally, one can use the ratio of the two neutrino squared mass differences, Δm^2_{21} and Δm^2_{3i}[3] and divide them by the lightest mass μ_3 yielding to

$$r := \frac{\Delta m^2_{21}}{\Delta m^2_{3i}} = \frac{\frac{m_2^2}{m_3^2} - \frac{m_1^2}{m_3^2}}{1 - \frac{m_i^2}{m_3^2}} = \frac{|\frac{\mu_2^2}{\mu_3^2}| - |\frac{\mu_1^2}{\mu_3^2}|}{1 - |\frac{\mu_i^2}{\mu_3^2}|}. \tag{2.31}$$

Thus, one can replace Eqs. (2.29) in Eq. (2.31), obtaining an equation that relates the oscillation parameters: Δm^2_{12}, Δm^2_{3i}, θ_{12}, θ_{23}, θ_{13} and δ independently of μ_3. This relation is the basis for the analysis of the parameter regions of the models.

In summary, the two complex zeros impose four independent constrains for the twelve real parameters in a 3×3 Majorana mass matrix, leading to seven independent real parameters, a global phase can be removed. This seven parameters are the four complex parameters: a, b, c and d in Eqs. (2.14) and (2.19) minus a global phase. On the other hand, the neutrino observables are: Δm^2_{12}, Δm^2_{3i}, θ_{12}, θ_{23}, θ_{13}, δ, α_{21} and α_{31}. Thus, the models will give us two predictions.

A numerical scan with inputs the 3σ values for the five oscillations parameters: Δm^2_{12}, Δm^2_{3i}, θ_{12}, θ_{23} and θ_{13} from three global fit data [121–123] is performed as follows. From Eq. (2.31), we can solve for the phase δ, independently of the lightest mass. Then, we have to give the mass scale as an input in the scan completing the seven independent parameters and solve for the two remaining Majorana α phases.

As result of the numerical scans, two interesting correlations between the oscillation parameters are worth to show. The first one between the atmospheric mixing angle, $\sin^2\theta_{23}$, and the sum of light neutrino masses, $\sum m_\nu = m_{\nu_1} + m_{\nu_2} + m_{\nu_3}$ and the second correlation between the neutrinoless double beta decay effective mass parameter, $|m_{ee}|$, and the lightest neutrino mass, $m_{\nu_{\text{light}}}$, where $m_{\nu_{\text{light}}} = m_{\nu_1}$ for the NO and $m_{\nu_{\text{light}}} = m_{\nu_3}$ for the IO.

Figs. 2.1, 2.2, and 2.3 show the correlation between the less precise measured mixing angle, the atmospheric angle $\sin^2\theta_{23}$ and the sum of active neutrino masses, for model A (with B_3 texture) at the top panels and model B (with B_4 texture) at the bottom ones. In these plots, the allowed 3σ regions in the oscillation parameters are displayed in magenta for the normal ordering (NO) and in cyan for the inverted ordering (IO). The 1σ ranges in the atmospheric mixing angle are represented by the horizontal blue and red shaded bands for the inverted and normal mass ordering, respectively. The best fit values in θ_{23} correspond to the blue and red horizontal dashed lines for the inverse and normal ordering respectively.

[3] where the index i in Δm^2_{3i} is $i = 2$ for the NO, thus $\Delta m^2_{32} > 0$, and $i = 3$ for the IO, thus $\Delta m^2_{31} < 0$.

The global fit from Forero *et al.* [121] which has a local minimum in the atmospheric angle for the IO is shown as the red pointed horizontal line in Fig. 2.1. The global fit from Capozzi *et al.* [123] which has two different and separated 1σ regions in the atmospheric angle for the IO, are shown as two blue shaded horizontal bands in Fig. 2.3. Finally, the grey vertical band represents the disfavoured region in the sum of active neutrino masses, $\sum m_\nu < 0.23$ eV, coming from the cosmological data fits by the Planck Collaboration [124].

The plots in Figs. 2.1, 2.2, and 2.3 show that model A is in agreement with values for $\sin\theta_{23}$ within the 1σ region in both mass orderings, while model B this depends on what dataset is used. In the data from Forero *et al.* [121] and Gonzalez-Garcia *et al.* [122] only the NO have values for atmospheric angle within the 1σ region. Though, for the data from [122] this happens for large values of the neutrino masses disfavoured by Planck constraint. For data from Capozzi *et al.* [123], only the IO have values within 1σ in the second octant for the atmospheric angle. Finally, it is worth to mention that the regions for the NO and IO in model A are the same but flipped in model B, this because both textures are related by a permutation symmetry between the $2-3$ rows and the $2-3$ columns.

The second remarkable correlation between $|m_{ee}|$ and $m_{\nu_{\text{light}}}$, is displayed in Figs. 2.4, 2.5 and 2.6 for model A (with B_3 texture) at the top panels and model B (with B_4 texture) at the bottom ones. The region for the NO with values of $\sin^2\theta_{23}$ within 3σ is in dark magenta and within 1σ in magenta. Analogously, the region for the IO with values of $\sin^2\theta_{23}$ within 3σ is in dark cyan and within 1σ in cyan. The horizontal red shaded region corresponds the current experimental limit on the neutrinoless double beta decay effective mass parameter [130]. The red (blue) lines represent the forthcoming experimental sensitivities on the parameter $|m_{ee}|$ [125–127, 129] ($m_{\nu_{\text{light}}}$ [128]). The vertical blue shaded region displays the disfavoured neutrino mass region set by Planck data [124]. Finally, the graphics also show in yellow and green bands the corresponding 3σ "flavour-generic" IO and NO neutrino spectra respectively. Figs. 2.4 and 2.5 show that model B has no 1σ values in the atmospheric mixing angle, therefore it is only shown the data in the 3σ region in the IO. The Fig. 2.6, shows that model B does not have values within the 1σ region for the NO, as mentioned before.

The models have a prediction on the Majorana α phases giving a minimal cancellation for the parameter $|m_{ee}|$. As can been seen in Figs. 2.4, 2.5 and 2.6 the allowed regions for the $|m_{ee}|$ lie on the upper limits of the generic spectrum bands. The mass parameter of the two-zero textures B_3 and B_4 is also sensitive to the value of the atmospheric mixing angle, in the cases in which this mixing angle prediction overlaps with the experimental value

at 1σ, it translates into a localised region for the neutrinoless mass parameter. Another important feature of the models is related with the parameter $|m_{ee}|$. The flavour structure sets a lower bound on $|m_{ee}|$ for both models, irrespective of the mass ordering, within the range of sensitivity of the near-future experiments. Finally, it is worth mentioning that a better measurement of the atmospheric mixing angle is a crucial test for such models.

2.5 Dark matter phenomenology

The dark matter phenomenology arising from the models A and B is different from that in the original DDM setup, where the limit for large masses ($M_{\rm DM} > 100$ GeV) was not allowed. The dark matter phenomenology, in this case, is similar to the inert Higgs doublet model [131], but with two active and two inert Higgses. Unlike the first A_4 DDM model, there is no inconvenient in generating the right relic abundance even if the mass of the DM candidate is larger than the mass of the gauge bosons. One can see that the limits presented in the minimal dark matter model [132] apply, and for those masses the dark matter annihilates mainly into gauge bosons.

2.6 Conclusions

In this chapter, two models (A and B) based on the discrete dark matter mechanism with A_4 as flavour symmetry were presented. The family symmetry is spontaneously broken at the seesaw scale, into a remanent Z_2. In the models, three LH Majorana neutrinos acquire their masses through the type-I seesaw mechanism, by adding five RH neutrinos to the particle content of such models. After the flavour symmetry breaking, two RH neutrinos $N_{2,3}$ will be Z_2-odd and the remaining three $N_{1,4,5}$ will be Z_2-even. The latter three RH neutrinos are the only which participate in the seesaw. In addition, the scalar sector is enhanced by the $SU(3) \otimes SU(2)_L \otimes U(1)_Y$ singlet scalar fields ϕ which trigger the breaking of A_4, in such a way that two-zero textures for the active neutrino mass matrices are achieved. These textures are in agreement with current experimental data for the reactor mixing angle and allow the two neutrino mass orderings with non-zero lightest neutrino masses.

Another consequence of the A_4 breaking is that these models contain a dark matter candidate stabilised by the remnant Z_2 symmetry. The dark matter phenomenology in the models is different from the original DDM [103], where exists a limit for large DM masses

($M_{DM} \gtrsim 100$ GeV), and will be similar to the inert Higgs doublet model [131] with extra two active and two inert $SU(2)_L$ doublet scalar fields.

In addition, an updated analysis for the two-zero textures mass matrix obtained for both models, B_3 and B_4, is presented. The models predict a correlation between the atmospheric mixing angle and the sum of the active neutrino masses, as well as a lower bound for the neutrinoless double beta decay effective mass parameter being in the region of sensitivity of near future experiments.

Finally, if the flavon fields acquire *vevs.* at some scale larger than the seesaw scale, the remaining Z_2 symmetry at the seesaw scale could lead to a mixing between the three Z_2-even RH neutrinos. Such mixing is crucial in scenarios with matter-antimatter asymmetry, via leptogenesis, while in the original DDM A_4 setup, this is not possible.

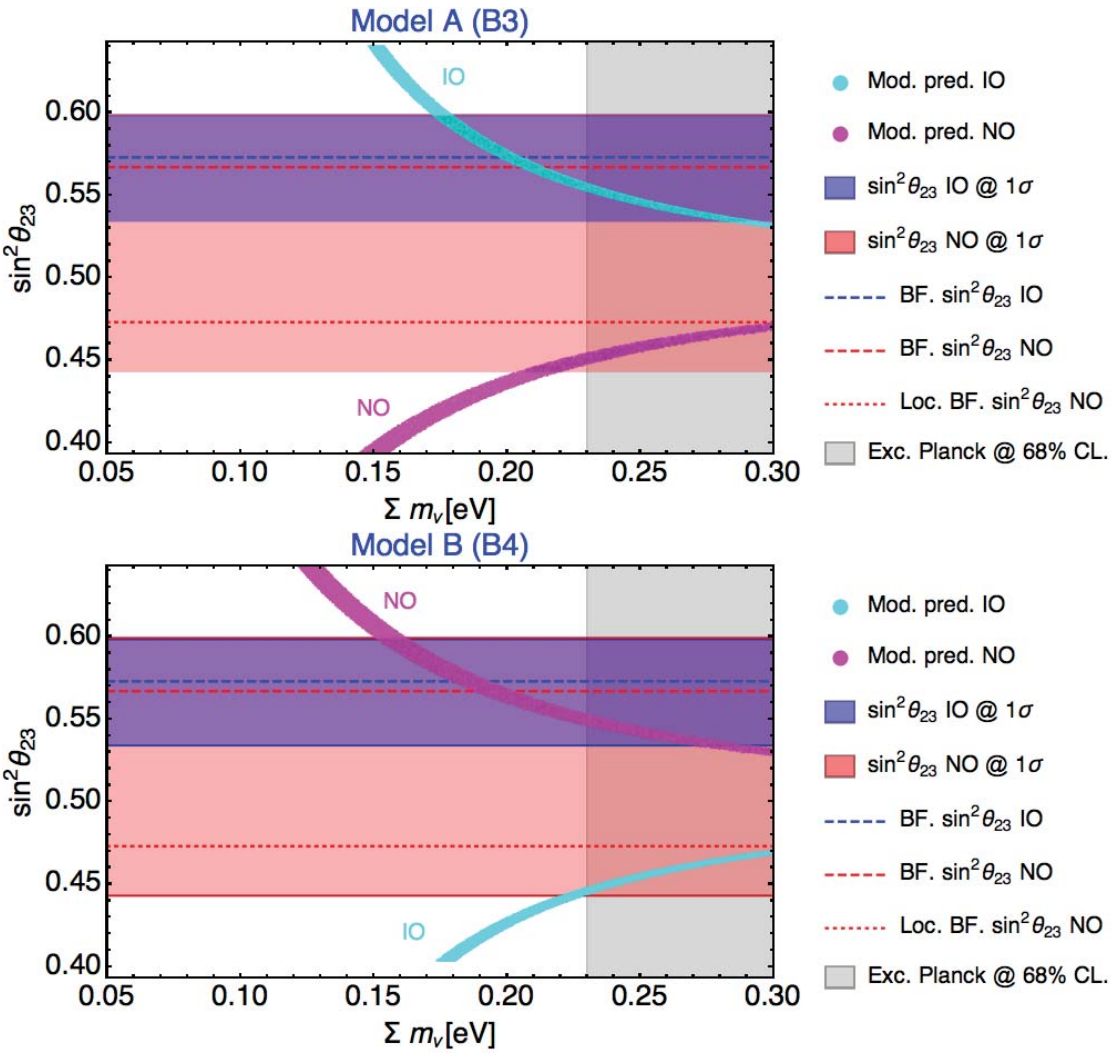

Fig. 2.1 *Correlation between* $\sin^2\theta_{23}$ *and the sum of the light neutrino masses,* $\sum m_\nu$*, in model A (with the* B_3 *texture) at the top and model B (with the* B_4 *texture) at the bottom, where NO (IO) allowed region is in magenta (cyan). The horizontal red (blue) shaded region corresponds to the* 1σ *value in* $\sin^2\theta_{23}$ *for NO (IO) from [121]. The red (blue) horizontal dashed line represent the* θ_{23} *best fit value in NO (IO), while the doted horizontal red line represents the value of local minimum in NO from from [121]. The vertical grey shaded region is disfavoured by Planck data [124].*

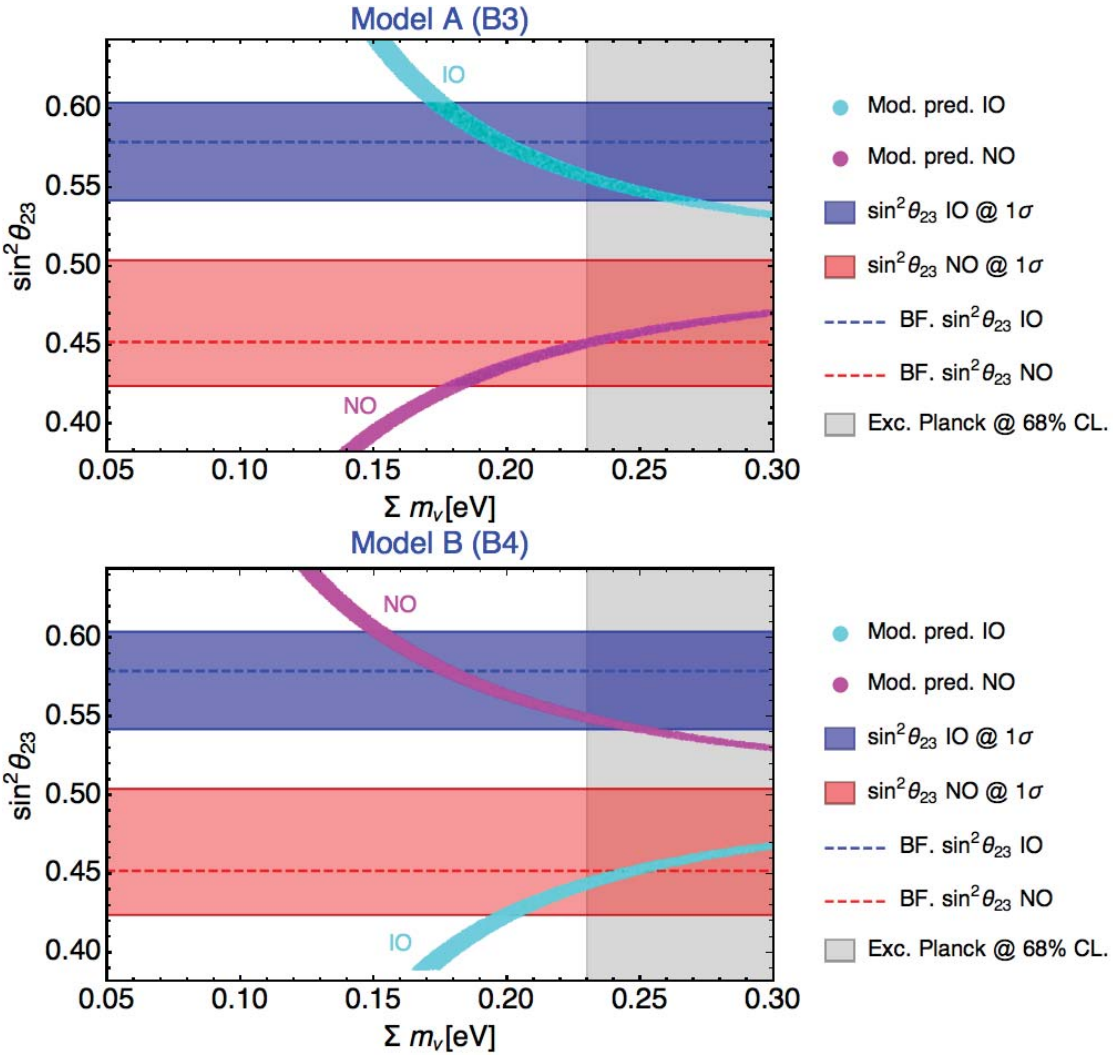

Fig. 2.2 *Correlation between* $\sin^2\theta_{23}$ *and the sum of the light neutrino masses,* $\sum m_\nu$*, in model A (with the* B_3 *texture) at the top and model B (with the* B_4 *texture) at the bottom, where NO (IO) allowed region is in magenta (cyan). The horizontal red (blue) shaded region corresponds to the* 1σ *value in* $\sin^2\theta_{23}$ *for NO (IO) from [122]. The red (blue) horizontal dashed line represents the best fit value in NO (IO) from [122]. The vertical grey shaded region is disfavoured by the Planck data [124].*

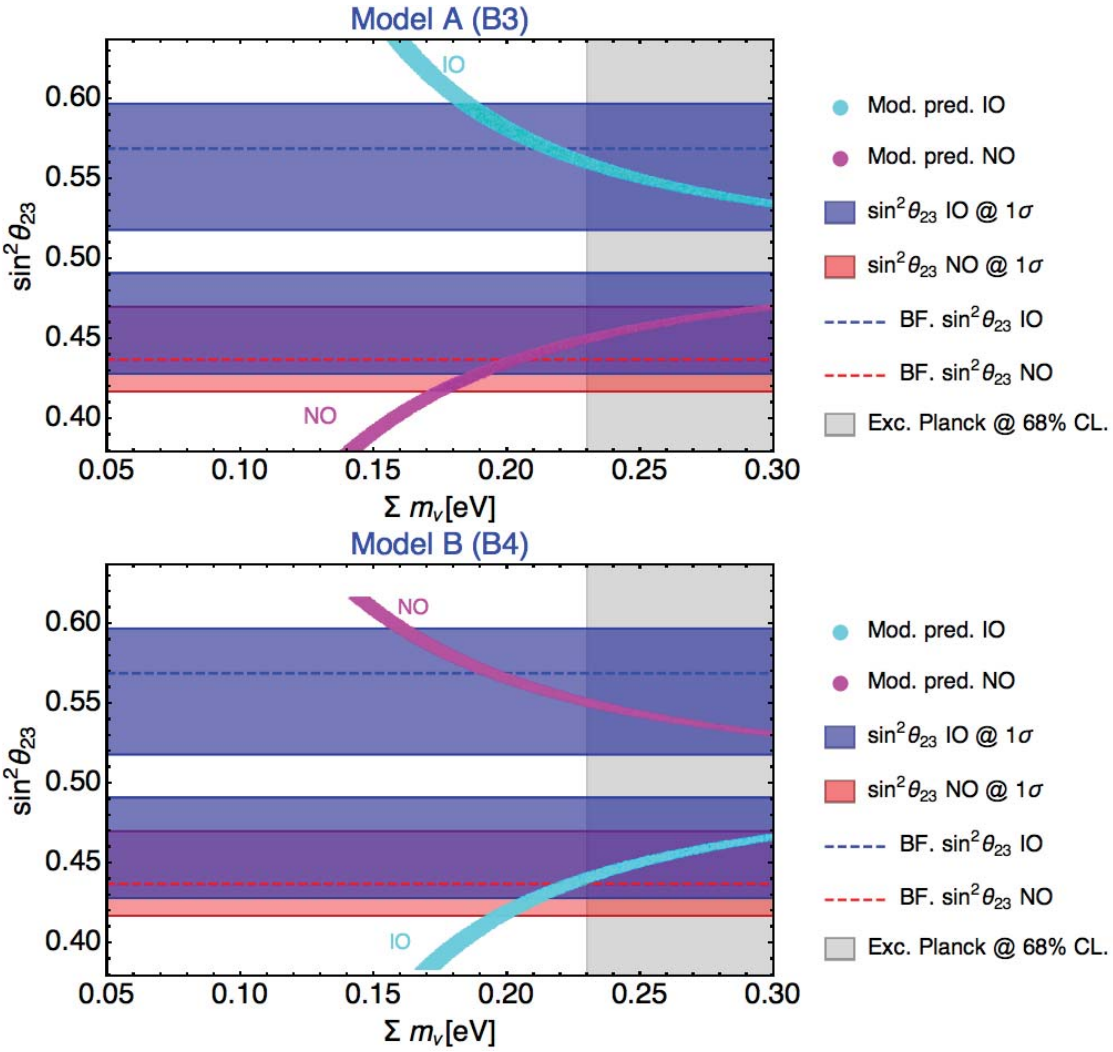

Fig. 2.3 *Correlation between* $\sin^2\theta_{23}$ *and the sum of the light neutrino masses,* $\sum m_\nu$*, in model A (with the* B_3 *texture) at the top and model B (with the* B_4 *texture) at the bottom, where NO (IO) allowed region is in magenta (cyan). The horizontal red (blue) shaded region correspond to the* 1σ *in* $\sin^2\theta_{23}$ *for NO (IO) from [123]. The case for IO has two* 1σ *regions in the data used. The red (blue) horizontal dashed line represents the best fit value in NO (IO) from [123]. The vertical grey shaded region is disfavoured by Planck data [124].*

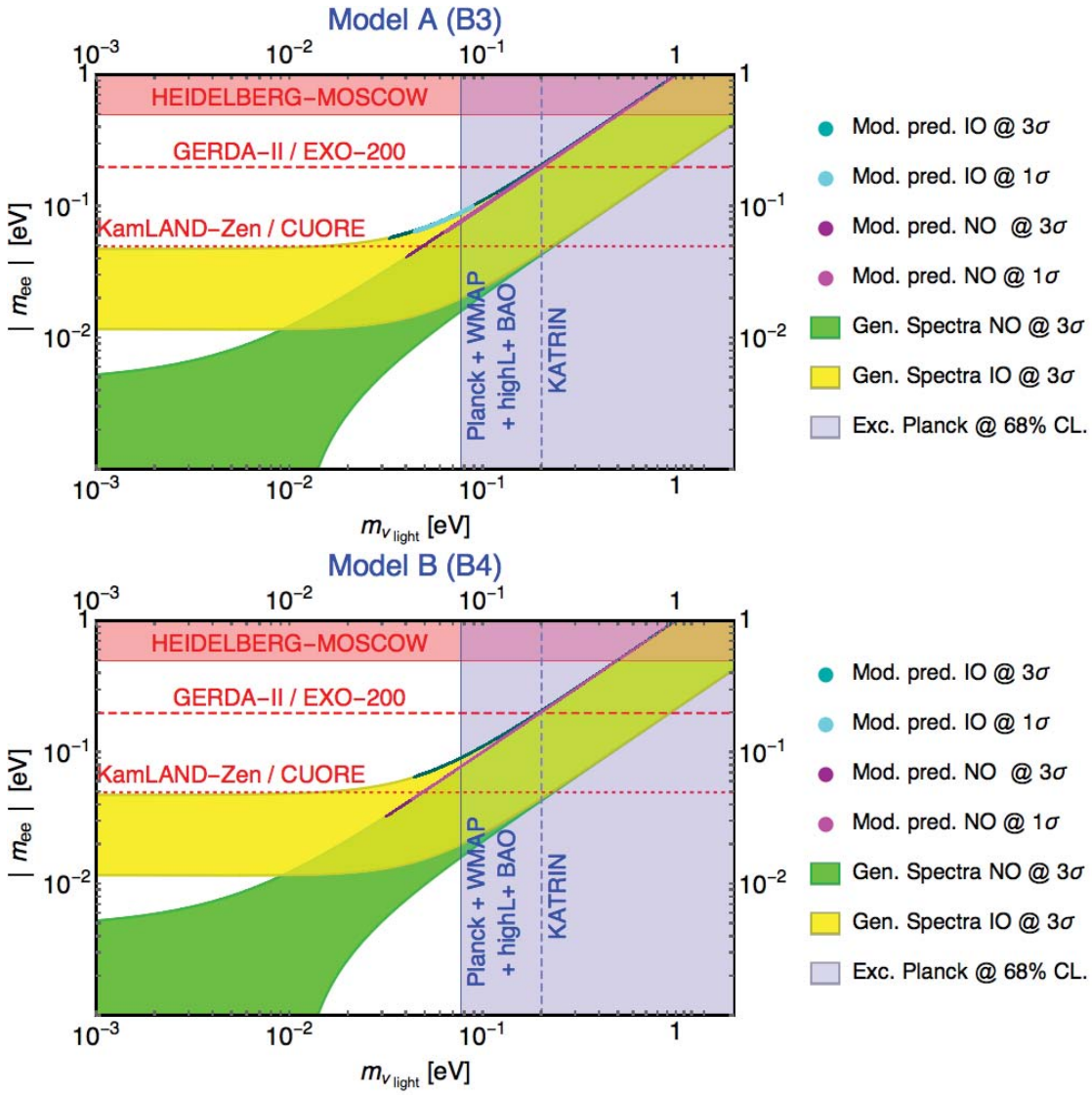

Fig. 2.4 *Effective* $0\nu\beta\beta$ *parameter* $|m_{ee}|$ *versus the lightest neutrino mass* $m_{\nu_{light}}$ *in model A (B) at the top (bottom). The* $m_{\nu_{light}}$ *is* $m_1 (m_3)$ *for NO (IO). The model allowed region for NO is in magenta (dark magenta) for the* 1σ *(*3σ*) atmospheric mixing angle and for IO in cyan (dark cyan) for the* 1σ *(*3σ*) atmospheric mixing angle region from [121]. The yellow (green) band correspond to the "flavour–generic" IO (NO) neutrino spectra at* 3σ*. The horizontal red shaded region is the experimental limit on* $0\nu\beta\beta$*, while the red (blue) horizontal (vertical) lines are the forthcoming experimental sensitivities on* $|m_{ee}|$ *(*$m_{\nu_{light}}$*) from [125–130]. The vertical blue shaded region is disfavoured by Planck data [124].*

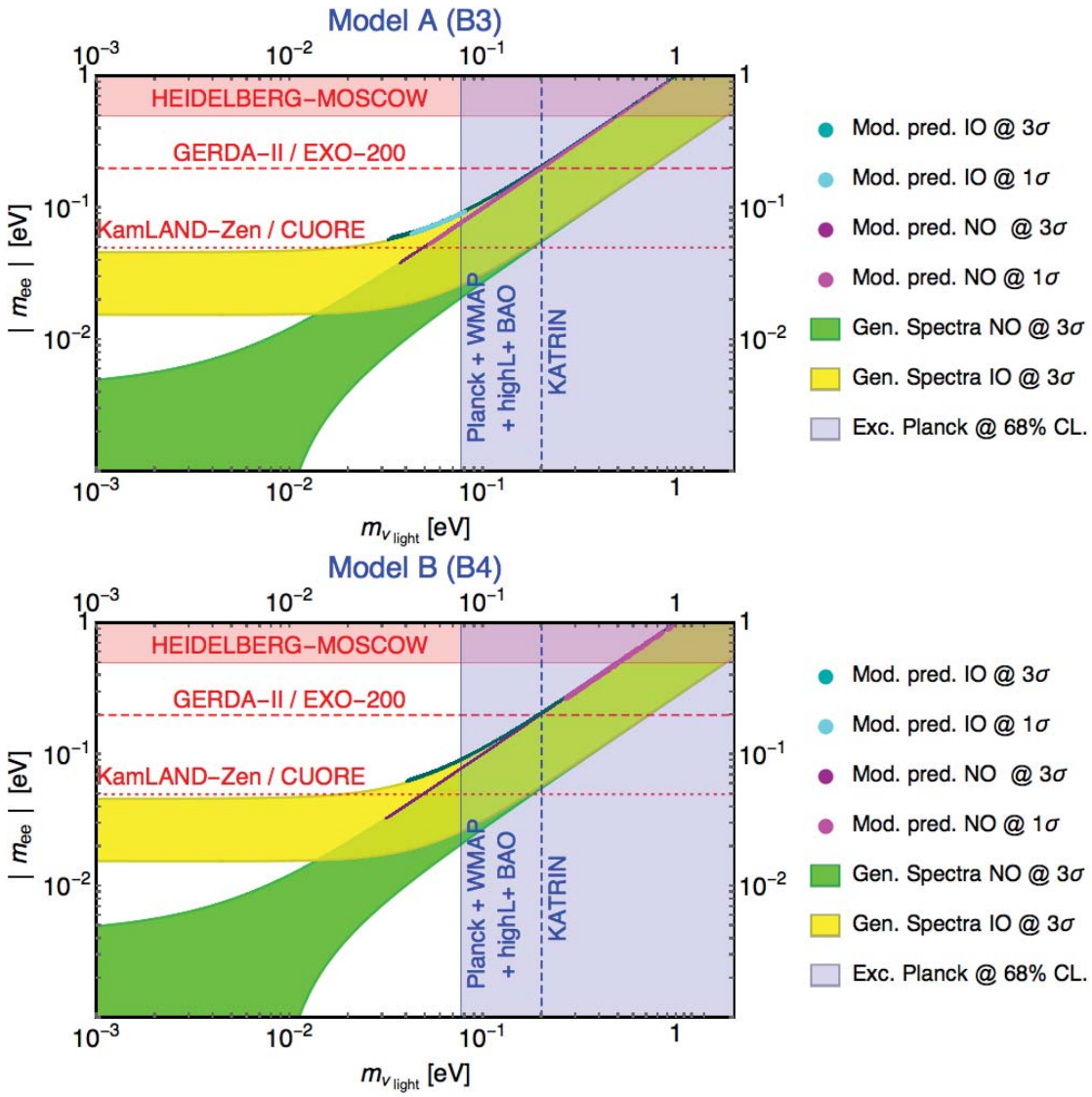

Fig. 2.5 *Effective* $0\nu\beta\beta$ *parameter* $|m_{ee}|$ *versus the lightest neutrino mass* $m_{\nu_{light}}$ *in model A (B) at the top (bottom). The* $m_{\nu_{light}}$ *is* $m_1(m_3)$ *for NO (IO). The* $m_{\nu_{light}}$ *is* $m_1(m_3)$ *for NO (IO). The model allowed region for NO is in magenta (dark magenta) for the* 1σ (3σ) *atmospheric mixing angle and for IO in cyan (dark cyan) for the* 1σ (3σ) *atmospheric mixing angle region from [122]. The yellow (green) band correspond to the "flavour–generic" IO (NO) neutrino spectra at* 3σ*. The horizontal red shaded region is the experimental limit on* $0\nu\beta\beta$*, while the red (blue) horizontal (vertical) lines are the forthcoming experimental sensitivities on* $|m_{ee}|$ $(m_{\nu_{light}})$ *from [125–130]. The vertical blue shaded region is disfavoured by Planck data [124].*

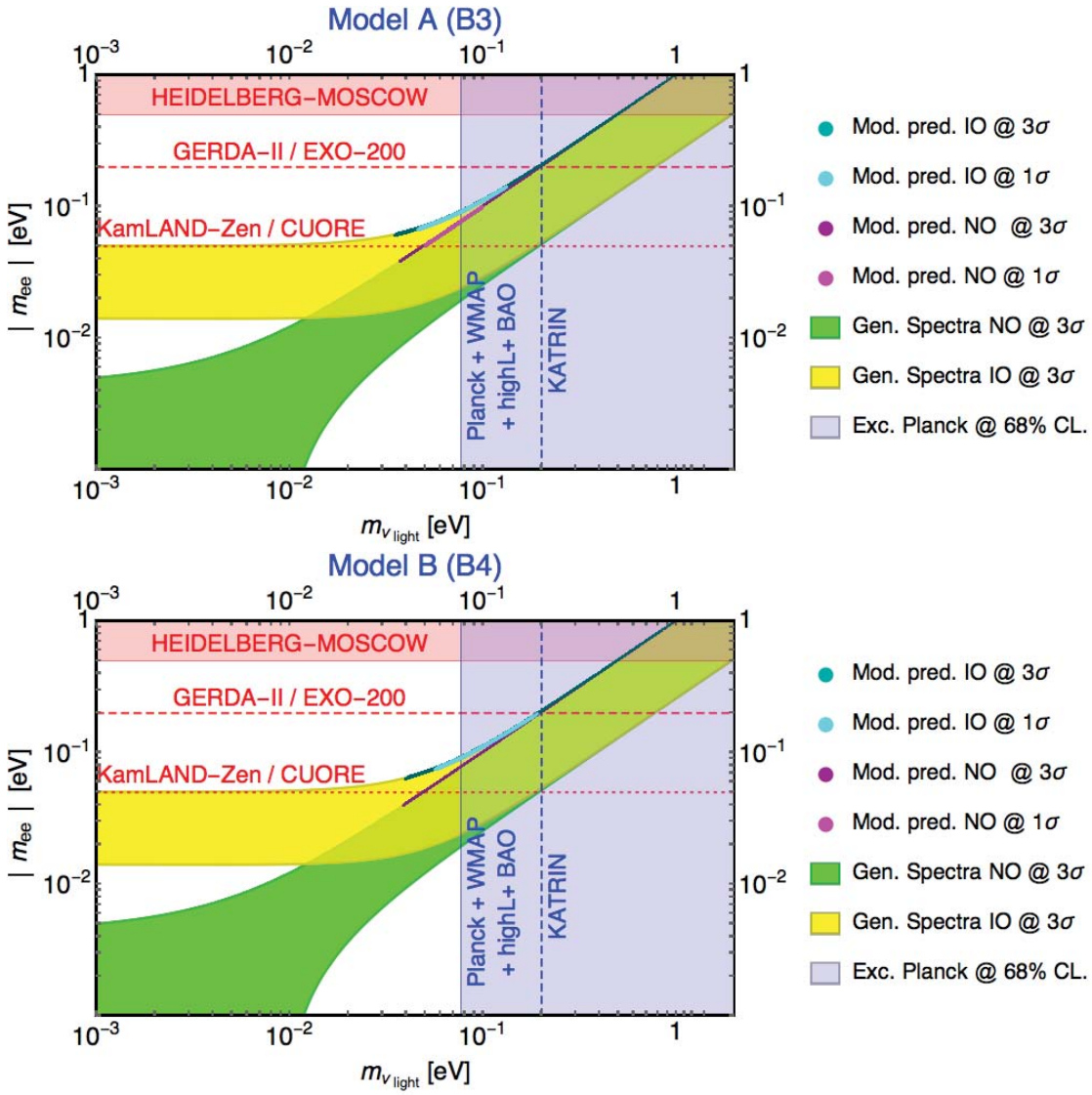

Fig. 2.6 *Effective* $0\nu\beta\beta$ *parameter* $|m_{ee}|$ *versus the lightest neutrino mass* $m_{\nu_{light}}$ *in model A (B) at the top (bottom). The* $m_{\nu_{light}}$ *is* $m_1(m_3)$ *for NO (IO). The model allowed region for NO is in magenta (dark magenta) for the* 1σ *(*3σ*) atmospheric mixing angle and for IO in cyan (dark cyan) for the* 1σ *(*3σ*) atmospheric mixing angle region from [123]. The yellow (green) band correspond to the "flavour–generic" IO (NO) neutrino spectra at* 3σ*. The horizontal red shaded region is the experimental limit on* $0\nu\beta\beta$*, while the red (blue) horizontal (vertical) lines are the forthcoming experimental sensitivities on* $|m_{ee}|$ *(*$m_{\nu_{light}}$*) from [125–130]. The vertical blue shaded region is disfavoured by Planck data [124].*

Chapter 3

Radiative Majorana neutrino mass generation and fermionic dark matter

In the following chapter, we will review a model where light Majorana neutrino masses arise radiatively at an one-loop level and a DM candidate emerges. This model is an extension of the Ma's Scotogenic model, where Z_2-odd particles enter in the loop generating neutrino masses and allowing two possible DM candidates: fermionic or scalar.

3.1 Preliminaries

The Scotogenic model [133] is a minimal extension of the SM where an exact Z_2 symmetry is imposed. The symmetry group is therefore enlarged to $SM \otimes Z_2$. This parity only charges additional particles to the SM particle content, in such way that active neutrinos get masses only at loop level. The parity also works as a stability mechanism for the particle DM candidates arising in the model.

	L	ℓ_R	H	η	N_i
$SU(2)_L$	**2**	**1**	**2**	**2**	**1**
Z_2	+	+	+	-	-

Table 3.1 *Relevant particle content and quantum numbers in Scotogenic model*

The model enhances the SM particle content by the addition of an extra $SU(2)_L$ scalar doublet η, and three generations of heavy RH neutrinos $\nu_{Ri} = N_i$, i $= \{1, 2, 3\}$. The particle

content and its assignments are shown in Tab. 3.1. As η is Z_2-odd and Z_2 is considered as a conserved symmetry, η cannot develop a *vev*, thus it is an inert doublet in the sense of [134].

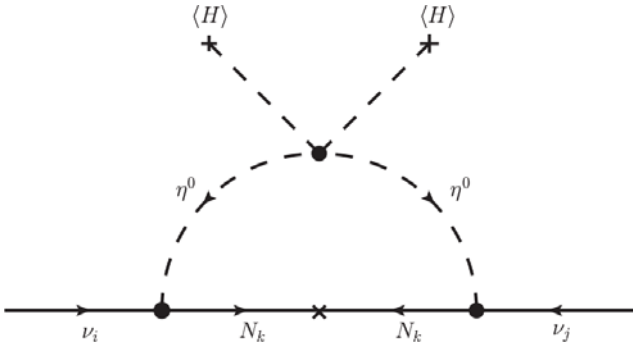

Fig. 3.1 *One-loop neutrino mass generation in Ma's Scotogenic model [133].*

There are no tree level mass terms for the active neutrinos. The Dirac mass term coming from the Yukawa interaction between the neutrinos and the SM Higgs H is forbidden by the Z_2-odd assignment of N_i, and the Yukawa interaction between neutrinos and η does not lead to a mass term as η is an inert doublet. The LH Majorana neutrinos acquire their masses through radiative corrections involving the Z_2-odd particles in the loop. The Feynman diagram in Fig. 3.1 shows the one-loop process.

From the particle content and assignments in Tab. 3.1, the relevant part of the Lagrangian is given by:

$$-\mathcal{L}_Y = Y^{\ell}\bar{L}H\ell + Y^{\nu}\bar{L}\tilde{\eta}N + \frac{1}{2}M_N\bar{N}^c N + h.c., \tag{3.1}$$

where the scalar $SU(2)_L$ doublets can be written as

$$H = \begin{pmatrix} H^+ \\ H^0 \end{pmatrix} \quad \text{and} \quad \eta = \begin{pmatrix} \eta^+ \\ \eta^0 \end{pmatrix}, \tag{3.2}$$

and $\tilde{\eta} = i\sigma^2\eta^*$. The Yukawa matrices $Y^{(\ell,\nu)}$ are 3×3 general complex matrices and M_N is the RH neutrino Majorana mass matrix.

The LH Majorana neutrino mass matrix is calculated from the one-loop diagram in Fig. 3.1 leading to:

$$(\mathcal{M}_\nu)_{ij} = \sum_k Y^{\nu}_{ik}Y^{\nu}_{jk}\Lambda_k \tag{3.3}$$

where Λ_k is a loop function, whose calculation is shown in the Appendix B.

The scalar potential, following the particle assignments in Tab. 3.1, is given by:

$$V = \mu_H^2 H^\dagger H + \mu_\eta^2 \eta^\dagger \eta + \frac{1}{2}\lambda_1 (H^\dagger H)^2 + \frac{1}{2}\lambda_2 (\eta^\dagger \eta) + \lambda_3 (H^\dagger H)(\eta^\dagger \eta) + \lambda_4 (H^\dagger \eta)(\eta^\dagger H) + \frac{1}{2}\lambda_5 \left[(H^\dagger \eta)^2 + (\eta^\dagger H)^2 \right], \quad (3.4)$$

where all the couplings λ_i are real, except for λ_5 if one considers the case of CP violation in scalar sector.

After EWSB, the iso-doublet η neutral component $\eta^0 \equiv \eta_R + i\,\eta_I$ and charged component $\eta^\pm$ acquire the tree level masses:

$$m_{\eta^\pm}^2 = \mu_\eta^2 + \lambda_3 v^2, \quad (3.5)$$

$$m_{\eta_R}^2 = \mu_\eta^2 + (\lambda_3 + \lambda_4 + \lambda_5) v^2, \quad (3.6)$$

$$m_{\eta_I}^2 = \mu_\eta^2 + (\lambda_3 + \lambda_4 - \lambda_5) v^2, \quad (3.7)$$

where $v = \langle H \rangle$. Notice that the mass squared splitting between the neutral components of the iso-doublet η is $m_{\eta_R}^2 - m_{\eta_I}^2 = 2\lambda_5 v^2$.

The DM candidates in the model are stable as Z_2 is a conserved symmetry. The DM could be either the lightest singlet fermion N_1 or the lightest neutral component of the scalar iso-doublet η. The case where η_R (or η_I) is the DM resembles the inert Higgs doublet model (IHDM), which has been studied in several works [135, 136]. Fig. 3.2 shows the relevant annihilation channels for the calculation of the relic abundance in the case of $\eta^0 = \eta_R$ or $\eta^0 = \eta_I$ as DM.

In the case of fermionic DM, the relevant annihilation channels in the calculation of the relic abundance are shown in Fig. 3.3. It is worth to mention that in order to have the right relic density, the Yukawa couplings relevant to these processes should be $\mathcal{O}(Y^\nu) \sim 1$. However, lepton flavour violating (LFV) processes as: $\mu \to e\,\gamma$, $\tau \to \mu\gamma$ and $\mu \to 3e$ are generated in the Scotogenic model at one-loop level in a process similar to the way neutrino mass is generated and depending on the same Yukawa couplings Y^ν. Therefore, experimental bounds on such LFV processes have provided several constraints over the viable parameter region for the fermionic DM in Scotogenic model. Even forthcoming experiments potentially could rule out the entire parameter region in the case of fermionic DM with no $\eta^0 - N_1$ co-annihilations.

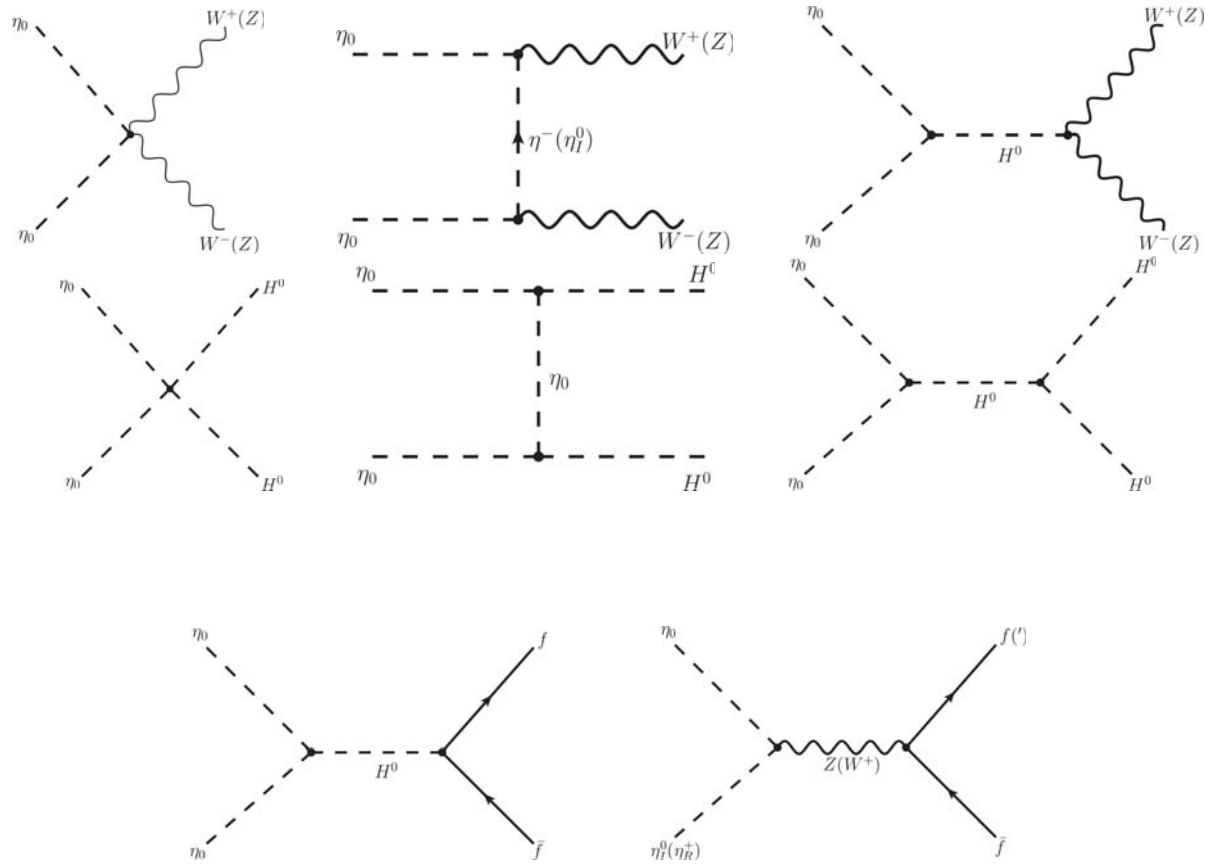

Fig. 3.2 *Relevant annihilation channels for scalar DM η_0 in Ma's Scotogenic model.*

3.2 The model

The model considered in [137] is an extension of the Scotogenic model motivated by the issues in generating the right relic density and at the same time being consistent with the LFV constraints in the case of fermionic DM. In this model a $\mathrm{SU(3)_C} \otimes \mathrm{SU(2)_L} \otimes \mathrm{U(1)_Y}$ singlet complex scalar field ϕ is added, such that when ϕ acquires a *vev.* $\langle\phi\rangle = v_\phi$ lepton number is broken and the RH neutrinos get masses dynamically. The addition of the scalar field opens up a new annihilation channel for the DM which relaxes the constraints in the Yukawa couplings for generating the right relic density.

The relevant particle content and quantum numbers are shown in Table 3.2. The scalar sector in the model consists in addition to the SM-like Higgs doublet, H, and the inert

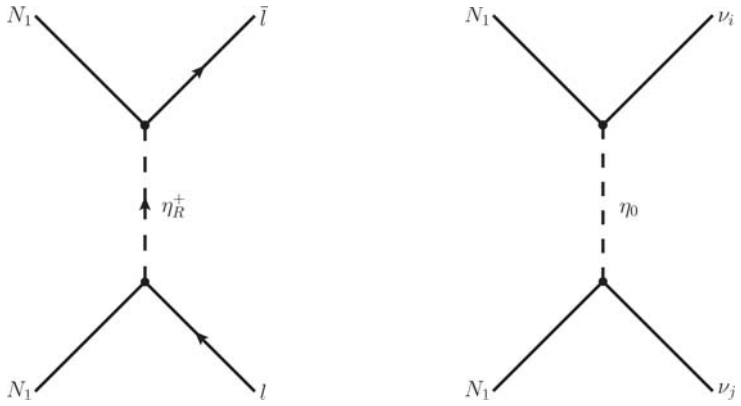

Fig. 3.3 *Relevant annihilation channel for fermionic DM N_1 in Ma's Scotogenic model.*

	$\bar{L}_i$	ℓ_i	H	η	N_i	ϕ
$SU(2)_L$	**2**	1	**2**	**2**	1	1
$U(1)_L$	1	-1	0	0	-1	2
Z_2	$+$	$+$	$+$	$-$	$-$	$+$

Table 3.2 *Summary of the relevant particle content and quantum numbers in the model.*

doublet η, of a SM singlet complex scalar field ϕ. The scalar fields are defined as:

$$H = \begin{pmatrix} H^+ \\ \frac{1}{\sqrt{2}}(v_h + h + i\,A) \end{pmatrix}, \quad \eta = \begin{pmatrix} \eta^+ \\ \frac{1}{\sqrt{2}}(\eta_R + i\,\eta_I) \end{pmatrix} \text{ and } \phi = \frac{1}{\sqrt{2}}(v_\phi + \phi_R + i\,\phi_I). \tag{3.8}$$

The lepton sector remains the same as in the Scotogenic model. This consist of LH doublets L_i, RH charged leptons ℓ_i and three additional RH Majorana neutrinos N_i, $i = \{1, 2, 3\}$. Where the three RH neutrinos allow the possibility for non-zero masses for the three active neutrinos. The Z_2 symmetry remains the same as in the Scotogenic model, where it only charges the RH neutrinos N_i and the inert iso-doublet η.

Considering the matter content shown in Table 3.2, the relevant part of Lagrangian is given by:

$$\mathcal{L}_{\rm Y} = Y^\ell_{ij}\,\bar{L}_i H \ell_j + Y^\nu_{ij}\,\bar{L}_i \tilde{\eta} N_j + h^\phi_{ij}\,\phi\,\bar{N}^c_i N_j + \text{ h.c.}, \tag{3.9}$$

with $\tilde{\eta} = i\tau_2\eta^*$ and $i = \{1, 2, 3\}$. The Yukawa coupling matrices Y^ν and the singlet scalar–RH neutrinos Yukawa coupling matrix h^ϕ_{ij} are hereafter assumed to be real and diagonal. Then,

$$Y^\nu_{ij} = Y^\nu_i \delta_{ij} \qquad \text{and} \qquad h^\phi_{ij} = h_{N_i}\delta_{ij}.$$

The breaking of the global $U(1)_L$ is generated dynamically by the gauge singlet scalar field ϕ, which has being assigned with $L = 2$. After the lepton number breaking, ϕ acquires a *vev.* and the RH neutrinos get Majorana masses dynamically. Form the last term in Eq. (3.9), we have that such masses are

$$m_{N_i} = \sqrt{2}\, v_\phi\, h_{N_i}. \tag{3.10}$$

The scalar potential for the model enhances the Scotogenic model scalar potential in Eq. (3.4) as:

$$\begin{aligned} V = {} & \mu_1^2 H^\dagger H + \mu_2^2 \eta^\dagger \eta + \mu_3^2 \phi^\star \phi + \lambda_1 (H^\dagger H)^2 + \lambda_2 (\eta^\dagger \eta)^2 + \lambda_3 (\eta^\dagger \eta)(H^\dagger H) \\ & + \lambda_4 (\eta^\dagger H)(H^\dagger \eta) + \frac{\lambda_5}{2}\left((\eta^\dagger H)^2 + (H^\dagger \eta)^2\right) + \lambda_6 (\phi^\star \phi)^2 \\ & + \lambda_7 (\phi^\star \phi)(H^\dagger H) + \lambda_8 (\phi^\star \phi)(\eta^\dagger \eta). \end{aligned} \tag{3.11}$$

We have assumed no contribution from the scalar sector into the CP violation. Therefore, all the quartic couplings λ_i and *vevs.* $v_{h,\phi}$ are considered real.

After EWSB, the neutral CP-even part of the iso-doublet H and the CP-even part of the gauge singlet ϕ mix. Then, the physical fields labelled as h_1 and h_2, where h_1 is the SM Higgs with $m_{h_1} \approx 125$ GeV and $\langle H \rangle = v_h \approx 246$ GeV, while h_2 is an additional neutral scalar field. The $h - \phi_R$ mixing is parametrised by a rotation matrix with angle θ as:

$$\begin{pmatrix} h \\ \phi_R \end{pmatrix} = \begin{pmatrix} \cos\theta & \sin\theta \\ -\sin\theta & \cos\theta \end{pmatrix} \begin{pmatrix} h_1 \\ h_2 \end{pmatrix}. \tag{3.12}$$

The tree level masses of the fields h_1 and h_2 are calculated from the potential Eq. (3.9) leading after EWSB to:

$$m_{h_1}^2 = v_h^2 \lambda_1 + v_\phi^2 \lambda_6 + \sqrt{v_h^2 v_\phi^2 \lambda_7^2 + (v_h^2 \lambda_1 - v_\phi^2 \lambda_6)^2}, \tag{3.13}$$

$$m_{h_2}^2 = v_h^2 \lambda_1 + v_\phi^2 \lambda_6 - \sqrt{v_h^2 v_\phi^2 \lambda_7^2 + (v_h^2 \lambda_1 - v_\phi^2 \lambda_6)^2}. \tag{3.14}$$

Additionally, the tree level masses of the charged and neutral CP-even and CP-odd components of the inert doublet η split as:

$$m^2_{\eta^\pm} = \mu_2^2 + \frac{\lambda_3}{2} v_h^2 + \frac{\lambda_8}{2} v_\phi^2, \tag{3.15}$$

$$m^2_{\eta_R} = \mu_2^2 + \frac{\lambda_3 + \lambda_4 + \lambda_5}{2} v_h^2 + \frac{\lambda_8}{2} v_\phi^2, \tag{3.16}$$

$$m^2_{\eta_I} = \mu_2^2 + \frac{\lambda_3 + \lambda_4 - \lambda_5}{2} v_h^2 + \frac{\lambda_8}{2} v_\phi^2. \tag{3.17}$$

The η neutral components squared mass splitting is $\lambda_5 v_h^2 = (m^2_{\eta_R} - m^2_{\eta_I})$.

Finally, the CP-odd component of the gauge singlet scalar field, ϕ_I, will be the Nambu–Goldstone boson, also known as Majoron, associated with the symmetry breaking of the global lepton number, $U(1)_L$. This breaking triggers the neutrino mass generation. The

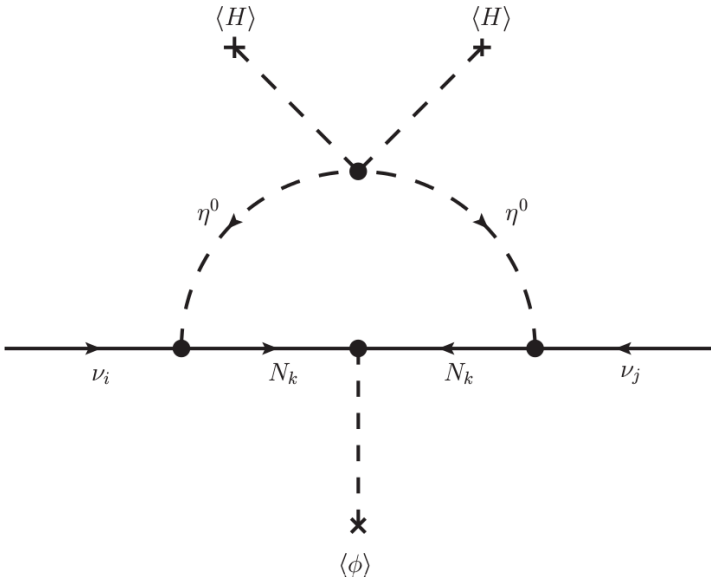

Fig. 3.4 *One-loop neutrino mass generation in the model.*

LH neutrinos acquire masses at the one-loop level, as in the Scotogenic model, mediated by the Z_2-odd particles. The neutrino mass matrix can be calculated from the diagram in Fig. 3.4 giving [133, 138]:

$$(\mathcal{M}_\nu)_{ij} = \sum_k Y^\nu_{ik} \Lambda_k Y^\nu_{jk} \tag{3.18}$$

with the loop function:

$$\Lambda_k = \frac{m_{N_k}}{2(4\pi)^2}\left[\frac{m^2_{\eta_R}}{m^2_{\eta_R}-m^2_{N_k}}\log\frac{m^2_{\eta_R}}{m^2_{N_k}} - \frac{m^2_{\eta_I}}{m^2_{\eta_I}-m^2_{N_k}}\log\frac{m^2_{\eta_I}}{m^2_{N_k}}\right]. \tag{3.19}$$

The LH Majorana neutrino mass matrix, Eq. (3.18), has three key approximations. If we denote $m_0^2 := (m^2_{\eta_R} + m^2_{\eta_I})/2$, then we have:

1. If $m_0^2 \ll m^2_{N_k}$ and the splitting $\lambda_5 v_h^2 \ll m_0^2$, then

$$(\mathcal{M}_\nu)_{ij} \simeq \frac{\lambda_5 v_h^2}{8\pi^2}\sum_k \frac{Y^\nu_{ik}Y^\nu_{jk}}{m_{N_k}}\left[\log\frac{m^2_{N_k}}{m_0^2} - 1\right]. \tag{3.20}$$

2. If $m_0^2 \gg m_k^2$ and the splitting $\lambda_5 v_h^2 \ll m_0^2$, then

$$(\mathcal{M}_\nu)_{ij} \simeq \frac{\lambda_5\, v_h^2}{8\pi^2}\sum_k Y^\nu_{ik}Y^\nu_{jk}\frac{m_{N_k}}{m_0^2}. \tag{3.21}$$

3. Finally, if $m_0^2 \simeq m^2_{N_k}$, then

$$(\mathcal{M}_\nu)_{ij} \simeq \frac{\lambda_5 v_h^2}{16\pi^2}\sum_k \frac{Y^\nu_{ik}Y^\nu_{jk}}{m_{N_k}}. \tag{3.22}$$

In the case where the dark matter candidate is the singlet fermion N_1, the DM self-annihilation t-channel is the same as in the Scotogenic model, shown in Fig. 3.3. However, the addition of the gauge singlet scalar field, ϕ, to the model opens two new annihilation channel for the DM. The first one is a new t-channel shown up in Fig. 3.5. Such t-channel contributes mostly to the self-annihilation of DM into dark radiation, Goldstone boson ϕ_I, as discussed for instance in [139]. Such dark radiation is severely constrained by Cosmological data to be not very abundant. Thus, we will try to suppress this channel and focus our attention in the another new annihilation channel. After EWSB, the new scalar mixes with the SM Higgs, resulting in a s-channel annihilation of dark matter to SM particles shown bottom in Fig. 3.5. This new annihilation s-channel relaxes the constraint on the Y^ν Yukawa couplings coming from dark matter relic density below the bounds set by LFV processes without the need of DM-inert scalar $(N_1 - \eta_{R,I})$ co-annihilation. We will shown this in following sections.

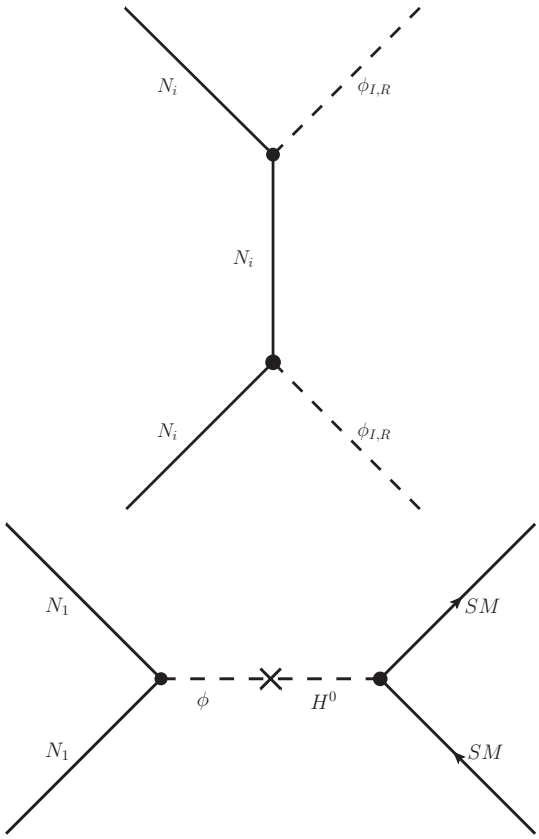

Fig. 3.5 *New annihilation channels for fermionic DM, N_1, in the model. Up: t-channel. Down: s-channel resonance.*

3.3 Constraints

In the following section, we will discuss the constraints we have implemented in the analysis of our model. These come form theoretical as well as experimental considerations.

Theoretical constraints

The perturbative nature of the scalar potential quartic couplings, Eq. (3.11), and the Yukawa couplings in the Lagrangian, Eq. (3.9), require:

$$|\lambda_i|,\ |h_{N_i}|^2,\ |Y_i^\nu|^2 \lesssim \sqrt{4\pi}. \tag{3.23}$$

Furthermore, stability of the scalar potential is guaranteed if it is bounded from bellow, then the vacuum has a minimum. This leads to the couplings of the scalar potential, Eq. (3.11), must follow [140]:

$$\lambda_1, \lambda_2, \lambda_6 \geq 0, \tag{3.24}$$

$$\lambda_3 \geq -2\sqrt{\lambda_1 \lambda_2}, \tag{3.25}$$

$$\lambda_3 + \lambda_4 - |\lambda_5| \geq -2\sqrt{\lambda_1 \lambda_2}, \tag{3.26}$$

$$4\,\lambda_1\,\lambda_6 \geq \lambda_7^2, \tag{3.27}$$

$$4\,\lambda_2\,\lambda_6 \geq \lambda_8^2. \tag{3.28}$$

Experimental constraints

The following constraints we considered as experimental, as they are derived from experiments directly or indirectly.

Dark matter relic density: The Planck global fit of CMB temperature anisotropies, using low multipoles and lensing data combined with spatial distribution of the galaxies (BAO), constrains the dark matter relic density to be [124]:

$$\Omega_{\rm DM} h^2 = 0.1186 \pm 0.0020, \quad \text{at } 68\% \text{ c.l.}, \tag{3.29}$$

with h the Hubble constant in units of 100 Km/s/Mpc.

Gauge boson widths: Several measurements have precisely determined the gauge boson widths [24]. In order to avoid altering the value of such widths from their SM values, we have kinematically forbid the decay of W and Z into the inert scalars: η_R, η_I and $\eta^\pm$. This condition impose that the masses satisfy:

$$\begin{aligned} m_Z &< m_{\eta_R} + m_{\eta_I}, \qquad & m_W &< m_{\eta^\pm} + m_{\eta_I}, \\ m_Z &< 2\, m_{\eta^\pm}, \qquad & m_W &< m_{\eta^\pm} + m_{\eta_R}. \end{aligned} \tag{3.30}$$

Scalar mass constraints from LEP: In the context of the inert Higgs doublet model, an analysis of LEP-II data [141] allows charged and neutral inert scalar field masses above:

$$m_{\eta^\pm} > 135 \text{ GeV}, \quad \min\{m_{\eta_R}, m_{\eta_I}\} > 100 \text{ GeV}. \tag{3.31}$$

Higgs width and branching to invisible decays: From LHC data, the branching ratio of SM Higgs to invisible decays has an upper bound of 28% and its total width an upper bound at 13 MeV, both at 95% CL [24]. In our model, the SM Higgs h_1 always can decay into pair of Majorons, $h_1 \to \phi_I\ \phi_I$. When $m_{N_i} < m_{h_1}/2$ into a pair of RH neutrinos, $h_1 \to N_i\ N_i$, which contribute to the Higgs invisible decay and enhances its width. In addition, when kinematically allowed $m_{h_2} < m_{h_1}/2$, the SM Higgs can decay into a h_2 pair, $h_1 \to h_2\ h_2$, leading to a further enhancement of its decay width and depending on the h_2 width and decays could contribute to the SM Higgs invisible channel. Thus, in our analysis of the Higgs phenomenology we have followed the constraints derived in [139] which lead to a bound in the mixing parameter

$$\sin\theta < 0.2. \tag{3.32}$$

Electroweak precision parameters S and T: The additional $SU(2)_L$ iso-doublet η and the mixing of the flavon ϕ with the SM Higgs contribute to the W and Z self-energies. The deviations from SM are parametrised by the S, T and U [142, 143]. In the appendix C, we have calculated the S and T parameters, following [144], and used the bounds set by the electroweak global fits constraints taking $U = 0$ [24]:

$$-0.1 < S < 0.3, \quad -0.1 < T < 0.25, \tag{3.33}$$

to constrain the model parameter region.

Direct detection of dark matter: Dark matter direct detection experiments have set bounds over the dark matter-nucleon scattering cross section. For the spin-independent (SI) process in a dark matter mass range from 10 GeV to 10 TeV, the most stringent bound is set by PandaX-II 54 ton-day results [145]. The lowest bound value is set at $\sigma_{SI} \lesssim 8.6 \times 10^{-47}$ cm^2 for a dark matter mass of 40 GeV.

Indirect detection of dark matter: Astronomical gamma ray observations constrain the velocity averaged cross section of dark matter annihilation into gamma rays $\langle\sigma v\rangle_\gamma$. The search for gamma rays with the Fermi-LAT satellite has constrained $\langle\sigma v\rangle_\gamma \lesssim 10^{-29}\text{cm}^3\text{s}^{-1}$ [146].

Lepton flavour violating processes: In the Scotogenic model, it is known that the cross section of the LFV processes such as the radiative decays $\mu \to e\gamma$ and the decay $\mu \to ee$ are proportional to the Yukawa coupling between the inert Higgs and RH neutrinos. Experimental bounds on these LFV processes translate into stringent limits over the Yukawa couplings Y^ν in the case of fermionic dark matter without co-annihilation with the inert scalars [147, 148]. In our analysis, we have considered the same experimental bounds on

the LFV processes $l' \to \gamma\, l$ and $l' \to 3l$, with $l, l' = \{e, \mu, \tau\}$ as in [147, 148] for comparison with the Scotogenic model.

3.4 Results and discussion

In the analysis of the model, we have performed a numerical scan over the model parameter space using MicrOMEGAS [149]. The model has in total 12 independent parameters, which have been scanned over the intervals:

$$10^{-5} \leq |\lambda_{2,8}| \leq 1, \qquad 10^{-6} \leq \lambda_5 \leq 1, \tag{3.34}$$

$$10^{-4} \leq \sin\theta \leq 0.2, \qquad 10 \text{ GeV} \leq m_{h_2} \leq 1 \text{ TeV}, \tag{3.35}$$

$$100 \text{ GeV} \leq m_{\eta_0} \leq 5 \text{ TeV}, \qquad 135 \text{ GeV} \leq m_{\eta^\pm} \leq 5 \text{ TeV}, \tag{3.36}$$

$$10^{-5} \text{ eV} \leq m_{\nu_1} \leq 0.07 \text{ eV}, \qquad 100 \text{ GeV} \leq m_{N_{2,3}} \leq 5 \text{ TeV}, \tag{3.37}$$

$$10 \text{ GeV} \leq m_{N_1} \leq 1 \text{ TeV} \qquad 500 \text{ GeV} \leq v_\phi \leq 100 \text{ TeV}. \tag{3.38}$$

Such parameter ranges choice obeys the theoretical and the most straightforward experimental constraints discussed previously. The remaining experimental constraints, are calculated for each point and then filtered in our scan. We have also assumed a normal ordering (NO) for LH neutrino masses and used the best fit values for the mixing angles and squared mass differences from the global fit given by [24]. In addition, we have taken into account the Planck limit for the sum of the active neutrino masses ($\sum m_\nu \lesssim 0.23$ eV), which sets the upper bound on the lightest neutrino mass $m_{\nu_1} \lesssim 0.07$ eV.

Choosing a normal ordering for the LH neutrinos, we obtain the same ordering for the RH neutrinos. Then, N_1 is the lightest dark fermion. In order to have fermionic dark matter, we have set the inert scalar masses to be heavier than the heaviest RH neutrino, N_3. Furthermore, we have set the dark sector masses to be at least 10% heavier than N_1, avoiding the co-annihilation enhancements. The gauge singlet scalar *vev.*, v_ϕ, range is chosen so that the Yukawa couplings h_{N_i} in Eq. (3.10) are perturbative and not unnaturally small.

In Fig. 3.6 we have plotted the dark matter thermal averaged velocity annihilation cross section to gammas $\langle\sigma v\rangle_\gamma$ and the dark matter-nucleon spin independent (SI) scattering cross section σ_{SI} as a function of dark matter mass m_{N_1}. We have found that the dark

matter annihilation into gammas lies below the Fermi bound for most of the generated points, therefore this observable does not further constrain the model. For the nucleon–dark matter spin independent scattering cross section, we have found some points above the experimental bound set by PandaX–II. However, this bound does not represent any stringent constraint in the model, as one can generate points bellow the bound without any tuning of the parameters.

In Fig. 3.7 we have plotted the total decay width of the SM Higgs Γ_{h_1} as a function of the dark matter mass m_{N_1} at the top and as a function of the sine of the mixing angle at the bottom. The 6 MeV value corresponds to the SM Higgs width prediction. Points above this value represent parameter space points where additional decay channels enhance the SM Higgs width.

In Fig. 3.8 we have shown the correlation between the SM Higgs branching to invisible as a function of $\sin\theta/v_\phi$. As mentioned before, the model introduces the decay modes: $h_1 \to \phi_I\ \phi_I$, $h_1 \to N_1\ N_1$ as well as $h_1 \to h_2 h_2$. The process is always present, but is controlled by $\sin\theta/v_\phi$. The other decays modes, when kinematically allowed, depends on the Yukawa coupling to dark matter $h_{N_1}\sin\theta$ in the first case and on $\sin\theta\cos\theta/v_\phi$ in the latter. The SM Higgs branching to invisible is correlated in all the cases to $\sin\theta/v_\theta$ as shown in the Fig. 3.8.

In Fig. 3.9 we have shown at the top the lightest active neutrino mass m_{ν_1} against the dark matter mass m_{N_1}. The full range of neutrino masses is allowed by the constraints and any DM mass value. At the bottom, we have plotted the inert Higgs – neutrinos Yukawa couplings, Y_i^ν, against the gauge singlet scalar–dark matter Yukawa coupling, h_{N_1}. Notice that the Yukawas Y_i^ν range between 10^{-6} – 10^{-2}, showing that the addition of the new dark matter annihilation channel relaxes the LFV constraints over these Yukawa couplings.

Finally, in Fig. 3.10 we show the dependence of $\sigma_{\rm SI}$ with the Yukawa coupling h_{N_1}. As one can see, this new annihilation channel, Higgs portal in Fig. 3.5, whose effective coupling is $h_{N_1}\sin\theta$, dominates over the Scotogenic channels (Fig. 3.3) the dark matter spin-independent scattering cross section.

3.5 Conclusion

In this work, we have extended the Scotogenic model to include an additional gauge singlet scalar ϕ which spontaneously gives masses to the RH neutrinos. The lightest RH neutrino has been considered to be the dark matter candidate. The new scalar mixes with the SM Higgs doublet, introducing a Higgs portal to dark matter. This portal enhances dark matter annihilation in the early universe, relaxing the tension between the constraints of LFV processes and the DM relic density existing in the Scotogenic model. We present a numerical analysis of the parameter space of the model confirming this hypothesis. Unfortunately, the addition of this new channel also gives an important contribution of dark matter annihilating into the Nambu–Goldstone boson ϕ_I, associated with the breaking of lepton number, as well as SM Higgs decaying into ϕ_I. In order to avoid these phenomena, we need a slight fine-tuning in the parameters.

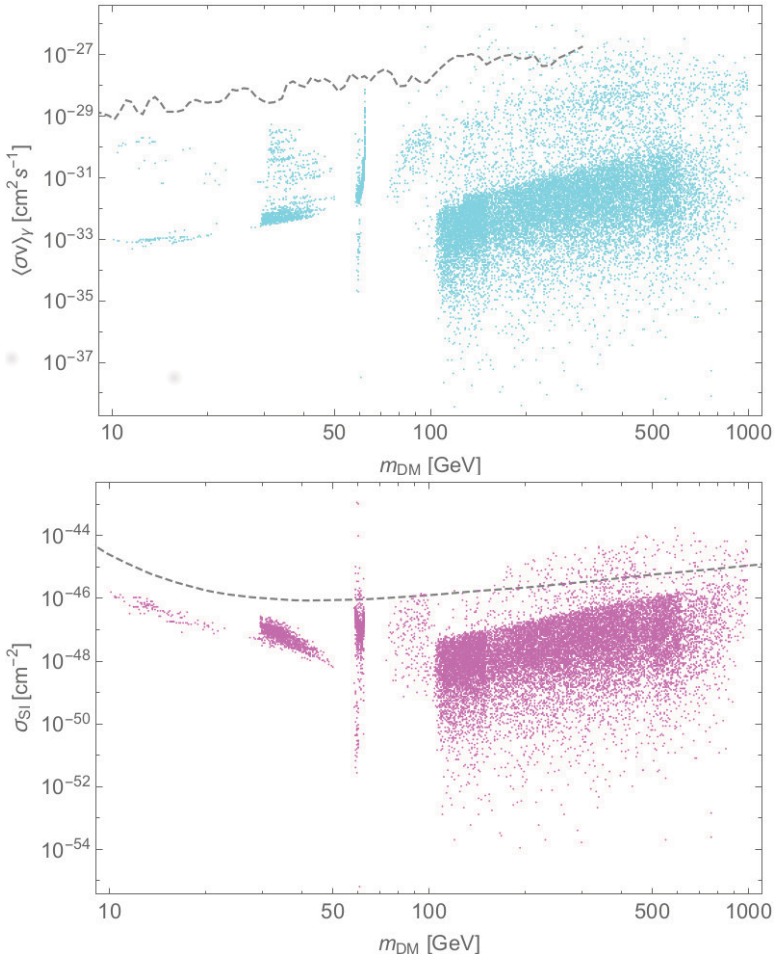

Fig. 3.6 *Up: Dark matter velocity averaged annihilation cross section to gammas* $\langle\sigma v\rangle_\gamma$ *as a function of the dark matter mass* m_{N_1}*. The Fermi-LAT [146] indirect detection exclusion curve is shown in blue. Bottom: Dark matter–nucleon spin independent scattering cross section* σ_{SI} *as a function of dark matter mass* m_{N_1}*. The PandaX–II [145] 54 ton-day exclusion curve is shown in blue.*

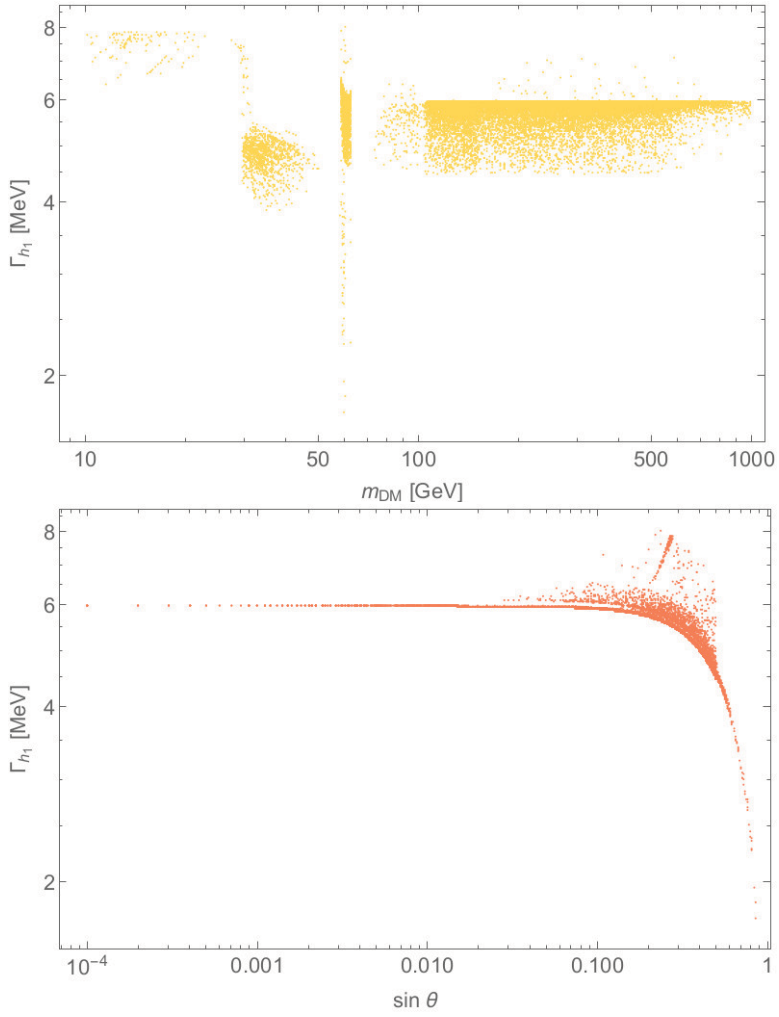

Fig. 3.7 *Up: SM Higgs total width* Γ_{h_1} *as a function of dark matter mass* m_{N_1}. *Bottom: SM Higgs total width* Γ_{h_1} *as a function of the mixing parameter* $\sin\theta$.

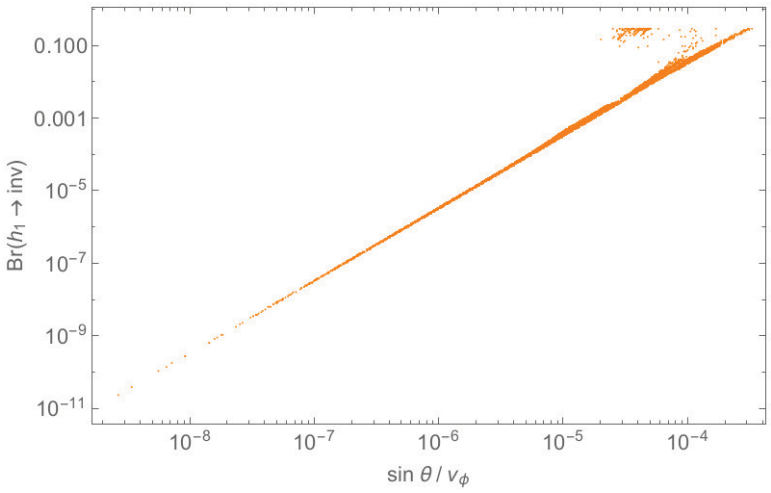

Fig. 3.8 *Correlation between the of SM Higgs branching ratio to invisible* $Br(h_1 \to inv)$ *and the effective coupling* $\sin\theta/v_\phi$.

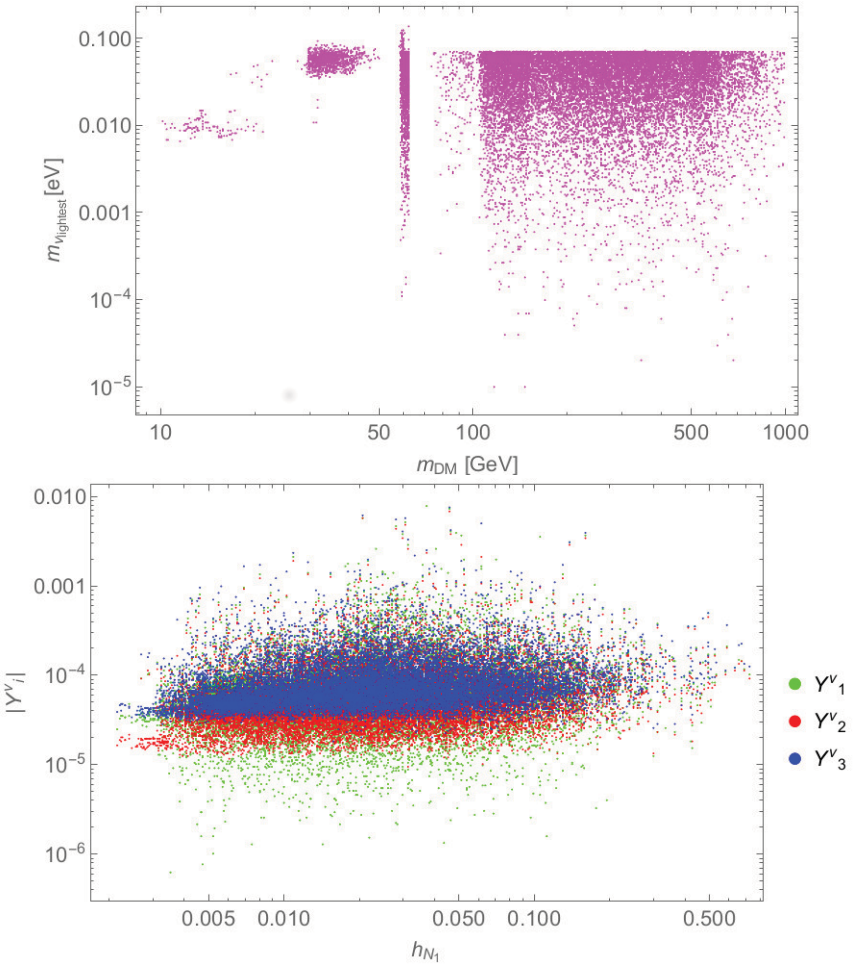

Fig. 3.9 *Up: lightest LH neutrino mass m_{ν_1} as a function of dark matter mass m_{N_1}. Bottom: gauge singlet scalar–dark matter Yukawa coupling h_{N_1} as a function of inert Higgs–neutrinos Yukawa couplings Y_i^{ν}.*

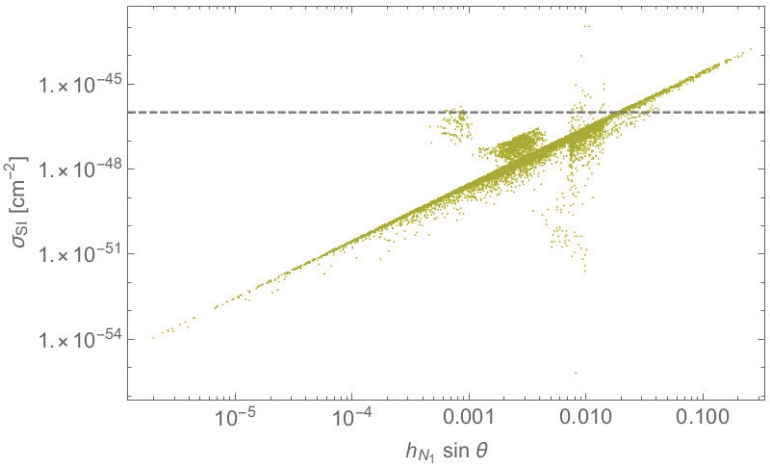

Fig. 3.10 *Correlation between the dark matter spin-independent scattering cross section* σ_{SI} *as a function of the Higgs portal effective coupling* h_{N_1}.

Chapter 4

A_4 flavour symmetric model for a type-II Dirac neutrino seesaw

In this chapter, we present an extension of the SM with an underlying flavour symmetry such that natural small Dirac masses for the neutrinos could be generated in an analogous way to the type-II seesaw for Majorana neutrinos. The non-abelian discrete group A_4 is chosen as flavour symmetry in addition with the product of discrete abelian cyclic groups $Z_3 \otimes Z_2$. Where the Z_3 ensures the "diracness" of the neutrinos at higher order operators and loop corrections and Z_2 forbids the tree level Dirac neutrino mass term. The model has the interesting feature of partially addressing the flavour problem: explaining the quarks and leptons mass hierarchies and mixing pattern in each sector. Notably, the model addresses the former, via the prediction of a flavour-dependent mass relation between charged leptons and down-type quarks.

4.1 Preliminaries

Given their colour and charge neutrality, neutrinos have been theorised as Majorana [50] fermions and exploited this fact to construct mechanisms generating natural small Majorana masses. Such mechanisms include the canonical seesaw realisations [50, 46, 48, 150, 54] and radiative processes [61, 62, 65, 64, 133]. However, as was mentioned in chapter 1 via the black-box theorem [43, 44], the neutrinoless double beta decay detection would provide the only robust way to establish the Majorana nature of neutrinos. Even though, such process

has not yet been detected [151, 129, 125, 126], suggesting the possibility for neutrinos to be Dirac fermions.

On the other hand, a full quark–lepton correspondence within the SM and extensions, suggests neutrinos to be Dirac fermions and the lepton mixing matrix completely analogous to the CKM matrix. Moreover, the existence of RH states, required for Dirac masses, may be necessary in order to have a consistent high energy completion, or for realising a higher symmetry such as the gauged B–L symmetry, present in the conventional $SO(10)$ seesaw scenarios, see for instance [54].

Dirac neutrinos within the SM can be generated by just adding three RH neutrinos, and generating neutrino masses though Higgs mechanism via Yukawa interaction term, Eq. (1.26)

$$\Gamma^{\nu}\, \bar{L}\, H^{c}\, \nu_{R}.$$

However, in this way, one has two issues. The first, as the RH neutrinos are SM singlets, their Majorana mass terms $M_R \bar{\nu}_R^c \nu_R$ are allowed, and then neutrinos will become Majorana. Therefore, there has to exist some additional mechanism forbidding such Majorana mass terms and protects the Dirac nature of neutrinos or "diracness". The second issue, as mentioned in chapter 1, is that there is no explanation about the suppression of neutrino Yukawa couplings, $Y^{\nu} \lesssim \mathcal{O}(10^{-11})$.

Nevertheless, there exist natural ways to generate small Dirac neutrino masses in extensions of the SM, which are analogous to the Majorana seesaw mechanisms. One can write down a generalised dimension-5 operator, Eq. (1.52), generating Dirac neutrino masses and finding its high energy realisations. It has been shown that Dirac seesaw mechanisms exist within the type I [152, 71, 72], as well as type-II [69, 153, 154] realisations, and even also the possibility of having radiative Dirac neutrino mass models [155–157]. A brief classification for the Dirac seesaw is shown in [158–160].

In addition, the need of a new unbroken symmetry protecting the diracness of the neutrinos has several possibilities which involve an extra $U(1)$ [74, 68] or its discrete subgroups Z_N [69, 155] or flavour symmetries [72, 73]. In the following, we will discuss a particular realisation for these possibilities.

4.2 The model

In this section, we will explain the details in the construction of the model where we have considered the possibility of Dirac neutrinos resulting from a family symmetry construction, in which small neutrino masses arise dynamically via a type-II seesaw mechanism for Dirac neutrinos. This setup complements the idea of having Dirac neutrinos arising from flavour symmetries proposed in [161].

The tree level completion of the generalised dimension-5 operator in Eq. (1.52),

$$\mathcal{O}_5 = \frac{g}{\Lambda}(\bar{L}\tilde{H})\,\sigma\nu_R,$$

by the exchange of a heavy scalar $SU(2)_L$ doublet mediator ϕ is diagrammaftically illustrated in Fig. 4.1. In order to have such realisation of this type-II Dirac neutrino seesaw, the

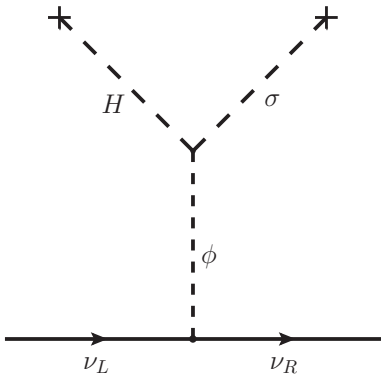

Fig. 4.1 *Neutrino mass generation in the type-II seesaw for Dirac neutrinos, as in [69, 153, 154].*

model has to enhance the SM particle content adding the iso-doublet ϕ and the scalar iso-singlet σ. Tab. 4.1 shows the relevant particles and assignments for this type-II Dirac neutrino realisation.

As mentioned before, a mechanism protecting the diracness of the neutrinos must be added. In this scenario, we have introduced the symmetry product $Z_3 \otimes Z_2$, such that it forbids the appearance of Majorana mass operators at the loop level, thus protecting

	$\bar{L}$	ℓ_R	ν_R	H	ϕ	σ
$SU(2)_L \otimes U(1)_Y$	$(\mathbf{2}, 1/2)$	$(1, -1)$	$(1, 0)$	$(\mathbf{2}, 1/2)$	$(\mathbf{2}, -1/2)$	$(1, 0)$
Z_3	ω^2	ω	ω	1	1	1
Z_2	$+$	$+$	$-$	$+$	$-$	$-$

Table 4.1 *Charge assignments for the particles involved in the type-II Dirac neutrino seesaw realisation, as in [69].*

the diracness of neutrinos. The A_4 flavour assignments of the model are not necessary for realising this type-II Dirac seesaw but will be relevant for the predictions of the model, as we will see in the following section.

4.2.1 Lepton sector

The specific particle assignments for the lepton sector and scalars are given in Tab. 4.2. The

	$\bar{L}$	ℓ_R	ν_R	H^d	ϕ	σ or σ_i
$SU(2)_L \otimes U(1)_Y$	$(\mathbf{2}, 1/2)$	$(1, -1)$	$(1, 0)$	$(\mathbf{2}, 1/2)$	$(\mathbf{2}, -1/2)$	$(1, 0)$
A_4	$\mathbf{3}$	$\mathbf{3}$	$\mathbf{3}$	$\mathbf{3}$	$\mathbf{3}$	$\mathbf{3}$ or 1_i
Z_3	ω^2	ω	ω	1	1	1
Z_2	$+$	$+$	$-$	$+$	$-$	$-$

Table 4.2 *Charge assignments for the particles involved in the neutrino mass generation mechanism, where* $\omega^3 = 1$

scalar $SU(2)_L$ doublets $H^d = (H_1^d, H_2^d, H_3^d)^T$ and $\phi = (\phi_1, \phi_2, \phi_3)^T$ transform as triplets, $\mathbf{3}$, under A_4. Where each component can be written as follows:

$$H_i^d = \begin{pmatrix} h_i^{d+} \\ h_i^{d0} \end{pmatrix}, \qquad \phi_i = \begin{pmatrix} \phi_i^0 \\ \phi_i^- \end{pmatrix}, \qquad i = \{1, 2, 3\}. \tag{4.1}$$

The *vev.* of these scalar triplets are given by:

$$\left\langle H^d \right\rangle = (v_{h_1^d}, v_{h_2^d}, v_{h_3^d}), \qquad \langle \phi \rangle = (v_{\phi_1}, v_{\phi_2}, v_{\phi_3}). \tag{4.2}$$

The SM singlet complex scalars σ_i, $i = \{1, 2, 3\}$, are responsible for inducing the small *vevs.* of the ϕ and could transform as an A_4 triplet $\sigma = (\sigma_1, \sigma_2, \sigma_3)^T \sim \mathbf{3}$ or as different

singlets $\sigma_i \sim \mathbf{1_i}$ under the flavour group. On the other hand, the LH lepton chiral components $L = (L_1, L_2, L_3)^T$, RH charged leptons $\ell_R = (\ell_{1R}, \ell_{2R}, \ell_{3R})^T$ and RH neutrinos $\nu_R = (\nu_{1R}, \nu_{2R}, \nu_{3R})^T$ transform as A_4 triplets **3**.

From the model assignments in Tab. 4.2, one can see that Z_3 is a conserved symmetry, because all scalars developing *vevs.* are blind (uncharged) under this symmetry. This Z_3 symmetry forbids the Majorana mass terms as well as the dimension-5 operators:

$$M_R\, \bar{\nu}_R^c\, \nu_R, \qquad \bar{L}^c H^d L H^d, \qquad \bar{L}^c \tilde{\phi} L \tilde{\phi} \qquad \text{and} \qquad \bar{L}^c H^d L \tilde{\phi}, \tag{4.3}$$

where $\tilde{\phi} = i\sigma_2 \phi^*$ and $\tilde{H^d} = i\sigma_2 H^{d*}$. The Z_3 symmetry also forbids higher order operators giving rise to Majorana mass terms:

$$(\bar{L}^c H^d L H^d)(H^{d\dagger} H^d)^n, \qquad (\bar{L}^c \tilde{\phi} L \tilde{\phi})(H^{d\dagger} H^d)^n \qquad (\bar{L}^c H^d L \tilde{\phi})(H^{d\dagger} H^d)^n, \tag{4.4}$$

$$(\bar{L}^c H^d L H^d)(\phi^\dagger \phi)^n, \qquad (\bar{L}^c \tilde{\phi} L \tilde{\phi})(\phi^\dagger \phi)^n, \qquad (\bar{L}^c H^d L \tilde{\phi})(\phi^\dagger \phi)^n, \tag{4.5}$$

$$(\bar{L}^c H^d L H^d)(H^{d\dagger} \tilde{\phi})^n, \qquad (\bar{L}^c \tilde{\phi} L \tilde{\phi})(H^{d\dagger} \tilde{\phi})^n, \qquad (\bar{L}^c H^d L \tilde{\phi})(H^{d\dagger} \tilde{\phi})^n, \tag{4.6}$$

$$\bar{\nu}_R^c\, \nu_R\, \sigma^n. \tag{4.7}$$

Finally, the Z_2 charges ν_R, σ and ϕ while the remaining particles are Z_2-even. Such symmetry acts in a complementary way to Z_3 forbidding the unwanted renormalisable Yukawa couplings:

$$\bar{L}\, \tilde{\phi}\, \ell_R \qquad \text{and} \qquad \bar{L}\, \tilde{H}^d\, \nu_R, \tag{4.8}$$

where the first operator allows the extra Higgses ϕ_i of giving mass to charged leptons, and the second operator provides the tree level Dirac neutrino mass term.

Before proceeding, we summarise our model structure by saying that compared with the minimal SM case, here one has three copies of the Higgs doublet $H^d_{1,2,3}$, three extra scalar iso-doublets $\phi_{1,2,3}$ and three RH neutrinos $\nu_{1R,\,2R,\,3R}$ all of them forming A_4 triplets. Moreover, one has three iso-singlet scalars $\sigma_{1,2,3}$ which could be assigned as a triplet or singlets of A_4. After flavour and EWSB, neutrinos get small type-II seesaw masses, Eq. (1.58), as result of the small *vev.* $\langle\phi\rangle$. This *vev.* is induced by means of the *vevs.* of the scalar iso-singlet $\sigma_{1,2,3}$, $\langle\sigma\rangle \sim v_\sigma$, through the seesaw relation

$$v_\phi \approx \kappa v_h \left(\frac{1}{\lambda_{H\phi} \frac{v_h^2}{v_\sigma} + \lambda_{\sigma\phi} - 2\frac{\mu_\phi^2}{v_\sigma}} \right), \tag{4.9}$$

as proposed in [69, 153, 154].

Finally, in accordance with the previous discussion the relevant part of Yukawa Lagrangian for leptons is given as:

$$\mathcal{L}_Y \supset Y_\ell^i \left[\bar{L}\, H^d\right]_{3_i} \ell_R + Y_\nu^i \left[\bar{L}\, \phi\right]_{3_i} \nu_R + \text{h.c.}, \tag{4.10}$$

where the symbol $[a\, b]_{3_i}$ stands for the two ways of contracting two triplets of A_4 a and b into a triplet, as shown in the Appendix A.

4.3 Results and discussion

In this section we will discuss the features of the model. The first one is how the model leads to a mass formula relating quark and lepton masses, despite the absence of grand unification, which leads to a flavour dependent generalisation of bottom-tau unification previously proposed in [162] and studied in [163–166, 72]. Another feature is related with the specific predictions for the lepton mixing matrix in the neutrino sector. Despite there are no predictions for the CKM, it can be shown that this can be adequately fitted following [163].

4.3.1 The generalised bottom-tau mass relation

The complete model particle assignment is based in the model [163], shown in Tab. 4.3, including both $SU(2)_L \otimes U(1)_Y$ gauge and flavour transformation properties. In this complete flavour assignment, only one new SM-like Higgs A_4 triplet is added H^u, which is responsable for giving mass to the u-type quarks. In addition, a new parity is added Z_2^d, that ensures d-type quark masses only come from H^d and forbids terms where H^u couples to d-type quarks and H^d couples to u-type quarks.

From the lepton Yukawa Lagrangian, Eq. (4.10), one sees that the charged lepton as well as the d-type quarks mass matrices[1], following [162–164], can be parametrised as:

$$m_\ell = \begin{pmatrix} 0 & a_\ell \alpha_\ell e^{i\theta_\ell} & b_\ell \\ b_\ell \alpha_\ell & 0 & e^{i\theta_\ell} a_\ell \rho_\ell \\ a_\ell e^{i\theta_\ell} & b_\ell \rho_\ell & 0 \end{pmatrix}, \tag{4.11}$$

[1] As the d-type quarks have the same flavour assignments than charged leptons, then their masses come from an analogous term involving H^d: $Y_d^i\, [\bar{Q}, H^d]_{3_i}\, d_R + h.c.$

	$\bar{Q}$	$\bar{L}$	u_{R_i}	d_R	ℓ_R	ν_R	H^u	H^d	ϕ	σ or σ_i
$SU(2)_L$	**2**	**2**	1	1	1	1	**2**	**2**	**2**	1
Y	-1/6	1/2	2/3	-1/3	-1	0	1/2	1/2	-1/2	0
A_4	**3**	**3**	$\mathbf{1_i}$	**3**	**3**	**3**	**3**	**3**	**3**	**3** or 1_i
Z_3	1	ω^2	1	1	ω	ω	1	1	1	1
Z_2	+	+	+	+	+	−	+	+	−	−
Z_2^d	+	+	+	−	+	+	+	−	+	+

Table 4.3 *Particle content and quantum numbers for the complete model.*

where

$$a_\ell = v_{h_2^d}\,(Y_\ell^1 + Y_\ell^3) \qquad \text{and} \qquad b_\ell = v_{h_2^d}\,(Y_\ell^2 + Y_\ell^4), \tag{4.12}$$

are real Yukawa couplings, θ_ℓ is the only unremovable complex phase, which we could assume $\theta_\ell = 0$, i.e. CP violation comes entirely from the neutrino and also u-type quark sectors, and the H^d *vev.* alignment is parameterised as:

$$\left\langle H^d \right\rangle = (v_{h_1^d}, v_{h_2^d}, v_{h_3^d}) = v_{h_2^d}\,(\rho_\ell, 1, \alpha_\ell), \tag{4.13}$$

with

$$\alpha_\ell = v_{h_3^d}/v_{h_2^d}, \qquad \text{and} \qquad \rho_\ell = v_{h_1^d}/v_{h_2^d}, \tag{4.14}$$

and $v_{h_i}^d$ (therefore α_ℓ and ρ_ℓ) real.

Now to determine the generalised bottom-tau mass relation, we can calculate the bi–unitary invariants of the squared mass matrix in Eq. (4.11), $M_\ell^2 = m_\ell m_\ell^\dagger$, where

$$m_\ell^D = \text{diag}\,(m_1, m_2, m_3) = V_\ell^\dagger m_\ell U_\ell, \tag{4.15}$$

with V_ℓ and U_ℓ unitary matrices, yielding to

$$\begin{aligned}
\mathrm{Tr}\, M_\ell^2 &= m_1^2 + m_2^2 + m_3^2 && (4.16)\\
&= (a_\ell^2 + b_\ell^2)(1 + \alpha_\ell^2 + \rho_\ell^2), && (4.17)\\
\det\, M_\ell^2 &= m_1^2 m_2^2 m_3^2 && (4.18)\\
&= (a_\ell^6 + b_\ell^6)\alpha_\ell^2 \rho_\ell^2, && (4.19)\\
(\mathrm{Tr}\, M_\ell^2)^2 - \mathrm{Tr}\,(M_\ell^2)^2 &= 2m_1^2 m_2^2 + 2m_2^2 m_3^2 + 2m_1^2 m_3^2, && (4.20)\\
&= a_\ell^2 b_\ell^2 (1 + \alpha_\ell^4 + \rho_\ell^4) + (a_\ell^4 + b_\ell^4)\left(\rho_\ell^2 + \alpha_\ell^2(1 + \rho_\ell^2)\right). && (4.21)
\end{aligned}$$

Under the assumptions $\rho_\ell \gg \alpha_\ell$, $\rho_\ell \gg 1$, $b_\ell > a_\ell$ and $\rho_\ell \gg \frac{b_\ell}{a_\ell}$ which, at leading order, ensure adequate family mass hierarchy ($m_1 < m_2 < m_3$) as well as the Cabibbo mixing pattern. One can expand Eqs. (4.17, 4.19, 4.21) and use the mass hierarchy on Eqs. (4.16, 4.18, 4.20), yielding at leading order to:

$$\begin{aligned}
(b_\ell \rho_\ell)^2 &\approx m_3^2, && (4.22)\\
(b_\ell^3 \rho_\ell \alpha_\ell)^2 &\approx m_1^2 m_2^2 m_3^2, && (4.23)\\
(a_\ell b_\ell \rho_\ell^2)^2 &\approx m_2^2 m_3^2. && (4.24)
\end{aligned}$$

Solving the system in Eqs. (4.22-4.24), one can find the approximate expressions [2]:

$$\begin{aligned}
a_\ell &\approx \frac{m_2}{m_3}\sqrt{\frac{m_1 m_2}{\alpha_\ell}}, && (4.25)\\
b_\ell &\approx \sqrt{\frac{m_1 m_2}{\alpha_\ell}}, && (4.26)\\
\frac{\rho_\ell}{\sqrt{\alpha_\ell}} &\approx \frac{m_3}{\sqrt{m_1 m_2}}. && (4.27)
\end{aligned}$$

As previously mentioned, d-type quarks couple only to H^d and hence have the same flavour structure. This implies that the parameters ρ_ℓ and α_ℓ in Eq. (4.27) are common to the charged leptons and the d–type quarks. Therefore,

$$\rho_\ell = \rho_d \quad \text{and} \quad \alpha_\ell = \alpha_d. \tag{4.28}$$

[2] These approximations are in 1% agreement with the exact numerical solution.

Using this fact, we can equate Eq. (4.27) for charged leptons and d-type quarks, and derive the generalised bottom-tau mass relation, proposed in [167, 162]:

$$\frac{m_\tau}{\sqrt{m_e m_\mu}} \simeq \frac{m_b}{\sqrt{m_d m_s}}. \tag{4.29}$$

It is worth to mention that this mass relation is scale invariant, as the running of the masses cancels out. Furthermore, Eq. (4.29) follows only from the flavour group assignments for the fields in the model; although it has been also obtained in other non-equivalent realisations of A_4 family symmetry [167, 163, 164, 72] and other family groups [166].

4.3.2 CKM fitting

In this section, we focus on the CKM matrix which can be adequately described, providing in addition an input for the lepton mixing matrix. Although the model has no family symmetry prediction for the CKM matrix, we can, however, accommodate the CKM elements in the same way as described in [163]. This fixes the value for the α_d parameter which enters also in the leptonic sector.

A numerical fit for quarks masses and mixing matrix is performed for the model. From the family assignments in Tab. 4.3, the Yukawa Lagrangian for the quarks sector is:

$$\mathcal{L}_Y = Y_u^i \, [\bar{Q} \, \tilde{H}^u]_{1_i} \, u_R + Y_d^i \, [\bar{Q} \, H^d]_{3_i} \, d_R + h.c., \tag{4.30}$$

where $Y_{u,d}^i$ are complex Yukawa couplings, and the symbol $[a\, b]_i$ stands for the contraction of two triplets a and b into the *irrep.* $i = \{1, 1', 1'', \mathbf{3}\}$ of A_4.

From the Lagrangian in Eq. (4.30), the mass matrix for the d-type quarks is:

$$m_d = \begin{pmatrix} 0 & a_d \alpha_d & b_d e^{i\theta_d} \\ b_d \alpha_d & 0 & a_d \rho_d \\ a_d & b_d e^{i\theta_d} \rho_d & 0 \end{pmatrix}, \tag{4.31}$$

which has been parametrised in a similar way as the mass matrix for the charged leptons, Eq. (4.11), and the u-type quark mass matrix can be written as:

$$m_u = \frac{1}{\sqrt{3}} \begin{pmatrix} v_u^1 & 0 & 0 \\ 0 & v_u^2 & 0 \\ 0 & 0 & v_u^3 \end{pmatrix} \begin{pmatrix} 1 & 0 & 0 \\ 0 & \omega & \omega^* \\ 0 & \omega^* & \omega \end{pmatrix} \begin{pmatrix} Y_u^1 & 0 & 0 \\ 0 & Y_u^3 & 0 \\ 0 & 0 & Y_u^2 \end{pmatrix}, \tag{4.32}$$

with $\langle H^u \rangle = (v_1^u, v_2^u, v_3^u)$ and $\omega^3 = 1$.

It is known that such mass matrices can be diagonalised by the bi-unitary transformation:

$$V^{u,d\dagger} m_{u,d} U^{u,d} = \text{diag } (m_{u,d}, m_{c,s}, m_{t,b}) \,. \tag{4.33}$$

Therefore, diagonalisation of the squared matices $m_u\, m_u^\dagger$ and $m_d\, m_d^\dagger$ give the left-diagonalising unitary matrices V_u and V_d, whose product give the CKM matrix, V_{CKM},

$$V_{CKM} = V^{u\dagger}\, V^d. \tag{4.34}$$

Analytical approximation for V^d establishes that in order to generate the Cabbibo mixing $\lambda_c \approx 0.2$ in the plane $1-2$, we need $\alpha_d \sim \mathcal{O}(1)$. This also implies that the other mixings, on the planes $1-3$ and $2-3$, are negligible.

Finally, as the contribution from the down sector has been shown to generate the Cabbibo mixing, the remaining smaller mixings can be generated from the contribution of the up sector V^u. Thus, in [163] is proposed that the structure for $M_u^2 = m_u\, m_u^\dagger$ is in a hierarchical way

$$M_u^2 \sim \begin{pmatrix} \lambda_c^8 & \lambda_c^6 & \lambda_c^4 \\ \lambda_c^6 & \lambda_c^4 & \lambda_c^2 \\ \lambda_c^4 & \lambda_c^2 & 1 \end{pmatrix}, \tag{4.35}$$

which have been proven to generate $V_{23}^u \approx \lambda_c^2$, $V_{13}^u \approx \lambda_c^4$ and $V_{12}^u \approx \lambda_c^2$. This could be achieved if the *vevs.* of H^u, $\langle H^u \rangle = (v_1^u, v_2^u, v_3^u)$, have the hierarchy:

$$v_1^u : v_2^u : v_3^u = 1 : \lambda_c^2 : \lambda_c^4. \tag{4.36}$$

Regarding the CP violation in the quark sector, it is possible to generate the right amount only from the up sector contribution through ω, i.e. one can set the CP-violating phase form the down sector to zero, $\theta_d = 0$.

The fitting of the CKM matrix is performed by numerical minimisation of a χ–squared function. Such χ^2 function is defined as

$$\chi^2 = \sum_i \left(\frac{m_i^{\text{ob}} - m_i^{\text{th}}}{\sigma m_i} \right)^2 + \sum_{j,k}{}' \left(\frac{|V_{jk}^{\text{ob}}| - |V_{jk}^{\text{th}}|}{\sigma V_{jk}} \right)^2 + \left(\frac{J^{\text{ob}} - J^{\text{th}}}{\sigma J} \right)^2, \tag{4.37}$$

where the first summation index accounts for all quarks, $i = \{u, c, t, d, s, b\}$, the primed summation refers only to the elements CKM elements[3] V_{12}, V_{13} and V_{23}, and J is the Jarlskog invariant, Eq. (1.14),

$$J = \mathrm{Im}\left[V_{\mathrm{us}} V_{\mathrm{cb}} V_{\mathrm{ub}}^{*} V_{\mathrm{cs}}^{*}\right].$$

The observed values and uncertainties for the CKM elements, the Jarlskog parameter and the charged leptons masses are taken from updated references [24], while the quark masses are taken from [168], at the Z mass scale. The best-fit values are shown in Tab. 4.4 in accordance with the results of [163].

Observable	Exp. value	Mod. pred.	| Pull | $[\sigma]$
m_u [Mev]	1.45 ± 0.51	1.51	0.16
m_c [Mev]	635 ± 86	585.7	0.12
m_t [Gev]	172.1 ± 1.5	172.0	0.04
m_d [Mev]	2.9 ± 0.51	2.7	0.39
m_s [Mev]	57.7 ± 16.8	56.5	0.07
m_b [Mev]	2820 ± 80	2835	0.19
$\lvert V_{12}\rvert$	0.22534 ± 0.00065	0.22504	0.47
$\lvert V_{13}\rvert$	0.00351 ± 0.00015	0.00359	0.51
$\lvert V_{23}\rvert$	0.0412 ± 0.008	0.0390	0.28
$J \times 10^{-5}$	2.96 ± 0.20	2.99	0.16

Table 4.4 *Experimental and predicted quark masses and mixing parameters from the CKM fit.*

4.3.3 Lepton masses and mixing

In this section, we will focus on the lepton mixing matrix, because it is in this sector that our model makes non-trivial predictions. In analogy with the previous subsection, Eq. (4.10) gives the neutrino mass matrix, which can also be parametrised as:

$$m_\nu = \begin{pmatrix} 0 & a_\nu \alpha_\nu & b_\nu e^{i\theta_\nu} \\ b_\nu e^{i\theta_\nu} \alpha_\nu & 0 & a_\nu \rho_\nu \\ a_\nu & b_\nu e^{i\theta_\nu} \rho_\nu & 0 \end{pmatrix}, \tag{4.38}$$

[3] We have assumed the unitarity of the CKM matrix.

where

$$a_\nu = v_{\phi_2}(Y^1_\nu + Y^3_\nu) \quad \text{and} \quad b_\nu = v_{\phi_2}(Y^2_\nu + Y^4_\nu) \tag{4.39}$$

are real Yukawa couplings, θ_ν is the complex phase that cannot be rotated away under $SU(2)_L$ transformations and characterises the strength of CP violation in the lepton sector. The *vev.* alignment of the iso-doublets ϕ can be parametrised as

$$\langle\phi\rangle = (v_{\phi_1}, v_{\phi_2}, v_{\phi_3}) = v_{\phi_2}\,(\rho_\nu, 1, \alpha_\nu), \quad \alpha_\nu = v_{\phi 3}/v_{\phi 2} \quad \rho_\nu = v_{\phi 1}/v_{\phi 2}. \tag{4.40}$$

The number of free parameters in the leptonic sector is nine. Four independent parameters (a_ℓ, b_ℓ, α_ℓ and ρ_ℓ) from the charged leptons, Eq. (4.11), and five parameters (a_ν, b_ν, α_ν, ρ_ν and θ_ν) from the neutrinos, Eq. (4.38). However, two of them α_ℓ and ρ_ℓ are fixed from the quark sector. The remaining seven parameters are used to fit three masses plus two mass squared splittings, three mixing angles and a Dirac CP violating phase. This is done using the invariants Eqs. (4.16 – 4.20) of the squared neutrino mass matrix $M^2_\nu = m_\nu m^\dagger_\nu$:

$$\begin{aligned}
\mathrm{Tr}(M^2_\nu) &= m^2_{\nu 1} + m^2_{\nu_2} + m^2_{\nu_3}, && (4.41)\\
&= (a^2_\nu + b^2_\nu)(1 + \alpha^2_\nu + \rho^2_\nu) && (4.42)\\
\det(M^2_\nu) &= m^2_{\nu_1}\, m^2_{\nu_2}\, m^2_{\nu_3} && (4.43)\\
&= \left(a^6_\nu + b^6_\nu + 2a^3_\nu b^3_\nu \cos(3\theta_\nu)\right) \alpha^2_\nu \rho^2_\nu, && (4.44)\\
\frac{1}{2}\left[(\mathrm{Tr}M^2_\nu)^2 - \mathrm{Tr}(M^4_\nu)\right] &= m^2_{\nu_1} m^2_{\nu_2} + m^2_{\nu_2} m^2_{\nu_3} + m^2_{\nu_1} m^2_{\nu_3} && (4.45)\\
&= a^2_\nu b^2_\nu (1 + \alpha^4_\nu + \rho^4_\nu) + (a^4_\nu + b^4_\nu)(\rho^2_\nu + \alpha^2_\nu(1 + \rho^2_\nu)), && (4.46)
\end{aligned}$$

and performing numerical scan over the parameter regions of solutions of these, Eqs. (4.41 – 4.46), that reproduce the measured elements of the leptonic mixing matrix. The leptonic mixing matrix, Eq (1.18):

$$V = V^{\ell\dagger} V^\nu,$$

have a fixed and calculable contribution from the left-diagonalising unitary matrix of charged leptons V^ℓ; V^ℓ is a close to s diagonal matrix. The inputs used in the scan are the 3σ values for three neutrino global fit [33]: the mixing angles (θ_{12}, θ_{23}, θ_{13}) and two mass squared differences (Δm^2_{12} , Δm^2_{3i}).

Neutrino oscillation predictions

In order to determine the model neutrino oscillation predictions, a random numerical scan is performed over the free parameters ranges:

$$\alpha_\nu \in [-10, 10]\,, \quad \rho_\nu \in [-10, 10] \qquad \theta_\nu \in [0, 2\pi] \quad \text{and} \quad m_{\text{light}} \in \left[10^{-5}, 0.23\right] \text{ eV}. \tag{4.47}$$

The parameter space points for which the oscillation parameters are within 3σ of the global fit data [33] are determined. This phenomenological requirement constrains the allowed regions for the neutrino mass matrix parameters, Eq. (4.38):

$$0.75 \lesssim |\alpha_\nu, \rho_\nu| \lesssim 1.25, \qquad 0.03 \lesssim |a_\nu, b_\nu| \lesssim 0.04, \qquad -\pi/3 \lesssim \theta_\nu \lesssim \pi/3. \tag{4.48}$$

This way, it has been obtained the model–allowed regions for the oscillation parameters. Correlations among the interesting and poorly determinated atmospheric mixing angle θ_{23}, the CP phase δ_{CP} and the lightest neutrino mass eigenvalue are shown as green shaded regions in Figs. 4.2, 4.3 and 4.4. Also,t the numerical scan has found that the model is only compatible with the inverted ordering (IO) of the neutrino masses. The consistent parameter regions for the atmospheric mixing angle $\sin^2\theta_{23}$ vs. m_3 the lightest neutrino mass are given in shaded (green) regions in Fig. 4.2. The green horizontal band represents the 1σ value for θ_{23} and the dashed line the best fit value in the data used. It is interesting to notice that the model is not compatible with a maximal mixing angle $\theta_{23} = 45°$.

The allowed regions for the CP violation parameters δ_{CP} and J_{CP} vs. m_3 are displayed in Fig. 4.3. From the plots one sees that the allowed region for the lightest neutrino mass m_3 is within the range

$$6.4 \times 10^{-4} \text{ eV} \lesssim m_3 \lesssim 2.7 \times 10^{-3} \text{ eV}. \tag{4.49}$$

It is worth to notice that only masses above ~ 0.002 eV allow $J_{CP} = 0$, i.e. no CP violation, while for lower masses such value is always non-zero.

Finally, the parameter regions for the atmospheric mixing angle θ_{23} vs. δ_{CP} the CP phase are shown as green shaded areas in Fig. 4.4, where the contours lines represent the 90 and 99% C.L. regions obtained directly from the unconstrained three neutrino oscillation global fit [33].

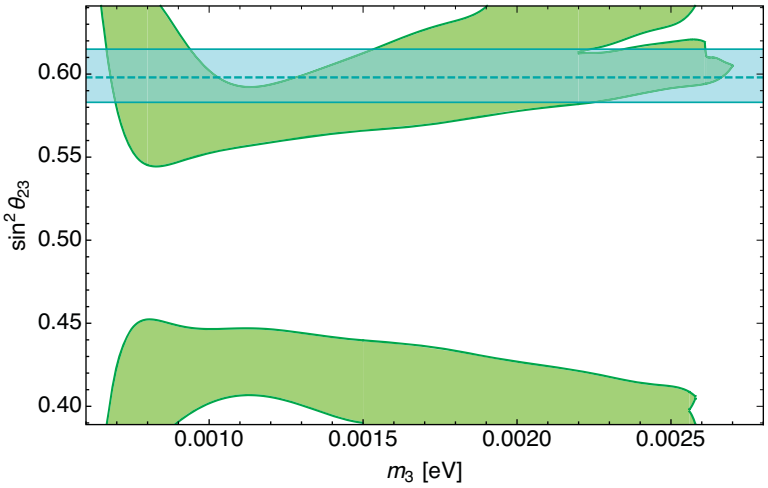

Fig. 4.2 *The regions in the atmospheric mixing angle θ_{23} and the lightest neutrino mass m_3 allowed by oscillation data in shaded (green) areas. The horizontal dashed line represents the best-fit value for $\sin^2\theta_{23}$, whereas the horizontal shaded region corresponds to the 1σ allowed region from Ref. [33].*

4.4 Conclusions

It this chapter, we have shown a model with $A_4 \otimes Z_3 \otimes Z_2$ flavour extension of the SM where the small Dirac neutrino masses are generated from a realisation of a type-II Dirac seesaw mechanism. The model partially addresses both aspects of the flavour problem explaining the mass hierarchy of quark and leptons and restricting the structure of the mixing matrix. Concerning the first point, the model leads to a golden mass relation between quark and lepton masses, which has been proposed in previous works. Regarding the latter point, the model gives flavour predictions for the lepton mixing matrix.

The model predicts an inverted neutrino mass ordering (IO) with non-maximal atmospheric mixing angle. The model also suggests a slight preference for the higher octant, since it predicts inverted neutrino mass ordering. This could be at odds with the latest results of the neutrino oscillation global fit [33], but one could argue that neither preference for normal ordering nor lower octant are statistically significant, since the general three–neutrino fit gives four possible closely separated local minima.

The model also has a positive hint for CP violation, $\delta_{CP} \neq 0$, if $m_{\nu_{\text{lightest}}} \lesssim 0.002$ eV, while bigger masses are consistent with CP-conserving solutions. In addition, the regions

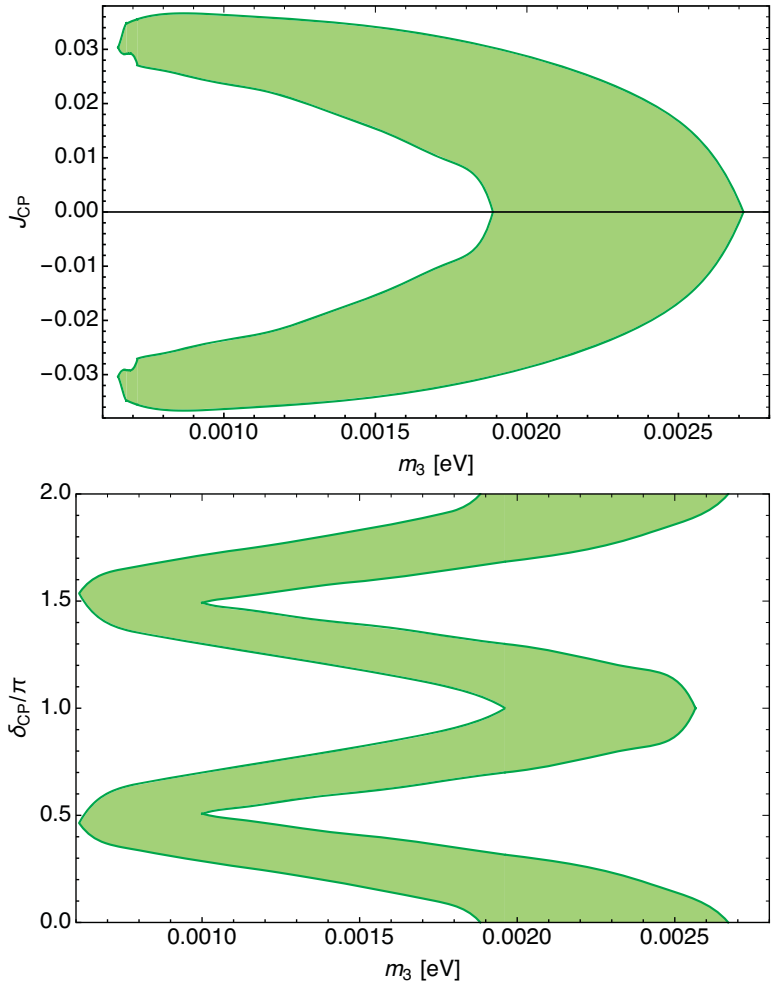

Fig. 4.3 *Correlation between the CP violation and the lightest neutrino mass. Up: correlation between the Jarlskog invariant J and the lightest neutrino mass m_3 allowed by the current oscillation data [33]. Bottom: Allowed regions for the correlation between the Dirac CP phase δ_{CP} and the lightest neutrino mass m_3.*

for the CP phase and the atmospheric angle nicely agree with the currently preferred ones, though these global fit determinations are not yet very robust.

Regarding the quark mixing matrix, although no predictions are made, the CKM matrix elements can be fitted which also fix the charged lepton contribution to the lepton mixing matrix. Finally, it is worth to notice that the Z_3 symmetry forbids the neutrino Majorana mass terms at any order and provides by construction a natural realisation of a type-II Dirac seesaw mechanism.

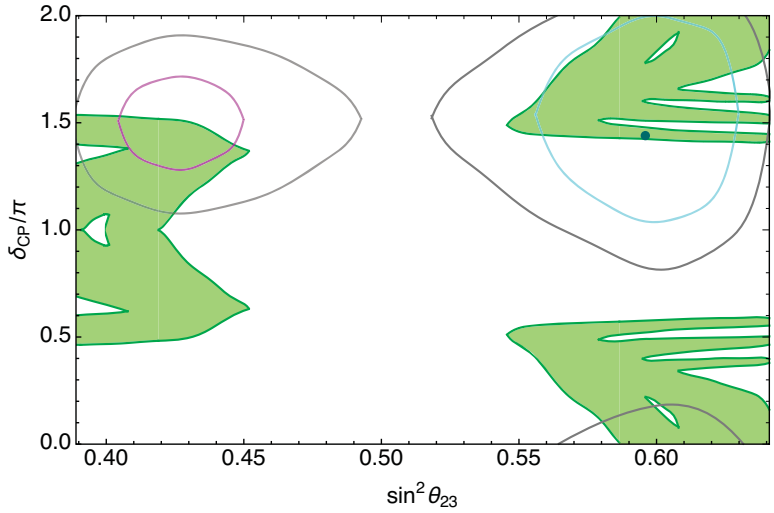

Fig. 4.4 *The allowed regions of the atmospheric mixing angle and δ_{CP} are indicated in green shaded. The unshaded contour regions represent the 90 and 99%CL regions obtained directly in the unconstrained three neutrino oscillation global fit [33].*

Chapter 5

Summary and final remarks

Here we present a very brief concluding summary, while detailed remarks can be found at the end of each chapter. This thesis collects the results of three projects which investigate the origin of neutrino masses by the use of abelian and non-abelian discrete symmetries. Furthermore, two of these works also explore the connection between the neutrino mass generation mechanism and dark matter. Each work addresses the neutrino mass generation in different ways, but all have in common the guidance of a predictive bottom-up model building. That is, a high energy extension of the SM where the particle content and symmetries are enhanced as minimal as possible and being consistent with existing low energy constraints.

The first work presents two A_4 extensions of the SM. The A_4 symmetry is spontaneously broken down into a remanent Z_2, in such a way, this symmetry provides a mechanism for the dark matter stability. The leptons transform non-trivially under the flavour symmetry, while the quarks remain blind, and their masses and mixing pattern may be explained by another complementary mechanism. The models are successful reproducing the neutrino masses and mixing pattern, which are a consequence of the flavour assignments and specific breaking. The flavour symmetry leads to mass matrices for light neutrinos with two-zero textures which accommodate current neutrino oscillation data for both mass orderings with a non-zero lightest neutrino mass. The models predict correlations among oscillation parameters, from which we have obtained lower bounds to the $0\nu\beta\beta$ effective mass parameter in a region of sensitivity of forthcoming experiments. Regarding dark matter phenomenology, the models provide an explanation on the dark matter stability mechanism and have as dark matter candidates: two RH neutrinos not participating in the neutrino mass generation and two inert Higgs doublets. Considering the last option, the dark matter phenomenology

is expected to be analogous to a model with two active and two inert Higgs doublets. Additionally, as the flavour symmetry breaking is driven by scalar gauge singlet fields, the scale of such breaking could be chosen to be above the seesaw scale, providing a plausible scenario for the generation of the matter-antimatter asymmetry via leptogenesis.

In the second work, we have studied a SM extension where an exact abelian discrete symmetry Z_2 is added such that it stabilises the dark matter and in addition is responsible for the neutrino mass generation. The latter through the one-loop realisation of the dimension-5 Weinberg operator in which dark matter participates in the loop. We have also added a gauge singlet scalar field charged under lepton number, such that it gives mass dynamically to the RH neutrinos. In addition, this gauge singlet scalar field mixes with the Higgs leading to a new dark matter annihilation channel. We have shown that this new channel leads to a relaxation on the tension between the dark matter relic abundance and lepton flavour violation constraints. The mixing between the Higgs and the gauge singlet scalar field leads to a richer Higgs phenomenology. Further constraints on the model parameter region can be considered taking into account a detailed analysis of the Higgs sector phenomenology. Although the model does not provide any prediction on the neutrino masses nor mixing pattern, it is consistent with current oscillation parameters through the LFV constraints.

Finally, in the last work we have presented an A_4 flavour symmetric realisation of a type-II Dirac neutrino seesaw. The model can reproduce successfully the patterns for fermion masses and mixings. The former through a flavour dependent golden mass relation between the charged leptons and down type quarks, which has been derived in previous works. Concerning the fermion mixing patterns, the model adequately describes the CKM elements, which fixes the charged lepton contribution to the lepton mixing matrix. The model flavour predictions for the leptons are consistent with a non-zero lightest neutrino mass with an inverted mass ordering, non-maximal atmospheric mixing angle and non-zero CP violating phase for the lightest neutrino mass < 0.002 eV. In this way, a better determination on the atmospheric mixing angle and the δ_{CP} phase as well as the determination of the neutrino mass ordering could test this model flavour realisation. This is expected to happen in the forthcoming years by long baseline experiments as NOνA and atmospheric neutrino oscillation experiments as Hyper-Kamiokande, etc. The model fails to account for a dark matter candidate. However, there are several ways to incorporate a dark matter candidate into this setup, one that has been explored in similar constructions is to enlarge the exact

Z_3 symmetry responsible for the "diracness" of neutrinos into a larger group as Z_n, leading to a dark matter stability symmetry.

In this thesis, we have assumed that neutrino masses and mixing pattern could be explained by some underlying discrete symmetry. Also, we have relied upon the hypothesis that neutrino mass generation mechanism and dark matter are somehow related. In particular, we have exploited this idea through the use of local discrete symmetries. However, it is worth mentioning that these bottom-up approaches fail to provide a natural relation between neutrinos and dark matter, in the sense that at one point one has to assume some symmetry assignments. It would be more appealing, from the theoretical point of view, to achieve this relation from a high energy fundamental theory. Thus, in our conservative model building approach, one could also consider the possibility that these models based on discrete (flavour) symmetries have to account for more complex interaction not possible within the SM. It would be interesting to investigate high energy extensions of the SM, with or without flavour symmetries, where the relation between dark matter and neutrinos is more natural, and look for its testable predictions. However, one should be cautious in this unification endeavour. There always exists the possibility that neutrinos and dark matter are completely independent phenomena.

Acknowledgements

I would like to express my kind gratitude to my advisor Eduardo Peinado for being so generous with his time and his pragmatism. To Genaro Toledo Sanchez and Mariano Chernicoff Minsberg, members of my PhD advisory committee. I am also grateful to the members of the committee of my thesis for generously accepting to review the manuscript and for their thoughtful comments. I wish to thank the co-authors of all the papers this thesis is based on for the excellent collaborations.

During my PhD, I had the chance to do a short stay with the Astroparticle and High Energy Physics (AHEP) group in the IFIC–University of Valencia, Spain. I want to express my deep acknowledge to Professor Jose W. F. Valle for the financial support during this staying and the whole people in the group for his kind hospitality and excitement discussions.

Last but not least, I acknowledge the financial support from the Mexico CONACyT fellowship, German-Mexican research collaboration grant SP 778/4-1 (DFG), 278017 (CONACyT) and Papiit: IA101516, RA101516 and IN107118 grants.

Appendix A

The A_4 group

In this appendix, we will review the properties of the smallest non-abelian discrete group A_4. The A_4 group is just a realisation of a general class of group called the alternating group of N elements or A_N, which consists of all the even permutations of N elements (i.e. A_N is a sub-group of S_N, the permutation group of N elements). The order of A_N is $N!/2$.

One can easily realise that A_3 is isomorphic to the abelian group Z_3, being Z_N the cyclic group of order N[1]. On the other hand, the group A_4 could be associated with the group of symmetries of the tetrahedron. The A_4 group has twelve elements that can be written in terms of two generators S and T. These generators satisfy the algebraic relations

$$S^2 = T^3 = (S\,T)^3 = \mathbb{1}. \tag{A.1}$$

The elements of A_4 can be written in terms of the generators and the identity e as: e, S, T, T^2, TS, ST, STS, TST, ST^2, T^2S, TST^2 and T^2ST. These could be classified into four conjugacy classes as:

$$C_1 : \{e\}, \qquad h = 1, \tag{A.2}$$

$$C_3 : \{S, TST^2, T^2ST\}, \qquad h = 2, \tag{A.3}$$

$$C_4 : \{T, TS, ST, STS\}, \qquad h = 3, \tag{A.4}$$

$$C_4' : \{T^2, ST^2, T^2S, TST\}, \qquad h = 3. \tag{A.5}$$

[1]The cyclic group of order N is an abelian finite group which can be defined through one single generator X, following the relation $X^N = \mathbb{1}$.

where h is the order of each conjugacy class.
One can see from Eq. (A.1) that A_4 contains two sub-groups: Z_3 and Z_2 each one associated with the T and S generator respectively. Finally, it is remarkable to mention that A_4 is a finite sub-group of the $SO(3)$ as well as $SU(3)$.

A.1 A_4 irreducible representations product

The group A_4 has four irreducible representations. Finding those *irreps.* of A_4 requiere to look at the orthogonality relation

$$\sum_n m_n n^2 = N_G = 12, \tag{A.6}$$

where m_n is the multiplicity of the *irrep.* of dimension n and $N_G = 12$ is the order of A_4. On the other hand, we have that

$$\sum_n m_n = 4, \tag{A.7}$$

because there are four conjugacy classes of A_4, Eqs. (A.2)-(A.5). From Eqs. (A.6) and (A.7), the only solution is: $(m_1, m_2, m_3, \dots) = (1, 0, 1, 0, \dots)$. Therefore there exist three one-dimensional *irreps.*: $\mathbf{1}$, $\mathbf{1'}$, and $\mathbf{1''}$ and one three-dimensional *irrep.* $\mathbf{3}$.

The one-dimensional unitary *irreps.* are:

$$\begin{aligned} \mathbf{1}: &\quad S = 1, \quad T = 1, \\ \mathbf{1'}: &\quad S = 1, \quad T = \omega, \\ \mathbf{1''}: &\quad S = 1, \quad T = \omega^2, \end{aligned} \tag{A.8}$$

where $\omega^3 = 1$, and the three-dimensional *irrep.* in the basis where S is real and diagonal is

$$\mathbf{3}: S = \begin{pmatrix} 1 & 0 & 0 \\ 0 & -1 & 0 \\ 0 & 0 & -1 \end{pmatrix} \text{ and } \quad T = \begin{pmatrix} 0 & 1 & 0 \\ 0 & 0 & 1 \\ 1 & 0 & 0 \end{pmatrix}. \tag{A.9}$$

The product rule for the singlets are

$$\begin{aligned} &\mathbf{1} \times \mathbf{1} = \mathbf{1'} \times \mathbf{1''} = \mathbf{1}, \\ &\mathbf{1'} \times \mathbf{1'} = \mathbf{1''}, \\ &\mathbf{1''} \times \mathbf{1''} = \mathbf{1'}, \end{aligned} \tag{A.10}$$

and triplet multiplication rules are

$$\begin{aligned}
[a\,b]_{1} &= a_1 b_1 + a_2 b_2 + a_3 b_3, \\
[a\,b]_{1'} &= a_1 b_1 + \omega\, a_2 b_2 + \omega^2\, a_3 b_3\,, \\
[a\,b]_{1''} &= a_1 b_1 + \omega^2\, a_2 b_2 + \omega\, a_3 b_3\,, \\
[a\,b]_{3_1} &= (a_2 b_3,\, a_3 b_1,\, a_1 b_2)\,, \\
[a\,b]_{3_2} &= (a_3 b_2,\, a_1 b_3,\, a_2 b_1)\,,
\end{aligned} \tag{A.11}$$

where $a = (a_1, a_2, a_3)$, $b = (b_1, b_2, b_3)$ and $\omega = (1)^{1/3}$.

Appendix B

Radiative one-loop mass calculation for Scotogenic model

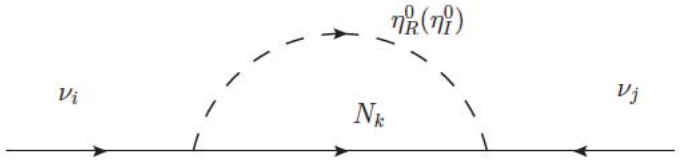

Fig. B.1 *Feynman diagram for the Scotogenic neutrino mass generation in mass eigenstates.*

In Ma's Scotogenic model, light neutrino masses arise from radiative correction to neutrino propagator. This correction shifts the pole of the propagator and therefore the physical mass of the neutrinos. The lowest order quantum correction in the Scotogenic model is the one-loop process shown in Fig. 3.1. Such loop generation of neutrino masses is guaranteed to be finite, though the superficial degree of divergence counting of the diagram leads to believe that this diverges. The reason behind this is that after EWSB there is a mass splitting between the neutral components of the scalar degree of freedom η^0, each contributing with opposite sign and thus the loop divergence cancels.

For the calculation of the loop, it is crucial to only use the mass eigenstates of the diagram, as shown in Fig. B.1. In the following, we will denote the Yukawa couplings in the Lagrangians in Eqs. (3.1) and (3.9) as $Y^\nu_{ij} = Y_{ij}$. From the diagram in Fig. B.1, it is

straightforward to see that the integral has the form:

$$-i\,\Sigma_{ij} = -\sum_k Y_{ik}Y_{jk}\int \frac{d^4k}{(2\pi)^2}\left[\frac{i(\not{k}+m_{N_k})}{k^2-m_{N_k}^2}\frac{i}{(p-k)^2-m_{\eta_R}^2} - \frac{i(\not{k}+m_{N_k})}{k^2-m_{N_k}^2}\frac{i}{(p-k)^2-m_{\eta_I}^2}\right] \tag{B.1}$$

$$= \sum_k Y_{ik}\,Y_{jk}\int \frac{d^4k}{(2\pi)^2}\,(\not{k}+m_{N_k})\left[\frac{1}{(k^2-m_{N_k}^2)\left((p-k)^2-m_{\eta_R}^2\right)} - \frac{1}{(k^2-m_{N_k}^2)\left((p-k)^2-m_{\eta_I}^2\right)}\right], \tag{B.2}$$

where the $i\varepsilon$ prescription for the poles is assumed in all squared masses. Then, we have been left with two one-loop integrals, one for the real and one for the imaginary part of η_0, where the minus sign in the second term of Eq. (B.1) comes from such splitting.

As we are interested in the mass correction, it is convenient to take zero total external momentum. Then, $p = 0$ and Eq. (B.2) takes the form:

$$-\,i\,\Sigma_{ij} = \sum_k Y_{ik}Y_{jk}\,I_k, \tag{B.3}$$

where

$$I_k = \int \frac{d^4k}{(2\pi)^4}\,(\not{k}+m_{N_k})\left[\frac{m_{\eta_R}^2-m_{\eta_I}^2}{(k^2-m_{N_k}^2)(k^2-m_{\eta_R}^2)(k^2-m_{\eta_I}^2)}\right]. \tag{B.4}$$

In order to calculate this integral, we use the Feynman parameter prescription (see for instance [169]), and combine the n propagators labelled as A_n appearing m_n times in the integral as:

$$\frac{1}{A_1^{m_1}A_2^{m_2}...A_n^{m_n}} = \frac{\Gamma(m_1+m_2+...+m_n)}{\Gamma(m_1)\Gamma(m_2)...\Gamma(m_n)}\int_0^1 dx_1\,x_1^{m_1-1}\int_0^1 dx_2\,x_2^{m_2-1}...\int_0^1 dx_n x^{m_n-1} \times \frac{\delta\left(1-x_1-x_2...-x_n\right)}{(x_1A_1+x_2A_2+...+x_nA_n)^{m_1+m_2+...+m_n}}. \tag{B.5}$$

In our case, the Feynman parametrisation technique yields to

$$I_k = (m_{\eta_R}^2 - m_{\eta_I}^2) \int \frac{d^4k}{(2\pi)^4} i\,(\not{k} + m_{N_k}) \left[\Gamma(3) \int_0^1 dx \int_0^{1-x} dy \right. \\ \left. \times \frac{1}{\left(x(k^2 - m_{N_k}^2) + y(k^2 - m_{\eta_R}^2) + (1-x-y)(k^2 - m_{\eta_I}^2)\right)^3} \right]. \quad \text{(B.6)}$$

Rearranging the integral denominator, we have

$$I_k = 2(m_{\eta_R}^2 - m_{\eta_I}^2) \int_0^1 dx \int_0^{1-x} dy \int \frac{d^4k}{(2\pi)^4} \left[\frac{(\not{k} + m_{N_k})}{(k^2 - \Delta)^3}\right], \quad \text{(B.7)}$$

where

$$\Delta = x\,(m_{N_k}^2 - m_{\eta_I}^2) + y\,(m_{\eta_R}^2 - m_{\eta_I}^2) + m_{\eta_I}^2.$$

Notice that the integral of k in Eq. (B.7) is zero by symmetry. The remaining integral is performed using the Wick rotation: $k_0 = i\,l_0$, so that $k^2 = -l^2$ and $d^4k = -i\,d^4l$. In this way, we can perform the integral in a four-dimensional spherical space as:

$$I_k = 2i \frac{(m_{\eta_R}^2 - m_{\eta_I}^2) m_{N_k}}{(2\pi)^4} \int_0^1 dx \int_0^{1-x} dy \int d^4l \left[\frac{1}{(l^2 + \Delta)^3}\right] \quad \text{(B.8)}$$

$$= 2i \frac{(m_{\eta_R}^2 - m_{\eta_I}^2) m_{N_k}}{(2\pi)^4} \int_0^1 dx \int_0^{1-x} dy \int d\Omega_3 \frac{dl\,l^3}{\Delta^3\,(1 + l^2/\Delta)^3} \quad \text{(B.9)}$$

$$= 2i \frac{(m_{\eta_R}^2 - m_{\eta_I}^2) m_{N_k}}{(2\pi)^4} \int_0^1 dx \int_0^{1-x} dy\,(2\pi^2) \int \frac{dl\,l^3}{\Delta^3\,(1 + l^2/\Delta)^3} \quad \text{(B.10)}$$

$$= i \frac{(m_{\eta_R}^2 - m_{\eta_I}^2) m_{N_k}}{4(2\pi)^2} \int_0^1 dx \int_0^{1-x} dy \frac{1}{x\,(m_{N_k}^2 - m_{\eta_I}^2) + y\,(m_{\eta_R}^2 - m_{\eta_I}^2) + m_{\eta_I}^2} \quad \text{(B.11)}$$

$$= i \frac{m_{N_k}}{4(2\pi)^2} \int_0^1 dx \frac{1}{x\,(m_{N_k}^2 - m_{\eta_I}^2) + y\,(m_{\eta_R}^2 - m_{\eta_I}^2) + m_{\eta_I}^2}. \quad \text{(B.12)}$$

The final integral, Eq. (B.12), can be performed by taking the derivative under the integral sign leading to:

$$I_k = i \frac{m_{N_k}}{16\pi^2} \left[\frac{m_{\eta_R}^2}{m_{\eta_R}^2 - m_{N_k}^2} \log \frac{m_{\eta_R}^2}{m_{N_k}^2} - \frac{m_{\eta_I}^2}{m_{\eta_I}^2 - m_{N_k}^2} \log \frac{m_{\eta_I}^2}{m_{N_k}^2}\right]. \quad \text{(B.13)}$$

Finally, from the propagator correction Eq. (B.3), we have that the mass matrix for the LH Majorana neutrinos is of the form $-\Sigma_{ij} = \mathcal{M}_{ij}$. Then,

$$\mathcal{M}_{ij} = \sum_k Y_{ik} Y_{jk} \frac{m_{N_k}}{16\pi^2} \left[\frac{m^2_{\eta_R}}{m^2_{\eta_R} - m^2_{N_k}} \log \frac{m^2_{\eta_R}}{m^2_{N_k}} - \frac{m^2_{\eta_I}}{m^2_{\eta_I} - m^2_{N_k}} \log \frac{m^2_{\eta_I}}{m^2_{N_k}} \right]. \tag{B.14}$$

Appendix C

Oblique parameters for a radiative Majorana neutrino mass generation

In this appendix, we give more details on the calculation of the electroweak parameters for the model in chapter 3. Following the notation in [170, 144], the oblique parameters T and S for a SM extension with n extra $SU(2)_L$ iso-doublets with hypercharge $-1/2$ are given by:

$$\begin{aligned} T &= \frac{g^2}{(8\pi)^2 \alpha\, m_W^2}\Bigg[F\left(m_{\eta^\pm}^2, m_{\eta_0}^2\right) + F\left(m_{\eta^\pm}^2, m_{\eta_A}^2\right) - F\left(m_{\eta_0}^2, m_{\eta_A}^2\right) \\ &\quad +3\sin^2\theta\Big(F\left(m_W^2, m_{h_1}^2\right) - F\left(m_Z^2, m_{h_1}^2\right) - F\left(m_W^2, m_{h_2}^2\right) + F\left(m_Z^2, m_{h_2}^2\right)\Big)\Bigg], \end{aligned} \tag{C.1}$$

and

$$\begin{aligned} S &= \frac{g^2 \sin^2\theta_W}{6(4\pi)^2\alpha}\Bigg[\left(2\sin^2\theta_W - 1\right)^2 G\left(m_{\eta^\pm}^2, m_{\eta^\pm}^2, m_Z^2\right) + G\left(m_{\eta_0}^2, m_{\eta_A}^2, m_Z^2\right) \\ &+ \log\left(m_{\eta_0}^2 m_{\eta_A}^2/(m_{\eta^\pm}^2)^2\right) + \sin^2\theta\Big(\log\left(m_{h_2}^2/m_{h_1}^2\right) + \hat{G}\left(m_{h_2}^2, m_Z^2\right) \\ &- \hat{G}\left(m_{h_1}^2, m_Z^2\right)\Big)\Bigg], \end{aligned} \tag{C.2}$$

where the functions F, G and $\hat{G}$ are defined as:

$$F(I,J) \equiv \begin{cases} \dfrac{I+J}{2} - \dfrac{IJ}{I-J}\log\dfrac{I}{J}, & \text{if} \quad I \neq J, \\ 0, & \text{if} \quad I = J. \end{cases} \tag{C.3}$$

$$\begin{aligned} G(I,J,Q) \equiv & -\frac{16}{3} + \frac{5(I+J)}{Q} - \frac{2(I-J)^2}{Q^2} \\ & + \frac{3}{Q}\left[\frac{I^2+J^2}{I-J} - \frac{I^2-J^2}{Q} + \frac{(I-J)^3}{3Q^2}\right]\log\frac{I}{J} + \frac{r}{Q^3} f(t,r)\,. \end{aligned} \tag{C.4}$$

$$\begin{aligned} \hat{G}(I,Q) \equiv & -\frac{79}{3} + 9\frac{I}{Q} - 2\frac{I^2}{Q^2} + \left(-10 + 18\frac{I}{Q} - 6\frac{I^2}{Q^2} + \frac{I^3}{Q^3} - 9\frac{I+Q}{I-Q}\right)\log\frac{I}{Q} \\ & + \left(12 - 4\frac{I}{Q} + \frac{I^2}{Q^2}\right)\frac{f(I, I^2-4IQ)}{Q}. \end{aligned} \tag{C.5}$$

and f is defined as

$$f(t,r) \equiv \begin{cases} \sqrt{r}\,\ln\left|\dfrac{t-\sqrt{r}}{t+\sqrt{r}}\right|, & \text{if} \quad r > 0, \\ 0, & \text{if} \quad r = 0, \\ 2\sqrt{-r}\,\arctan\dfrac{\sqrt{-r}}{t}, & \text{if} \quad r < 0. \end{cases} \tag{C.6}$$

References

[1] T. P. Cheng and L. F. Li. *GAUGE THEORY OF ELEMENTARY PARTICLE PHYSICS*. 1984.

[2] Paul Langacker. *The standard model and beyond*. 2010.

[3] G. 't Hooft and M. Veltman. Regularization and renormalization of gauge fields. *Nuclear Physics B*, 44(1):189 – 213, 1972.

[4] David J. Gross and Frank Wilczek. Ultraviolet behavior of non-abelian gauge theories. *Phys. Rev. Lett.*, 30:1343–1346, Jun 1973.

[5] H. David Politzer. Reliable perturbative results for strong interactions? *Phys. Rev. Lett.*, 30:1346–1349, Jun 1973.

[6] Steven Weinberg. Non-abelian gauge theories of the strong interactions. *Phys. Rev. Lett.*, 31:494–497, Aug 1973.

[7] M. Gell-Mann. Quarks. *Acta Phys. Austriaca Suppl.*, 9:733–761, 1972. [,5(2015)].

[8] H. Fritzsch, M. Gell-Mann, and H. Leutwyler. Advantages of the color octet gluon picture. *Physics Letters B*, 47(4):365 – 368, 1973.

[9] Steven Weinberg. A model of leptons. *Phys. Rev. Lett.*, 19:1264–1266, Nov 1967.

[10] Sheldon L. Glashow. Partial-symmetries of weak interactions. *Nuclear Physics*, 22(4):579 – 588, 1961.

[11] Abdus Salam. Weak and Electromagnetic Interactions. *Conf. Proc.*, C680519:367–377, 1968.

[12] G. S. Guralnik, C. R. Hagen, and T. W. B. Kibble. Global conservation laws and massless particles. *Phys. Rev. Lett.*, 13:585–587, Nov 1964.

[13] F. Englert and R. Brout. Broken symmetry and the mass of gauge vector mesons. *Phys. Rev. Lett.*, 13:321–323, Aug 1964.

[14] P.W. Higgs. Broken symmetries, massless particles and gauge fields. *Physics Letters*, 12(2):132 – 133, 1964.

[15] M. Gell-Mann. The interpretation of the new particles as displaced charge multiplets. *Nuovo Cim.*, 4(S2):848–866, 1956.

[16] Tadao Nakano and Kazuhiko Nishijima. Charge independence for v-particles*. *Progress of Theoretical Physics*, 10(5):581–582, 1953.

[17] Kazuhiko Nishijima. Charge independence theory of v particles*. *Progress of Theoretical Physics*, 13(3):285–304, 1955.

[18] G. Aad et al. Observation of a new particle in the search for the standard model higgs boson with the atlas detector at the lhc. *Physics Letters B*, 716(1):1 – 29, 2012.

[19] S. Chatrchyan et al. Observation of a new boson at a mass of 125 gev with the cms experiment at the lhc. *Physics Letters B*, 716(1):30 – 61, 2012.

[20] Yoichiro Nambu. Quasi-particles and gauge invariance in the theory of superconductivity. *Phys. Rev.*, 117:648–663, Feb 1960.

[21] J. Goldstone. Field theories with « superconductor » solutions. *Il Nuovo Cimento (1955-1965)*, 19(1):154–164, Jan 1961.

[22] Jeffrey Goldstone, Abdus Salam, and Steven Weinberg. Broken symmetries. *Phys. Rev.*, 127:965–970, Aug 1962.

[23] Ling-Lie Chau and Wai-Yee Keung. Comments on the parametrization of the kobayashi-maskawa matrix. *Phys. Rev. Lett.*, 53:1802–1805, Nov 1984.

[24] C. Patrignani et al. Review of Particle Physics. *Chin. Phys.*, C40(10):100001, 2016.

[25] C. Jarlskog. Commutator of the quark mass matrices in the standard electroweak model and a measure of maximal CP nonconservation. *Phys. Rev. Lett.*, 55:1039–1042, Sep 1985.

[26] Andrew Renshaw. Solar Neutrino Results from Super-Kamiokande. *Phys. Procedia*, 61:345–354, 2015.

[27] K. Abe et al. Solar neutrino results in Super-Kamiokande-III. *Phys. Rev.*, D83:052010, 2011.

[28] K. Abe et al. Observation of Electron Neutrino Appearance in a Muon Neutrino Beam. *Phys. Rev. Lett.*, 112:061802, 2014.

[29] P. Adamson et al. Electron neutrino and antineutrino appearance in the full MINOS data sample. *Phys. Rev. Lett.*, 110(17):171801, 2013.

[30] F. P. An et al. Observation of electron-antineutrino disappearance at Daya Bay. *Phys. Rev. Lett.*, 108:171803, 2012.

[31] Ziro Maki, Masami Nakagawa, and Shoichi Sakata. Remarks on the unified model of elementary particles. *Progress of Theoretical Physics*, 28(5):870–880, 1962.

[32] P. F. De Salas, S. Gariazzo, O. Mena, C. A. Ternes, and M. Tórtola. Neutrino Mass Ordering in 2018: Global Status. 2018.

[33] P. F. de Salas, D. V. Forero, C. A. Ternes, M. Tortola, and J. W. F. Valle. Status of neutrino oscillations 2017. 2017.

[34] V. N. Aseev, A. I. Belesev, A. I. Berlev, E. V. Geraskin, A. A. Golubev, N. A. Likhovid, V. M. Lobashev, A. A. Nozik, V. S. Pantuev, V. I. Parfenov, A. K. Skasyrskaya, F. V. Tkachov, and S. V. Zadorozhny. Upper limit on the electron antineutrino mass from the troitsk experiment. *Phys. Rev. D*, 84:112003, Dec 2011.

[35] V.M Lobashev, V.N Aseev, A.I Belesev, A.I Berlev, E.V Geraskin, A.A Golubev, O.V Kazachenko, Yu.E Kuznetsov, R.P Ostroumov, L.A Rivkis, B.E Stern, N.A Titov, C.V Zadoroghny, and Yu.I Zakharov. Direct search for neutrino mass and anomaly in the tritium beta-spectrum: Status of "troitsk neutrino mass" experiment. *Nuclear Physics B - Proceedings Supplements*, 91(1):280 – 286, 2001. Neutrino 2000.

[36] K. Eitel. Direct neutrino mass experiments. *Nucl. Phys. Proc. Suppl.*, 143:197–204, 2005. [,587(2005)].

[37] N. Aghanim et al. Planck 2018 results. VI. Cosmological parameters. 2018.

[38] Samoil M. Bilenky, J. Hosek, and S. T. Petcov. On Oscillations of Neutrinos with Dirac and Majorana Masses. *Phys. Lett.*, B94:495–498, 1980.

[39] W. H. Furry. On transition probabilities in double beta-disintegration. *Phys. Rev.*, 56:1184–1193, 1939.

[40] Heinrich Pas and Werner Rodejohann. Neutrinoless Double Beta Decay. *New J. Phys.*, 17(11):115010, 2015.

[41] Werner Rodejohann. Neutrinoless double beta decay and neutrino physics. *J. Phys.*, G39:124008, 2012.

[42] S. M. Bilenky and S. T. Petcov. Massive neutrinos and neutrino oscillations. *Rev. Mod. Phys.*, 59:671–754, Jul 1987.

[43] J. Schechter and J.W.F. Valle. Neutrinoless Double beta Decay in SU(2) x U(1) Theories. *Phys.Rev.*, D25:2951, 1982.

[44] Michael Duerr, Manfred Lindner, and Alexander Merle. On the Quantitative Impact of the Schechter-Valle Theorem. *JHEP*, 1106:091, 2011.

[45] Steven Weinberg. Varieties of Baryon and Lepton Nonconservation. *Phys. Rev.*, D22:1694, 1980.

[46] Peter Minkowski. mu -> e gamma at a rate of one out of 1-billion muon decays? *Phys. Lett.*, B67:421, 1977.

[47] Tsutomu Yanagida. HORIZONTAL SYMMETRY AND MASSES OF NEUTRINOS. *Conf. Proc.*, C7902131:95–99, 1979.

[48] Murray Gell-Mann, Pierre Ramond, and Richard Slansky. Complex Spinors and Unified Theories. *Conf.Proc.*, C790927:315–321, 1979.

[49] S. L. Glashow. The future of elementary particle physics, in Quarks and leptons. In *Cargèse Lectures, Plenum, NY (1980) 687.*, 1980.

[50] J. Schechter and J. W. F. Valle. Neutrino Masses in SU(2) x U(1) Theories. *Phys.Rev.*, D22:2227, 1980.

[51] J. Schechter and J. W. F. Valle. Neutrino Decay and Spontaneous Violation of Lepton Number. *Phys. Rev.*, D25:774, 1982.

[52] Rabindra N. Mohapatra and Goran Senjanovic. Neutrino Masses and Mixings in Gauge Models with Spontaneous Parity Violation. *Phys. Rev.*, D23:165, 1981.

[53] M. Magg and C. Wetterich. Neutrino Mass Problem and Gauge Hierarchy. *Phys. Lett.*, B94:61–64, 1980.

[54] G. Lazarides, Q. Shafi, and C. Wetterich. Proton lifetime and fermion masses in an SO(10) model. *Nucl. Phys.*, B181:287, 1981.

[55] C. Wetterich. Neutrino Masses and the Scale of B-L Violation. *Nucl. Phys.*, B187:343–375, 1981.

[56] Ernest Ma and D. P. Roy. Heavy triplet leptons and new gauge boson. *Nucl. Phys.*, B644:290–302, 2002.

[57] Robert Foot, H. Lew, X. G. He, and Girish C. Joshi. Seesaw Neutrino Masses Induced by a Triplet of Leptons. *Z. Phys.*, C44:441, 1989.

[58] Ernest Ma. Pathways to naturally small neutrino masses. *Phys. Rev. Lett.*, 81:1171–1174, 1998.

[59] R. N. Mohapatra and J. W. F. Valle. Neutrino Mass and Baryon Number Nonconservation in Superstring Models. *Phys. Rev.*, D34:1642, 1986.

[60] Michal Malinsky, J. C. Romao, and J. W. F. Valle. Novel supersymmetric SO(10) seesaw mechanism. *Phys. Rev. Lett.*, 95:161801, 2005.

[61] A. Zee. A Theory of Lepton Number Violation, Neutrino Majorana Mass, and Oscillation. *Phys. Lett.*, B93:389, 1980. [Erratum: Phys. Lett.B95,461(1980)].

[62] A. Zee. Charged Scalar Field and Quantum Number Violations. *Phys. Lett.*, B161:141–145, 1985.

[63] T. P. Cheng and Ling-Fong Li. Neutrino Masses, Mixings and Oscillations in SU(2) x U(1) Models of Electroweak Interactions. *Phys. Rev.*, D22:2860, 1980.

[64] A. Zee. Quantum Numbers of Majorana Neutrino Masses. *Nucl. Phys.*, B264:99–110, 1986.

[65] K. S. Babu. Model of 'Calculable' Majorana Neutrino Masses. *Phys. Lett.*, B203:132–136, 1988.

[66] Lincoln Wolfenstein. A Theoretical Pattern for Neutrino Oscillations. *Nucl. Phys.*, B175:93–96, 1980.

[67] Ernest Ma and Rahul Srivastava. Dirac or inverse seesaw neutrino masses with b-l gauge symmetry and s3 flavor symmetry. *Physics Letters B*, 741:217 – 222, 2015.

[68] Ernest Ma, Nicholas Pollard, Rahul Srivastava, and Mohammadreza Zakeri. Gauge $B - L$ Model with Residual Z_3 Symmetry. *Phys. Lett.*, B750:135–138, 2015.

[69] Cesar Bonilla and Jose W. F. Valle. Naturally light neutrinos in *Diracon* model. *Phys. Lett.*, B762:162–165, 2016.

[70] Cesar Bonilla, Ernest Ma, Eduardo Peinado, and Jose W.F. Valle. Two-loop dirac neutrino mass and wimp dark matter. *Physics Letters B*, 762:214 – 218, 2016.

[71] Salvador Centelles Chuliá, Ernest Ma, Rahul Srivastava, and José W. F. Valle. Dirac Neutrinos and Dark Matter Stability from Lepton Quarticity. *Phys. Lett.*, B767:209–213, 2017.

[72] Salvador Centelles Chuliá, Rahul Srivastava, and José W. F. Valle. Generalized Bottom-Tau unification, neutrino oscillations and dark matter: predictions from a lepton quarticity flavor approach. *Phys. Lett.*, B773:26–33, 2017.

[73] Salvador Centelles Chuliá, Rahul Srivastava, and José W. F. Valle. CP violation from flavor symmetry in a lepton quarticity dark matter model. *Phys. Lett.*, B761:431–436, 2016.

[74] Ernest Ma and Rahul Srivastava. Dirac or inverse seesaw neutrino masses with $B - L$ gauge symmetry and S_3 flavor symmetry. *Phys. Lett.*, B741:217–222, 2015.

[75] Ernest Ma and Utpal Sarkar. Radiative Left-Right Dirac Neutrino Mass. *Phys. Lett.*, B776:54–57, 2018.

[76] J. H. Jeans. The Motion of Stars in a Kapteyn Universe. *Monthly Notices of the Royal Astronomical Society*, 82:122, 1922.

[77] J. C. Kapteyn. First Attempt at a Theory of the Arrangement and Motion of the Sidereal System. *ApJ*, 55:302, 1922.

[78] F. Zwicky. Die Rotverschiebung von extragalaktischen Nebeln. *Helvetica Physica Acta*, 6:110, 1933.

[79] Vera C. Rubin and W. Kent Ford, Jr. Rotation of the Andromeda Nebula from a Spectroscopic Survey of Emission Regions. *Astrophys. J.*, 159:379–403, 1970.

[80] M. S. Roberts and A. H. Rots. Comparison of Rotation Curves of Different Galaxy Types. *Ast. and Astrophys J.*, 26:483–485, August 1973.

[81] J. Huchra, M. Davis, D. Latham, and J. Tonry. A survey of galaxy redshifts. IV - The data. *Astrophysical Journal Supplement Series*, 52:89–119, 1983.

[82] Christopher P. Ahn et al. The Ninth Data Release of the Sloan Digital Sky Survey: First Spectroscopic Data from the SDSS-III Baryon Oscillation Spectroscopic Survey. *Astrophys.J.Suppl.*, 203:21, 2012.

[83] S. Dodelson. *Modern Cosmology*. Academic Press. Academic Press, 2003.

[84] Craig J. Copi, David N. Schramm, and Michael S. Turner. Big bang nucleosynthesis and the baryon density of the universe. *Science*, 267:192–199, 1995.

[85] Henk Hoekstra, Howard Yee, and Mike Gladders. Current status of weak gravitational lensing. *New Astron.Rev.*, 46:767–781, 2002.

[86] Haakon Dahle. A compilation of weak gravitational lensing studies of clusters of galaxies. 2007.

[87] Alexey Vikhlinin, A. Kravtsov, W. Forman, C. Jones, M. Markevitch, et al. Chandra sample of nearby relaxed galaxy clusters: Mass, gas fraction, and mass-temperature relation. *Astrophys.J.*, 640:691–709, 2006.

[88] Mark Srednicki, Richard Watkins, and Keith A. Olive. Calculations of Relic Densities in the Early Universe. *Nucl.Phys.*, B310:693, 1988.

[89] P. Gondolo and G. Gelmini. Cosmic abundances of stable particles: improved analysis. *Nuclear Physics B*, 360:145–179, August 1991.

[90] Marco Taoso, Gianfranco Bertone, and Antonio Masiero. Dark Matter Candidates: A Ten-Point Test. *JCAP*, 0803:022, 2008.

[91] Julien Lesgourgues and Sergio Pastor. Massive neutrinos and cosmology. *Physics Reports*, 429(6):307 – 379, 2006.

[92] Julio F. Navarro, Carlos S. Frenk, and Simon D. M. White. The Structure of cold dark matter halos. *Astrophys. J.*, 462:563–575, 1996.

[93] Steven Weinberg. A new light boson? *Phys. Rev. Lett.*, 40:223–226, Jan 1978.

[94] R. D. Peccei and Helen R. Quinn. Constraints imposed by CP conservation in the presence of pseudoparticles. *Phys. Rev. D*, 16:1791–1797, Sep 1977.

[95] Jihn E. Kim. Weak Interaction Singlet and Strong CP Invariance. *Phys. Rev. Lett.*, 43:103, 1979.

[96] Mikhail A. Shifman, A. I. Vainshtein, and Valentin I. Zakharov. Can Confinement Ensure Natural CP Invariance of Strong Interactions? *Nucl. Phys.*, B166:493–506, 1980.

[97] Michael Dine, Willy Fischler, and Mark Srednicki. A Simple Solution to the Strong CP Problem with a Harmless Axion. *Phys. Lett.*, 104B:199–202, 1981.

[98] A. R. Zhitnitsky. On Possible Suppression of the Axion Hadron Interactions. (In Russian). *Sov. J. Nucl. Phys.*, 31:260, 1980. [Yad. Fiz.31,497(1980)].

[99] Gerard Jungman, Marc Kamionkowski, and Kim Griest. Supersymmetric dark matter. *Phys.Rept.*, 267:195–373, 1996.

[100] Jonathan L. Feng. Non-WIMP Candidates. 2010.

[101] Marco Cirelli. Indirect Searches for Dark Matter: a status review. *Pramana*, 79:1021–1043, 2012.

[102] M. Hirsch, S. Morisi, E. Peinado, and J. W. F. Valle. Discrete dark matter. *Phys. Rev.*, D82:116003, 2010.

[103] M. S. Boucenna, M. Hirsch, S. Morisi, E. Peinado, M. Taoso, and J. W. F. Valle. Phenomenology of Dark Matter from A_4 Flavor Symmetry. *JHEP*, 05:037, 2011.

[104] Wei Tang. Recent Results from the Daya Bay Neutrino Experiment. In *Proceedings, Workshop on Neutrino Physics : Session of CETUP* 2015 and 9th International Conference on Interconnections between Particle Physics and Cosmology (PPC2015): Lead/Deadwood, South Dakota, USA, July 6-17, 2015*, 2015.

[105] Myoung Youl Pac. Recent Results from RENO. 2018.

[106] Y. Abe et al. Improved measurements of the neutrino mixing angle θ_{13} with the Double Chooz detector. *JHEP*, 10:086, 2014. [Erratum: JHEP02,074(2015)].

[107] D. Meloni, S. Morisi, and E. Peinado. Neutrino phenomenology and stable dark matter with A4. *Phys. Lett.*, B697:339–342, 2011.

[108] D. Meloni, S. Morisi, and E. Peinado. Stability of dark matter from the D4xZ2 flavor group. *Phys. Lett.*, B703:281–287, 2011.

[109] M. S. Boucenna, S. Morisi, E. Peinado, Y. Shimizu, and J. W. F. Valle. Predictive discrete dark matter model and neutrino oscillations. *Phys. Rev.*, D86:073008, 2012.

[110] J. M. Lamprea and E. Peinado. Seesaw scale discrete dark matter and two-zero texture Majorana neutrino mass matrices. *Phys. Rev.*, D94(5):055007, 2016.

[111] Paul H. Frampton, Sheldon L. Glashow, and Danny Marfatia. Zeroes of the neutrino mass matrix. *Phys. Lett.*, B536:79–82, 2002.

[112] Zhi-zhong Xing. Texture zeros and Majorana phases of the neutrino mass matrix. *Phys. Lett.*, B530:159–166, 2002.

[113] Paul H. Frampton, Myoung C. Oh, and Tadashi Yoshikawa. Majorana mass zeroes from triplet VEV without majoron problem. *Phys. Rev.*, D66:033007, 2002.

[114] Atsushi Kageyama, Satoru Kaneko, Noriyuki Shimoyama, and Morimitsu Tanimoto. Seesaw realization of the texture zeros in the neutrino mass matrix. *Phys. Lett.*, B538:96–106, 2002.

[115] Alexander Merle and Werner Rodejohann. The Elements of the neutrino mass matrix: Allowed ranges and implications of texture zeros. *Phys. Rev.*, D73:073012, 2006.

[116] Harald Fritzsch, Zhi-zhong Xing, and Shun Zhou. Two-zero Textures of the Majorana Neutrino Mass Matrix and Current Experimental Tests. *JHEP*, 09:083, 2011.

[117] P. O. Ludl, S. Morisi, and E. Peinado. The Reactor mixing angle and CP violation with two texture zeros in the light of T2K. *Nucl. Phys.*, B857:411–423, 2012.

[118] D. Meloni, A. Meroni, and E. Peinado. Two-zero Majorana textures in the light of the Planck results. *Phys. Rev.*, D89(5):053009, 2014.

[119] Shun Zhou. Update on two-zero textures of the Majorana neutrino mass matrix in light of recent T2K, Super-Kamiokande and NOνA results. *Chin. Phys.*, C40(3):033102, 2016.

[120] Teruyuki Kitabayashi and Masaki Yasuè. Formulas for flavor neutrino masses and their application to texture two zeros. *Phys. Rev.*, D93(5):053012, 2016.

[121] D. V. Forero, M. Tortola, and J. W. F. Valle. Neutrino oscillations refitted. *Phys. Rev.*, D90(9):093006, 2014.

[122] M. C. Gonzalez-Garcia, Michele Maltoni, and Thomas Schwetz. Global Analyses of Neutrino Oscillation Experiments. *Nucl. Phys.*, B908:199–217, 2016.

[123] F. Capozzi, E. Lisi, A. Marrone, D. Montanino, and A. Palazzo. Neutrino masses and mixings: Status of known and unknown 3ν parameters. *Nucl. Phys.*, B908:218–234, 2016.

[124] P. A. R. Ade et al. Planck 2015 results. XIII. Cosmological parameters. *Astron. Astrophys.*, 594:A13, 2016.

[125] M. Agostini et al. Results on Neutrinoless Double-β Decay of ^{76}Ge from Phase I of the GERDA Experiment. *Phys. Rev. Lett.*, 111(12):122503, 2013.

[126] J. B. Albert et al. Search for Majorana neutrinos with the first two years of EXO-200 data. *Nature*, 510:229–234, 2014.

[127] A. Gando et al. Limit on Neutrinoless $\beta\beta$ Decay of ^{136}Xe from the First Phase of KamLAND-Zen and Comparison with the Positive Claim in ^{76}Ge. *Phys. Rev. Lett.*, 110(6):062502, 2013.

[128] Lutz Bornschein. KATRIN: Direct measurement of neutrino masses in the sub-Ev region. *eConf*, C030626:FRAP14, 2003. [,381(2003)].

[129] C. Alduino et al. CUORE sensitivity to $0\nu\beta\beta$ decay. *Eur. Phys. J.*, C77(8):532, 2017.

[130] V. E. Guiseppe et al. The Majorana Neutrinoless Double-Beta Decay Experiment. In *Proceedings, 2008 IEEE Nuclear Science Symposium, Medical Imaging Conference and 16th International Workshop on Room-Temperature Semiconductor X-Ray and Gamma-Ray Detectors (NSS/MIC 2008 / RTSD 2008): Dresden, Germany, October 19-25, 2008*, pages 1793–1798, 2008.

[131] Nilendra G. Deshpande and Ernest Ma. Pattern of Symmetry Breaking with Two Higgs Doublets. *Phys. Rev.*, D18:2574, 1978.

[132] Marco Cirelli, Nicolao Fornengo, and Alessandro Strumia. Minimal dark matter. *Nucl. Phys.*, B753:178–194, 2006.

[133] Ernest Ma. Verifiable radiative seesaw mechanism of neutrino mass and dark matter. *Phys. Rev.*, D73:077301, 2006.

[134] Nilendra G. Deshpande and Ernest Ma. Pattern of symmetry breaking with two higgs doublets. *Phys. Rev. D*, 18:2574–2576, Oct 1978.

[135] Laura Lopez Honorez, Emmanuel Nezri, Josep F. Oliver, and Michel H. G. Tytgat. The Inert Doublet Model: An Archetype for Dark Matter. *JCAP*, 0702:028, 2007.

[136] Laura Lopez Honorez and Carlos E. Yaguna. The inert doublet model of dark matter revisited. *JHEP*, 09:046, 2010.

[137] C. Bonilla, L. M. García de la Vega, J.M. Lamprea, R. Lineros, and E. Peinado. en prep.

[138] Alexander Merle and Moritz Platscher. Running of radiative neutrino masses: the scotogenic model — revisited. *JHEP*, 11:148, 2015.

[139] Cesar Bonilla, Jose W. F. Valle, and Jorge C. Romão. Neutrino mass and invisible Higgs decays at the LHC. *Phys. Rev.*, D91(11):113015, 2015.

[140] Mario Kadastik, Kristjan Kannike, and Martti Raidal. Dark Matter as the signal of Grand Unification. *Phys. Rev.*, D80:085020, 2009. [Erratum: Phys. Rev.D81,029903(2010)].

[141] Erik Lundstrom, Michael Gustafsson, and Joakim Edsjo. The Inert Doublet Model and LEP II Limits. *Phys. Rev.*, D79:035013, 2009.

[142] Michael E. Peskin and Tatsu Takeuchi. A New constraint on a strongly interacting Higgs sector. *Phys. Rev. Lett.*, 65:964–967, 1990.

[143] Michael E. Peskin and Tatsu Takeuchi. Estimation of oblique electroweak corrections. *Phys. Rev.*, D46:381–409, 1992.

[144] W. Grimus, L. Lavoura, O. M. Ogreid, and P. Osland. The Oblique parameters in multi-Higgs-doublet models. *Nucl. Phys.*, B801:81–96, 2008.

[145] Xiangyi Cui et al. Dark Matter Results From 54-Ton-Day Exposure of PandaX-II Experiment. *Phys. Rev. Lett.*, 119(18):181302, 2017.

[146] M. Ackermann et al. Search for Gamma-ray Spectral Lines with the Fermi Large Area Telescope and Dark Matter Implications. *Phys. Rev.*, D88:082002, 2013.

[147] Avelino Vicente and Carlos E. Yaguna. Probing the scotogenic model with lepton flavor violating processes. *JHEP*, 02:144, 2015.

[148] Takashi Toma and Avelino Vicente. Lepton Flavor Violation in the Scotogenic Model. *JHEP*, 01:160, 2014.

[149] G. Belanger, F. Boudjema, A. Pukhov, and A. Semenov. MicrOMEGAs: A Program for calculating the relic density in the MSSM. *Comput. Phys. Commun.*, 149:103–120, 2002.

[150] Rabindra N. Mohapatra and Goran Senjanovic. Neutrino mass and spontaneous parity nonconservation. *Phys. Rev. Lett.*, 44:91, 1980.

[151] A. Gando et al. Search for Majorana Neutrinos near the Inverted Mass Hierarchy Region with KamLAND-Zen. *Phys. Rev. Lett.*, 117(8):082503, 2016. [Addendum: Phys. Rev. Lett.117,no.10,109903(2016)].

[152] Ernest Ma and Rahul Srivastava. Dirac or inverse seesaw neutrino masses from gauged $B - L$ symmetry. *Mod. Phys. Lett.*, A30(26):1530020, 2015.

[153] Jose W. F. Valle and C. A. Vaquera-Araujo. Dynamical seesaw mechanism for Dirac neutrinos. *Phys. Lett.*, B755:363–366, 2016.

[154] Mario Reig, Jose W. F. Valle, and C.A. Vaquera-Araujo. Realistic $\mathrm{SU(3)_c} \otimes \mathrm{SU(3)_L} \otimes \mathrm{U(1)_X}$ model with a type II Dirac neutrino seesaw mechanism. *Phys. Rev.*, D94(3):033012, 2016.

[155] Cesar Bonilla, Ernest Ma, Eduardo Peinado, and Jose W. F. Valle. Two-loop Dirac neutrino mass and WIMP dark matter. *Phys. Lett.*, B762:214–218, 2016.

[156] Debasish Borah and Arnab Dasgupta. Naturally Light Dirac Neutrino in Left-Right Symmetric Model. 2017.

[157] Weijian Wang, Ronghui Wang, Zhi-Long Han, and Jin-Zhong Han. The $B - L$ Scotogenic Models for Dirac Neutrino Masses. 2017.

[158] Ernest Ma and Oleg Popov. Pathways to Naturally Small Dirac Neutrino Masses. *Phys. Lett.*, B764:142–144, 2017.

[159] Weijian Wang and Zhi-Long Han. Naturally Small Dirac Neutrino Mass with Intermediate $SU(2)_L$ Multiplet Fields. 2016.

[160] Salvador Centelles Chuliá, Rahul Srivastava, and José W. F. Valle. Seesaw roadmap to neutrino mass and dark matter. *Phys. Lett.*, B781:122–128, 2018.

[161] Alfredo Aranda, Cesar Bonilla, S. Morisi, E. Peinado, and J. W. F. Valle. Dirac neutrinos from flavor symmetry. *Phys. Rev.*, D89(3):033001, 2014.

[162] S. Morisi, E. Peinado, Yusuke Shimizu, and J. W. F. Valle. Relating quarks and leptons without grand-unification. *Phys. Rev.*, D84:036003, 2011.

[163] S. F. King, S. Morisi, E. Peinado, and J. W. F. Valle. Quark-Lepton Mass Relation in a Realistic A_4 Extension of the Standard Model. *Phys. Lett.*, B724:68–72, 2013.

[164] S. Morisi, M. Nebot, Ketan M. Patel, E. Peinado, and J.W.F. Valle. Quark-Lepton Mass Relation and CKM mixing in an A4 Extension of the Minimal Supersymmetric Standard Model. *Phys.Rev.*, D88:036001, 2013.

[165] Cesar Bonilla, Stefano Morisi, Eduardo Peinado, and Jose W. F. Valle. Relating quarks and leptons with the T_7 flavour group. *Phys. Lett.*, B742:99–106, 2015.

[166] Brenda Carballo-Perez, Eduardo Peinado, and Saul Ramos-Sanchez. $\Delta(54)$ flavor phenomenology and strings. *JHEP*, 12:131, 2016.

[167] S. Morisi and E. Peinado. An A(4) model for lepton masses and mixings. *Phys. Rev.*, D80:113011, 2009.

[168] Kalpana Bora. Updated values of running quark and lepton masses at GUT scale in SM, 2HDM and MSSM. *Horizon*, 2, 2013.

[169] M.E. Peskin and D.V. Schroeder. *An Introduction To Quantum Field Theory*. Frontiers in Physics. Avalon Publishing, 1995.

[170] W. Grimus, L. Lavoura, O. M. Ogreid, and P. Osland. A Precision constraint on multi-Higgs-doublet models. *J. Phys.*, G35:075001, 2008.